NOTICE

The quality of this microform is heavily dependent upon the quality of the original thesis submitted for microfilming. Every effort has been made to ensure the highest quality of reproduction possible.

If pages are missing, contact the university which granted the degree.

Some pages may have indistinct print especially if the original pages were typed with a poor typewriter ribbon or if the university sent us an inferior photocopy.

Reproduction in full or in part of this microform is governed by the Canadian Copyright Act, R.S.C. 1970, c. C-30, and subsequent amendments.

AVIS

La qualité de cette microforme dépend grandement de la qualité de la thèse soumise au microfilmage. Nous avons tout fait pour assurer une qualité supérieure de reproduction.

S'il manque des pages, veuillez communiquer avec l'université qui a conféré le grade.

La qualité d'impression de certaines pages peut laisser à désirer, surtout si les pages originales ont été dactylographiées à l'aide d'un ruban usé ou si l'université nous a fait parvenir une photocopie de qualité inférieure.

La reproduction, même partielle, de cette microforme est soumise à la Loi canadienne sur le droit d'auteur, SRC 1970, c. C-30, et ses amendements subséquents.

Electron Paramagnetic Resonance Linewidth and Spin-Lattice Relaxation in Single Crystals: Presence of Dissimilar Spins, Application of Site Percolation and Percolation-Limited Diffusion

Ufuk Orhun

A Thesis

in

The Department

of

Physics

Presented in Partial Fulfillment of the Requirements
for the Degree of Doctor of Philosophy at
Concordia University
Montréal, Québec, Canada

March 1991

ISBN 0-315-64665-9

ABSTRACT

Electron Paramagnetic Resonance Linewidth and Spin-Lattice Relaxation in Single Crystals: Presence of Dissimilar Spins, Application of Site Percolation and Percolation-Limited Diffusion

Ufuk Orhun

An expression, appropriate to calculate the spin-lattice relaxation time of the host paramagnetic ions, using the EPR linewidths of the impurity ion, is derived by use of the second moment for crystals consisting of two different kinds of spins. Estimations have been made of the spin-lattice relaxation time of the R^{3+} ions in Gd^{3+} doped $NH_4R(SO_4)_2 \cdot 4H_2O$ single crystals, with R = Pr, Sm, Ce, and Nd. Significant differences were found in the values of spin-lattice relaxation time as calculated using the presently derived expression from those calculated using the commonly used incorrect equation.

Three dimensional site-percolation calculations of Gd^{3+}-doped $LiYb_xY_{1-x}F_4$ and $Pr_xLa_{1-x}F_3$ single crystals have been made in order to explain the experimentally observed Gd^{3+} EPR linewidths in these hosts as functions of temperature and x. The calculated percolation thresholds are in agreement with the disappearance of the observed EPR linewidths at low temperatures for $LiYb_xY_{1-x}F_4$ crystals with $x \geq 0.3$, and with the disappearance of the observed EPR lines, when $0.2 < x < 0.8$, in $Pr_xLa_{1-x}F_3$. It is concluded

that the that the spin-lattice relaxation process is ineffective, as far as the linewidths are concerned, below x = x_c.

A model combining percolation and diffusion processes, referred to as percolation-limited diffusion (PLD), has been proposed, and applied to a square lattice. Two probabilities, one for site occupation and the other for spin orientation, have been employed to simulate three distinct cases - spin glasses, magnetically-dilute single crystals, and liquid crystals. Fractal dimension of PLD cluster, fractal dimension of random-walk, percolation thresholds, and critical exponents for the various cases have been estimated. It is found that the resulting PLD clusters exhibit the same fractal behaviour as those of the hulls of diffusion fronts. As well, they exhibit some properties of percolation clusters. In addition, they possess some unique critical exponents of their own. The presently-calculated values of percolation thresholds, p_c, the fractal dimensions D_H and d_{rw}, and the critical exponents ν and γ, are in agreement, within error bounds, with those reported previously.

ACKNOWLEDGEMENTS

The author expresses his sincere gratitude to Professor S. K. Misra for proposing the topics covered in this thesis, and for his continued willingness to help, and his guidance throughout the course of entire research, presented in this thesis. He is also thankful to him for providing partial financial support from his NSERC and Action-Structurante grants.

The teaching assistantship provided by the Department of Physics is also thankfully acknowledged.

TABLE OF CONTENTS

Chapter I

Introduction

This thesis consists of three distinct yet related topics, whose detailed introductions are given in the beginning of the corresponding chapters. They are:

(i) Calculation of the host-ion spin-lattice relaxation time in single crystals containing two different kinds of paramagnetic ions. Crystals consisting of one kind of paramagnetic ion, were mostly used in the early days of electron paramagnetic resonance (EPR) experiments. An expression was derived to calculate the spin-lattice relaxation time of the paramagnetic ion using its EPR linewidth. In the last few decades paramagnetic impurity ions, in addition to the paramagnetic host ions, have been used widely in EPR experiments. However, the same expression, mentioned above, applicable to the presence of one kind of paramagnetic ions had been frequently used to calculate the spin-lattice relaxation time (τ) of the host ions using the impurity-ion EPR linewidth. All these estimates of τ have, thus, been erroneous, since the second moment for crystals consisting of one kind of paramagnetic ion, used in these estimates of τ, excludes all interactions between dissimilar paramagnetic ions, which can be quite significant.

(ii) Percolation. This is a relatively recent subject. Percolation is basically the study of the extent of the connectivity via certain sites in a medium. It has been used to explain various physical phenomena. In this thesis, percolation phenomenon has been used as a model to represent the spin-lattice relaxation process and, in turn, to explain various critical behaviours observed in EPR experiments. This is the first-ever application of the percolation process to the study of the spin-lattice relaxation process in doped and magnetically dilute crystals.

(iii) Percolation-limited diffusion. A model, combining both percolation and diffusion processes, referred to as percolation-limited diffusion (PLD), has been proposed in this thesis. Three specific cases are discussed by way of detailed computer simulations.

The organization of this thesis is as follows. Chapter II describes the details of the phenomenon of electron paramagnetic resonance (EPR), EPR linewidth, and its relationship to spin-lattice relaxation, as a background necessary to understand the research presented in this thesis. The derivation of the impurity-ion second moment for crystals which contain two different species of paramagnetic ions, and the derivation of an equation to calculate the spin-lattice relaxation time of the host paramagnetic ions using the impurity-ion EPR linewidth are given in Chapter III. These will be followed by calculations of host-ion

spin-lattice relaxation times in several samples containing host paramagnetic ions, and comparisons of these relaxation times with the previously-reported values, estimated using the incorrect expression. Finally, a discussion is provided on how to identify the particular spin-lattice relaxation mechanism effective; this is accompanied by illustrative examples. The phenomenon of percolation, percolation threshold, its relevance to EPR and application to spin-lattice relaxation are discussed in detail in Chapter IV. A description is provided of the computer simulations used for the calculation of the second moment and percolation thresholds in $LiYb_xY_{1-x}F_4$ and $Pr_xLa_{1-x}F_3$ single crystals. An explanation of the reported data, i.e. dependence on concentration (x) and temperature of Gd^{3+} EPR linewidths in $LiYb_xY_{1-x}F_4$ and $Pr_xLa_{1-x}F_3$ is thus provided. Chapter V deals with the details of percolation-limited diffusion model. The parameters of interest, such as critical exponents and fractal dimensions, are calculated for PLD model. The calculated values of these parameters are compared, in limiting cases, to some previously-studied models, such as purely percolation and purely diffusion processes. The relationship between the percolation-limited diffusion and the spin-lattice relaxation processes is established. A discussion of the possible application of this model to various physical systems is also provided. Finally, the conclusions are given in Chapter VI.

Chapter II

The phenomenon of electron paramagnetic resonance

II.1 The mechanism of electron paramagnetic resonance

Electron paramagnetic resonance (EPR) is a form of spectroscopy in which an oscillating magnetic field induces magnetic dipole transitions between energy levels of a system of paramagnets. A paramagnet with a total angular momentum of J will have 2J+1 equally-spaced energy levels, in the presence of a static magnetic field, referred to as the Zeeman field (B). The spacing between the energy levels, ΔE, is directly proportional to the magnitude of the external magnetic field, B, and is given by

$$\Delta E = g\mu_B B, \qquad \text{(II.1)}$$

where μ_B is the Bohr magneton and g is a dimensionless constant that determines the magnetic dipole moment, called the Landé factor. Further splitting of the energy levels may occur due to spin-orbit coupling and crystal field effects. In an usual EPR experiment, the magnetic field value is varied, while the supplied microwave energy is kept constant and the resonance occurs when the supplied microwave energy ($h\nu$) equals ΔE, the spacing between the energy levels of a paramagnet. This particular frequency, corresponding to ΔE,

i.e. $\nu = \Delta E/h$, is called the Larmor frequency. Thus, an isolated, single paramagnet, supplied with constant microwave energy $h\nu$, while the magnetic field is varied, would have a single resonance line at $B_r = h\nu/g\mu_B$.[1] X-band EPR experiments, as those considered in this thesis, utilize microwave frequencies in 8.5 to 10 GHz. For this frequency range, for most paramagnets, the resonance condition is satisfied for external magnetic fields near 3500×10^{-4} T.

II.2 EPR linewidth

In a typical EPR experiment, crystals consisting of paramagnetic and/or diamagnetic host ions are doped by paramagnetic impurity ions, and it is the impurity ion whose resonance is of interest. The impurity ions are surrounded with paramagnetic host ions, and therefore the local magnetic field at an impurity site depends on the direction of the host-ion spins surrounding that particular impurity site. Some host spins contribute to increase the magnitude of the local magnetic field, while others tend to reduce it. This results in a distribution of the resonance magnetic field value for the impurity ion, causing the broadening of the EPR resonance line.[2] The linewidth, ΔB, is defined as the full width at half the maximum (FWHM) of an absorption line. An EPR absorption line along with its first derivative are depicted in Figure II.1. It is the first derivative of the absorption line, which is recorded in most EPR

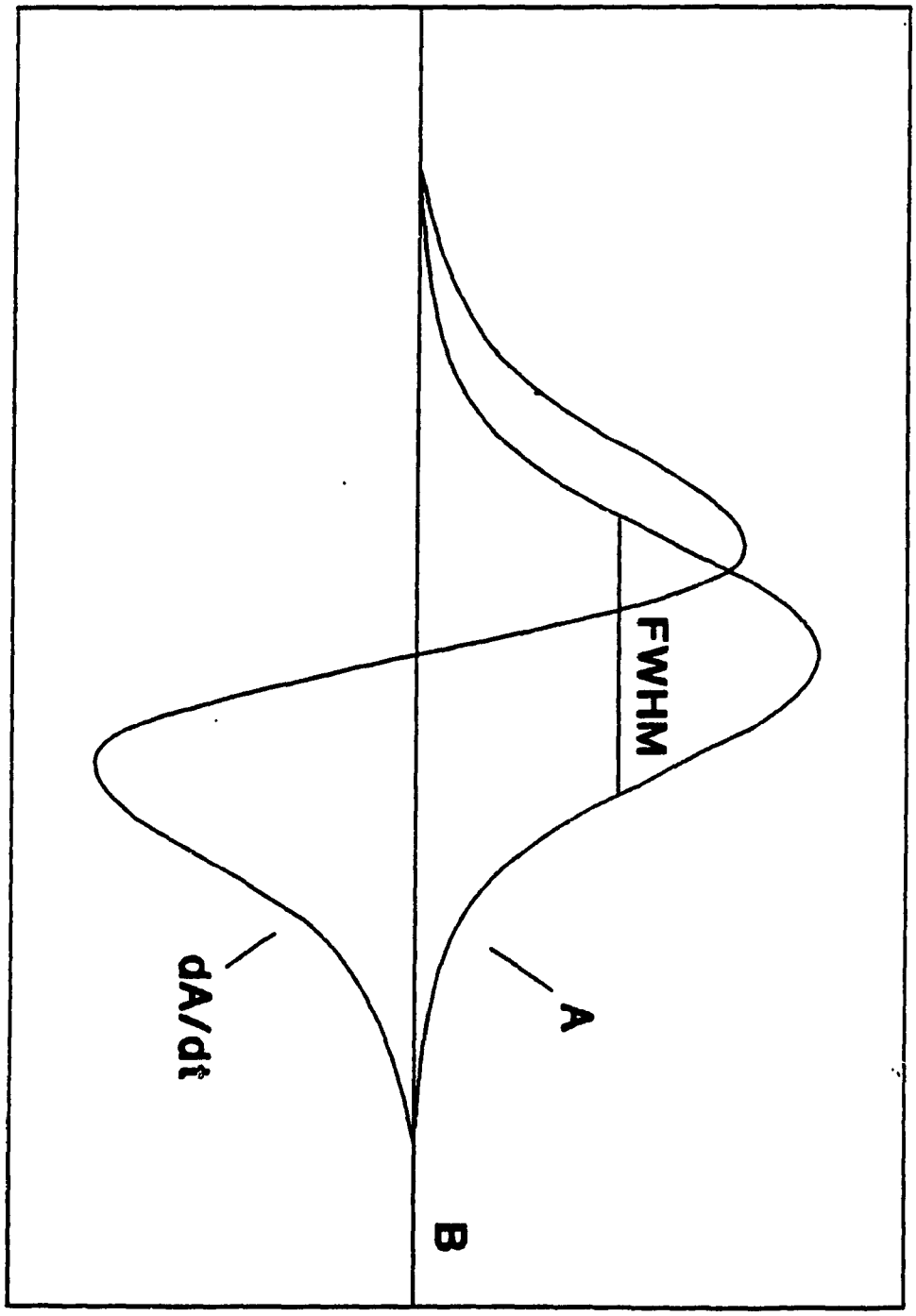

Figure II.1. The plot of EPR absorption, A, and its first derivative dA/dt as a function of the external magnetic field. The linewidth (FWHM), ΔB, is also indicated.

experiments.

There may exist other magnetic dipoles in the crystal (e.g., protons), besides the paramagnetic host ions, which will also cause variations of the local fields at the impurity ion sites and contribute to the linewidth. In addition, non-magnetic interactions can also affect the linewidth indirectly through their effect on magnetic interactions.

II.3 Spin-lattice relaxation and its effect on EPR lines

The transitions induced between the energy levels of a paramagnet, by the exchange of energy between the paramagnet and the rest of the lattice constitute spin-lattice relaxation. There are several spin-lattice relaxation processes, differing from each other through the way the energy exchange takes place. For example in direct process there are two energy levels involved in the spin-lattice relaxation process, while in the Orbach process there are three.[1]

The spin-lattice relaxation process is responsible for the return of an excited spin system to its equilibrium state. Assuming that this return has an exponential behaviour, and that the external magnetic field is along the z axis, the spin-lattice relaxation time, τ, is defined by the following equation:[1]

$$\frac{d}{dt}M_z = \frac{M_o - M_z}{\tau}. \qquad \text{(II.2)}$$

In eq. (II.2), M_z is the component of the magnetization along the z axis and M_o is its equilibrium value.

The spin-lattice relaxation process causes the paramagnetic host-ion spins to flip from one state to the other. These flips of the surrounding paramagnets result in fluctuations of the local field at the impurity site which affect the local field, and therefore the EPR linewidth. It has been shown that the host-ion spin-lattice relaxation can both narrow and broaden the EPR lines, depending on the ratio of the spin-lattice relaxation time of the impurity ion to that of the host ion.[2] Both the narrowing and the broadening of EPR lines are measured with respect to dipolar linewidth as calculated using the second moment. The second moment represents EPR linewidth that would have been measured in the absence of any spin motion in the lattice. The EPR lines broaden when the host-ion spin-lattice relaxation time is of the same order of that of the impurity ion, while they are narrowed when the host-ion spin-lattice relaxation time is much shorter than that of the impurity ion.[2] Generally, in the former case, the EPR lines broaden with increasing temperature, while in the latter case they narrow with increasing temperature. It should be noted that the spin-lattice relaxation time, always, decreases with

increasing temperature.

Chapter III

Calculation of the paramagnetic host spin-lattice relaxation time from impurity-ion EPR linewidth

III.1 Introduction

The effect of dipolar interactions on resonance line shape was first treated by Waller,[3] and later by Broer[4] and Van Vleck.[5] Subsequently, Anderson and Weiss[6] presented a theory, which treats the motion of spins induced by the exchange interactions as a stochastic process, and makes it possible to describe the line shape in a fairly reasonable way. This stochastic theory was developed further by Anderson.[7] His step goes a step further than the moment method of Van Vleck.[5] More quantitative calculations of relaxation times were later reported by Mitsuma.[8]

It has been shown by Anderson and Weiss,[6] that rapid motions of the host spins narrow the impurity EPR lines in crystals, consisting of only one paramagnetic species and considered the exchange interactions between the ions as the source of random spin motions, with the rate of motion being ω_e. They derived the EPR linewidth (ΔB) as

$$\Delta B = \frac{10}{3} B_{dip}^2 / B_e. \qquad \text{(III.1)}$$

It should be mentioned that the validity of eq. (III.1) is subject to the condition: $B_e >> B_{dip}$.[6] In eq. (III.1), B_e is, in fact, ω_e, as expressed in magnetic-field units, and B_{dip} is the linewidth due to dipole-dipole interactions between the impurity ion, responsible for EPR, and the paramagnetic ions of the host crystal, given by $B_{dip}^2 = h^2 <\Delta\nu^2>/g^2\mu_B^2$, (h is Planck's constant, g is the Lande's factor of the paramagnetic ions, μ_B is the Bohr magneton). $<\Delta\nu^2>$ is the second moment for a simple cubic lattice with one kind of magnetic ion, given by Van Vleck,[5] as

$$<\Delta\nu^2> = 36.8g^4\beta^4h^{-2}d^{-6}\ [\tfrac{1}{3}S(S+1)]\ (\lambda_1^4+\lambda_2^4+\lambda_3^4-0.187), \quad \text{(III.2)}$$

where d, S, and λ_1, λ_2, λ_3 are the spacing of a simple cubic lattice, the effective spin, and the direction cosines of the applied field, relative to the principal cubic axes, respectively. Using eq. (III.2), Anderson and Weiss[6] showed that

$$B_{dip}^2 = 5.1\ (g\beta n)^2 S(S+1), \quad \text{(III.3)}$$

where n is the number of host paramagnetic spins per unit volume.

In order to explain the highly temperature-dependent EPR linewidths, Mitsuma[8] suggested that the spin-lattice

relaxation process might be responsible for the narrowing of EPR lines in a way, which is similar to that caused by the exchange interactions, described above. In parallelism to the theory of Anderson and Weiss,[6] Mitsuma[8] derived the EPR linewidth as

$$\Delta B = \frac{10}{3} 2B_{dip}^2 / B_{mod}. \qquad \text{(III.4)}$$

The $\frac{10}{3}$ factor, both in eqs. (III.1) and (III.4), is due to the extreme narrowing, as pointed out by Anderson and Weiss.[6] The factor of 2 appearing in eq. (III.4) is due to Lorentzian line shape of the narrowed resonance lines. As seen from eq. (III.4), the quantity B_{mod} replaces B_e in eq. (III.1). B_{mod} is the host-ion spin-lattice relaxation time, τ , expressed in magnetic-field units:[8]

$$B_{mod} = h/\tau g\beta \qquad \text{(III.5)}$$

Combining eqs. (III.3), (III.4), and (III.5), τ can be expressed as

$$\tau = \frac{3h\Delta B}{102(g\beta)^3 n^2 S(S+1)} . \qquad \text{(III.6)}$$

Thus, τ can be calculated from eq. (III.6), using the experimentally observed EPR linewidth.

As already stated, eq. (III.3) is derived for a simple cubic lattice, consisting of only one kind of paramagnetic ion. Thus, eq. (III.6) is invalid for crystals, wherein the paramagnetic host ions are different from impurity paramagnetic ions. Papers after papers have been published in the literature dealing with such crystals, wherein eq. (III.6) has been employed to calculate the spin-lattice relaxation time of the host ions; for example, see Refs. 9-14. Nevertheless, as discussed above, use of eq. (III.6) is not, indeed, valid in such cases.

In this chapter, an expression is derived in order to calculate the spin-lattice relaxation time of paramagnetic host ions in crystals using the impurity-ion EPR linewidths, taking appropriately into account the presence of two different kinds of spins in the crystal. The derivation of this equation is given in Sec. III.2.

III.2 Theory

The second moment, for crystals, containing two kinds of paramagnetic spins, is given by Van Vleck,[5] as follows:

$$\langle \Delta\nu^2 \rangle_{II} = \frac{1}{3} S(S+1)\, h^{-2} \sum_k [-3g^2\beta^2 r_{jk}^{-3} \left(\tfrac{3}{2}\gamma_{jk}^2 - \tfrac{1}{2}\right)]^2 +$$

$$+\tfrac{1}{3}S'(S'+1)\, h^{-2} \sum_k [(-2z^2 J_{jk'}) + (1-3\gamma_{jk'}^2) gg'\beta^2 r_{jk'}^{-3}]^2. \quad \text{(III.7)}$$

In eq. (III.7), S, $r_{jk'}$, $\gamma_{jk'}$, z, and $J_{jk'}$ represent the

effective spin, the distance between the j and k ions, the direction cosine of the vector r_{jk} with the external field, the number of electrons in unfilled electronic shells of the host ions, and the exchange integral between the host (k') and the impurity ions (j), respectively; the primed quantities describe the host ions, while the unprimed ones the impurity ion. The external Zeeman field (B) is assumed to be along the z axis.[5] The impurity and host Lande factors (g, g') are assumed to be sufficiently different from each other, so that the resonances of these two different ions do not overlap each other.[3] It should be pointed out, here, that it is the impurity ion whose resonance is of interest. Assuming that the distances between the impurity ions are sufficiently large, the first term in eq. (III.7) can be neglected, compared to the other terms. If the number of the neighbors, to be considered, is limited to N, eq. (III.7) reduces to

$$<\Delta\nu^2> = \frac{1}{3} S'(S'+1)\, h^{-2} \left[N J_p^2 + (gg')^2 \beta^2 \mu_o^2 \sum_{k'}^{N} (1-3\gamma_{jk'}^2)^2 r_{jk'}^{-6} + 2 J_p gg' \beta^2 \mu_o \sum_{k'}^{N} (1-3\gamma_{jk'}^2) r_{jk'}^{-3}\right], \qquad \text{(III.8)}$$

In eq. (III.8), J_p is the average host-impurity pair-exchange constant. (μ_o is the permeability constant, required for the purpose of calculations in SI units.) In

reducing eq. (III.7) to eq. (III.8), it should be noted that J_p, the average host-impurity exchange constant,[15] stands for the quantity $\tilde{A}_{jk'} = -2z^2 J_{jk'}$, as defined by Van Vleck;[5] the same value (J_p) for $\tilde{A}_{jk'}$ has been assumed for all the neighbors taken into consideration. In magnetic-field units, the full width at half maximum (FWHM) of a Gaussian distribution, taking into account both the dipole-dipole and exchange interactions, can be expressed as

$$B^2_{dip-ex} = (2.35)^2 h^2 \langle \Delta\nu^2 \rangle_{II} / g^2 \beta^2, \qquad \text{(III.9)}$$

where $\langle \Delta\nu^2 \rangle_{II}$ is that given by eq. (III.8). Eq. (III.9) is, in fact, a generalization of eq. (III.3), which is valid for crystals consisting of only one kind of paramagnetic ion, to the presence of two different species of paramagnetic ions in the crystal. In eq. (III.9) the factor 2.35 should be replaced by 3.46 for the case when the EPR resonance lines have a Lorentzian shape. It should be noted here, that the second moment [and, therefore, eq. (III.3) which depends on it] for crystals consisting of only one kind of paramagnetic ions does not include exchange terms, whereas the second moment [and, therefore, eq. (III.9) which depends on it] for crystals consisting of two different kinds of paramagnetic ions, does include exchange between dissimilar ions as well. Further, the exchange between similar ions does not appear in the expression for the second moment.[5] Replacing B^2_{dip} in

eq. (III.4) by B^2_{dip-ex}, one obtains

$$\Delta B = \frac{10}{3} 2B^2_{dip-ex} / B_{mod}. \qquad \text{(III.10)}$$

Using eqs. (III.5), (III.8), (III.9), and (III.10) the spin-lattice relaxation time of the host ions in crystals with two different kinds of paramagnetic ingredients, τ, can be expressed as

$$\tau = (3\Delta B g^2 \beta)/(110hg' \langle \Delta\nu^2 \rangle_{II}), \qquad \text{(III.11)}$$

where ΔB is the impurity-ion EPR linewidth (FWHM), observed experimentally; the primed Landé factor is that for the host, while the unprimed one refers to the impurity.

Eq. (III.11), derived using the second moment for crystals with two kinds of paramagnetic ions, is, really, the appropriate equation for the usual EPR situation, i.e., for crystals consisting of paramagnetic host ions, doped with impurity paramagnetic ions, which are different from the host ions. One should, therefore, use eq. (III.11) in order to calculate the spin-lattice relaxation time of the host ions, rather than eq. (III.6), which is valid for crystals consisting of only one kind of paramagnetic ions.

As seen from eq. (III.11), the host-ion spin-lattice relaxation time is directly proportional to the impurity-ion EPR linewidth. Thus, as the temperature increases the

spin-lattice relaxation time becomes shorter, and the impurity-ion lines become narrower. Therefore, eq. (III.11) should not be used in cases when the experimentally observed lines broaden as the temperature increases. Obviously, in such a case, the EPR linewidths are not proportional to the host-ion spin-lattice relaxation time since the spin-lattice relaxation time, always decreases with increasing temperature. Some data have been reported, wherein the EPR linewidth is inversely proportional to the spin-lattice relaxation time,[16] to which eq. (III.11) does not apply.

III.3 Illustrative examples

In a typical EPR experiment paramagnetic impurity is introduced into a host crystal lattice in order to study the resonance spectrum, consisting of transition lines of the impurity ion. The host crystal may consist of diamagnetic and paramagnetic ions. By exploiting the resonance spectrum, one can get an understanding of the host lattice.

For illustration, the spin-lattice relaxation times of the host paramagnetic ions will be calculated presently for the following Gd^{3+}-doped single crystals:

(i) $NH_4Pr(SO_4)_2 \cdot 4H_2O$ (Pr^{3+})

(ii) $NH_4Sm(SO_4)_2 \cdot 4H_2O$ (Sm^{3+})

(iii) $NH_4Ce(SO_4)_2 \cdot 4H_2O$ (Ce^{3+})

(iv) $NH_4Nd(SO_4)_2 \cdot 4H_2O$ (Nd^{3+})

The host ions in the crystals above are those indicated in the brackets following the formulas.

The reasons for choosing these particular crystals is that the host-ion spin-lattice relaxation times for these crystal have been estimated previously using the wrong expression, and therefore a comparison of the presently calculated spin-lattice relaxation times can be made with those calculated using the incorrect expression. Relevant experimental data, e.g. crystal structure, EPR linewidths, which are needed to calculate the spin-lattice relaxation time using the appropriate second moment, are readily available for these crystals.

The structure, of all the crystals listed above, is monoclinic, characterized by the space group C_{2h}^5; there are four formulas per unit cell.[17,18] The unit cell parameters, used in the present calculations, are given in Table III.1. The effective spin, S', of the host ion, the Lande factors, g and g', of both the host and the impurity ions, and the experimentally observed impurity-ion linewidths at room temperature, ΔB, all required for the present calculations, are given in Table III.2.[19] No pair-exchange constant, J_p, values have been reported for these crystals. Therefore, the spin-lattice relaxation times have been presently calculated for the values of J_p = 0.1, 1.0, 5.0, and 10.0 GHz, thus covering a reasonable range. These values of the spin-lattice relaxation times, along with those reported

Table III.1. The unit cell parameters of the crystals considered, which are necessary for the calculation of $r_{jk'}$ and $\gamma_{jk'}$ values.

Crystal	a(Å)	b(Å)	c(Å)	β
$NH_4Pr(SO_4)_2 \cdot 4H_2O$ (monoclinic)	6.64	18.96	8.80	97°11′
$NH_4Sm(SO_4)_2 \cdot 4H_2O$ (monoclinic)	6.58	18.89	8.74	96°52′
$NH_4Ce(SO_4)_2 \cdot 4H_2O$ (monoclinic)	6.68	19.01	8.82	97°17′
$NH_4Nd(SO_4)_2 \cdot 4H_2O$ (monoclinic)	6.63	18.93	8.80	97°04′

Table III.2. τ of R in $NH_4R(SO_4)_2 \cdot 4H_2O$ (R = Pr, Sm, Ce, Nd) single crystals calculated at room temperature. The values of S', g, g', and ΔB used in the present calculations are also listed. τ values are given in seconds, while the figures inside the brackets following τ are J_p values in GHz.

R	Sm	Nd	Pr	Ce
S'	1/2	1/2	1/2	1/2
g	1.9922	1.9830	1.9949	1.9930
g'	0.57	2.82	0.80	2.01
ΔB (Gs)	21	41	30	28
τ (0.1)[a]	1.47×10^{-11}	2.41×10^{-13}	7.64×10^{-11}	4.69×10^{-13}
τ (1.0)[a]	2.40×10^{-12}	2.21×10^{-13}	2.23×10^{-12}	3.68×10^{-13}
τ (5.0)[a]	1.01×10^{-13}	3.79×10^{-14}	1.04×10^{-13}	3.81×10^{-14}
τ (10.0)[a]	2.51×10^{-14}	9.99×10^{-15}	2.57×10^{-14}	9.66×10^{-15}
τ [b]	2.10×10^{-10}	2.10×10^{-12}	———	1.00×10^{-11}

[a]Calculated presently.

[b]Reported in Refs. 18 and 20.

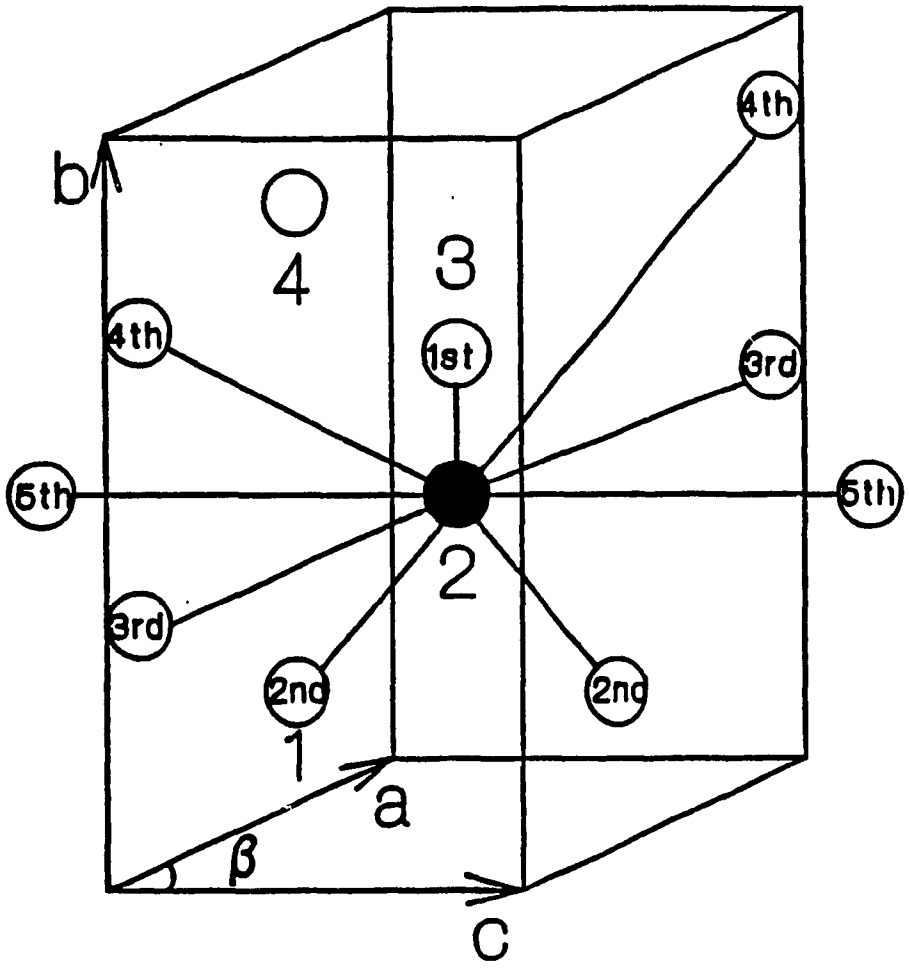

Figure III.1. The positions of the four R^{3+} ions in the unit cell of the $NH_4R(SO_4)_2 \cdot 4H_2O$ hosts. They are marked as 1, 2, 3, and 4, respectively. Considering that a Gd^{3+} ion replaces the R^{3+} ion 2, the positions of the nine R^{3+} ions (up to and including fifth nearest neighbors) surrounding the impurity ion are also exhibited.

previously,[18,20] calculated using the incorrect expression, are given in Table III.2.

It should be noted that the lattice sums required in eq. (III.8) were calculated taking into account up to and including fifth-nearest neighbors surrounding the impurity ion for these crystals. This was found to be quite sufficient,since the value of the second moment for the present crystals does not vary appreciably by including neighbours farther away in the lattice. However, depending on the crystal and the accuracy desired, neighbors located at larger distances can also be included in the calculations. A $NH_4R(SO_4)_2 \cdot 4H_2O$ unit cell along with the neighbouring ions, considered here, is shown in Figure III.1. A computer program, listed in Appendix I, was used to locate the host ions surrounding the impurity ion. This computer program will be described, in detail, in the next chapter.

Finally, it should be mentioned that the impurity linewidth, ΔB, used in eq. (III.11) is $\Delta B_{exp} - \Delta B_{dia}$, where ΔB_{exp} and ΔB_{dia} are the experimentally observed impurity linewidth in isostructural lattices consisting of paramagnetic and diamagnetic host ions, respectively. This enables the elimination of the effects which contribute to ΔB_{exp}, but do not contribute to the second moment, described by eq. (III.8).

III.4 Determination of the effective spin-lattice relaxation process

The values of τ, host ion spin-lattice relaxation time, listed in Table III.2 are calculated only at the room temperature. It should be noted that, the spin-lattice relaxation time is highly temperature dependent, always decreasing with increasing temperature. There are several processes responsible for spin-lattice relaxation, each having their own temperature dependence, i.e., direct process [$\tau^{-1} \propto \exp(-1/T)$], and $\tau^{-1} \propto T^n$ for some other processes.[21] One can calculate τ as a function of temperature using variable-temperature EPR data, thus allowing the determination of the effective spin-lattice relaxation process. For $NH_4Pr(SO_4)_2 \cdot 4H_2O$), the spin-lattice relaxation time, τ, of the paramagnetic host ion, Pr^{3+}, has been calculated in the 266-369 K temperature range. Figure III.2 shows the log-log plot of τ^{-1} versus T. By calculating the slopes of the fitted straight lines, it is found that $\tau^{-1} \propto T^7$ in the temperature range 266-296 K, and $\tau^{-1} \propto T^2$ in the temperature range 296-369 K. By comparing the temperature dependences, currently estimated, to those of the various spin-lattice relaxation processes, it is deduced that in the temperature range 266-296 K the predominant spin-lattice relaxation process is the "sum" process, while in the 296-369 K range the Raman process is dominant.[19,21]

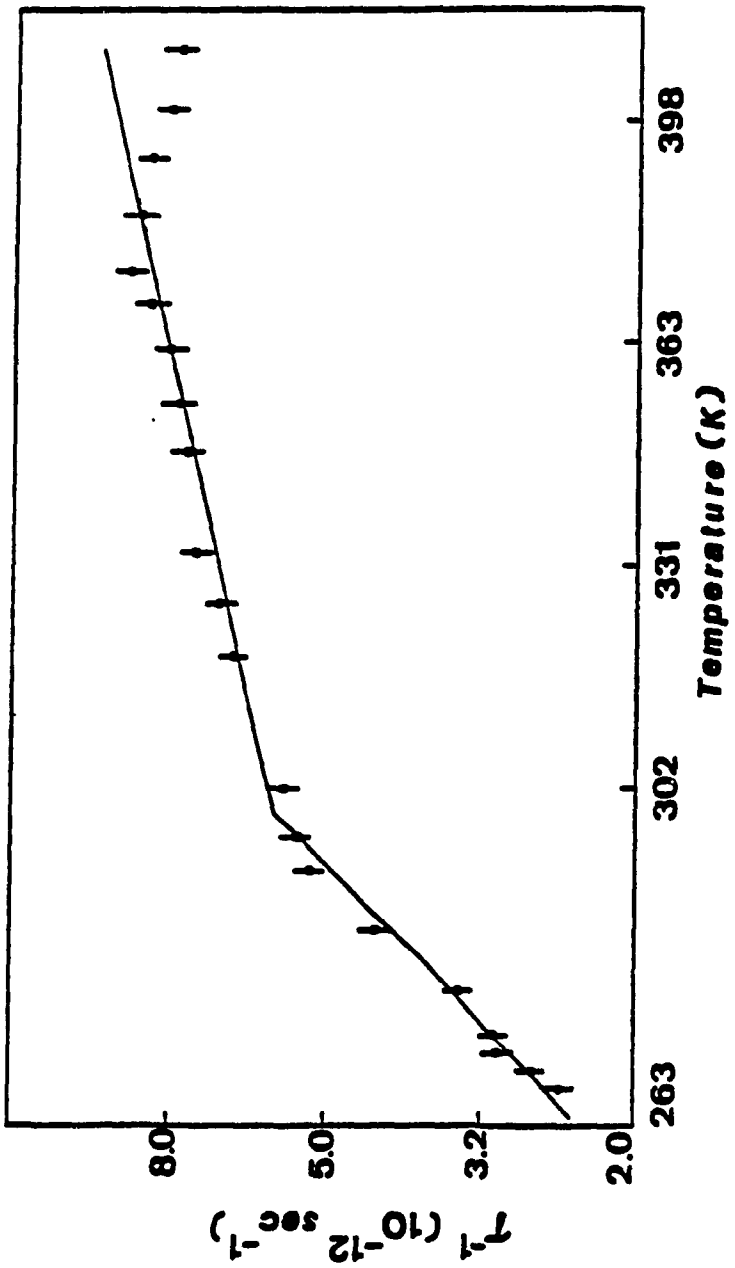

Figure III.2. The log-log plot of the spin-lattice relaxation time, τ, of Pr^{3+} in Gd^{3+} doped $NH_4Pr(SO_4)_2 \cdot 4H_2O$ versus the temperature.

III.5 Discussion

As seen from Table III.2, the presently calculated spin-lattice relaxation times, τ, using eq. (III.11) are quite different from those calculated using the incorrect eq. (III.6). The differences are, in some cases, as much as four orders (see Table III.2). The large differences arise from the fact that eq. (III.6) does not include the exchange and the dipolar interactions between the impurity and the host ions. Thus in an EPR situation, when the single crystal consists of paramagnetic host and paramagnetic impurity ions, and the impurity-ion lines narrow with increasing temperature, eq. (III.11) should be used instead of eq. (III.6) in order to calculate the spin-lattice relaxation time of the host ion.

In addition, as has been shown in the previous section, a variable temperature spin-lattice relaxation time calculation can be made in order to determine the effective spin-lattice relaxation process.

Chapter IV

Site Percolation

IV.1 Introduction

Site percolation has been used, mostly in the last several years, as a model for describing the behavior of many dilute physical systems. Percolation processes have been employed to study diverse physical phenomena, such as conduction and phase transitions. Various fractal-related properties of percolation clusters have also been studied extensively, see, e.g., the reviews by Stauffer[22] and Essam.[23] Basically, in site percolation, a random fraction p of the sites on a lattice structure is assumed to be occupied, while the rest of the lattice sites remain vacant. Then, the study of percolation on such a structure is to check, if there is a path across the lattice, through the occupied sites. The occupied sites, having other occupied sites as nearest neighbors form clusters. A cluster which stretches from one end of the medium to the other, is called an incipient or percolating cluster. The most remarkable feature of a percolation process is the existence of a occupation probability threshold, called the percolation threshold, below which a percolating cluster does not exist, thus, the spreading of quantity of interest in the medium is limited to a finite region only, i.e. to a finite cluster,

and does not propagate all the way through the sample. At and above the percolation threshold, the spreading quantity is always expected to reach from one end to the other end of the medium. Figure IV.1 shows a small part of a square lattice and the incipient cluster made up of occupied and connected sites. It should be remarked, here, that not all the occupied sites necessarily belong to the incipient cluster; finite clusters still exist above percolation threshold. The probability of an occupied site belonging to the largest cluster in the lattice shows critical behaviour around the percolation threshold. This characteristic behaviour of the percolation process is displayed in Figure IV.2 for a square lattice.

There are several interesting parameters to be studied in a percolation process, for instance the mass and the size of the clusters as functions of the occupation probability. These subjects will be discussed in detail in Chapter V. The present chapter concentrates on percolation threshold, which is for two different single crystals. After the calculation of the percolation threshold, its relevance to EPR situation will be described.

The single crystals studied here are Gd^{3+}-doped $LiYb_xY_{1-x}F_4$ and $Pr_xLa_{1-x}F_3$. The reasons for choosing these particular crystals are: (i) Ample data are available on their crystal structures. (ii) Detailed temperature and paramagnetic host-ion concentration (x) dependent EPR data

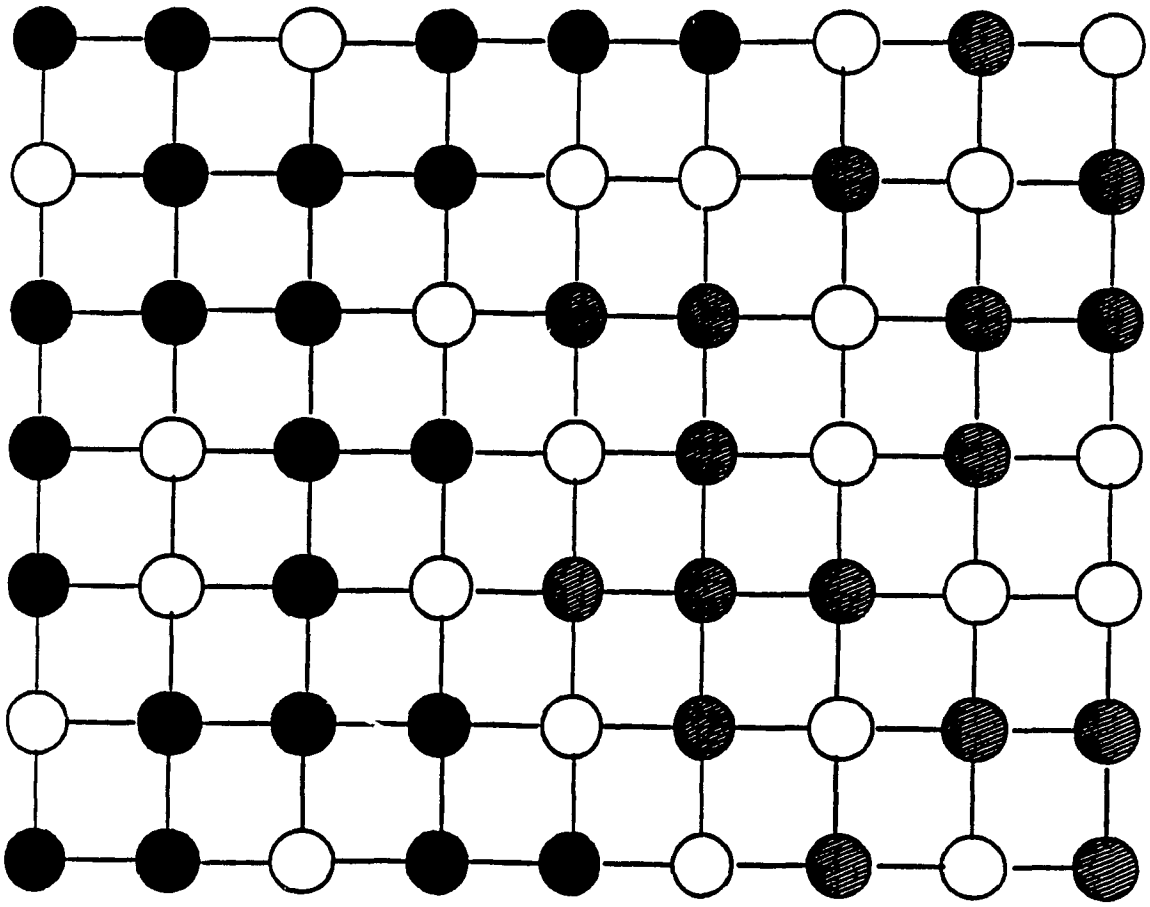

Figure IV.1. A sample portion of a square lattice displaying the incipient cluster depicted by solid circles. Empty circles represent unoccupied sites, while the hatched circles represent occupied sites which do not belong to the percolating cluster.

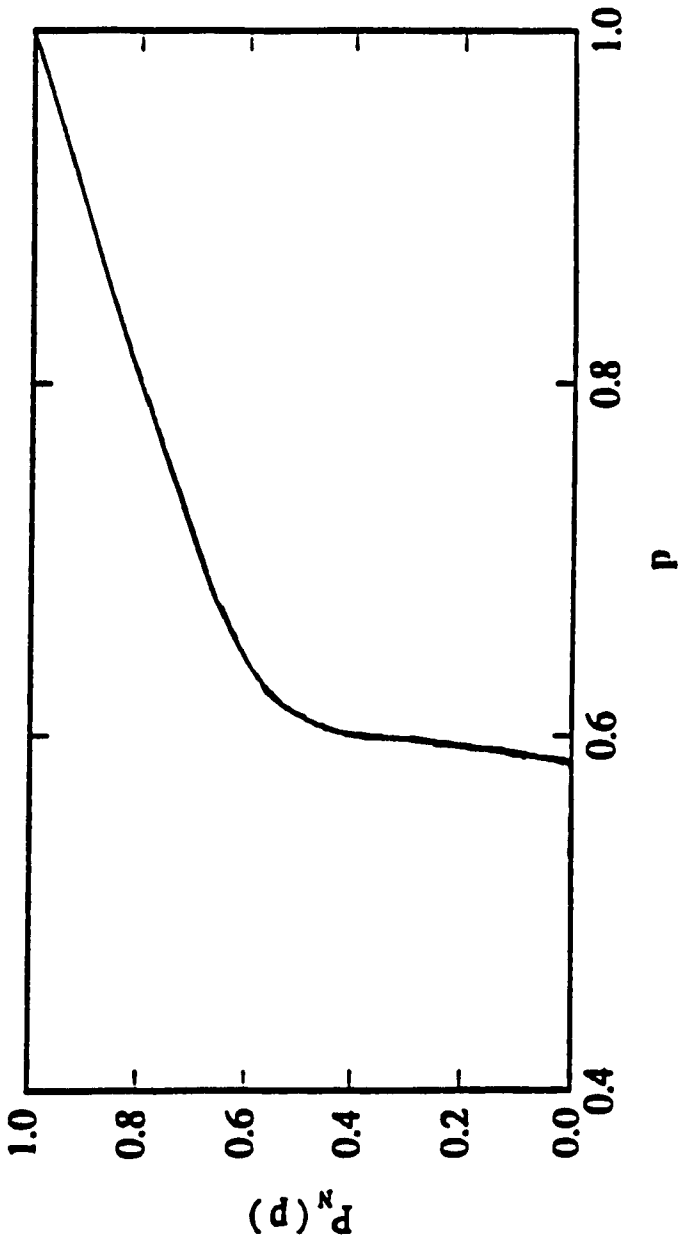

Figure IV.2. The probability of an occupied site belonging to the largest cluster versus occupation probability for a square lattice.

are available; and (iii) The EPR data are indicative of the existence of critical behaviours.

This is the first-ever application of the percolation process to study the influence of the host ion spin-lattice relaxation on the impurity linewidth. The details of the relevant computer programs used in Chapter III to generate lattices, will also be provided.

IV.2 EPR data on Gd^{3+}-doped $LiYb_xY_{1-x}F_4$ single crystals

X-band EPR measurements on single crystals of Gd^{3+}-doped $LiYF_4$ and $LiYbF_4$ have been previously reported by Vaills et al.[24] at room temperature, and by Misra et al.[25] from room temperature down to liquid-helium temperature. X-band EPR measurements on mixed crystals of Gd^{3+}-doped $LiYb_xY_{1-x}F_4$, with values of x = 0.0, 0.01, 0.05, 0.1, 0.2, 0.3, 0.4, 0.5, 0.6, 0.7, 0.8, 0.9, 0.95, 1.0, from room temperature down to liquid-helium temperature (LHT), have recently been reported by Misiak et al.,[26,27] who observed that Gd^{3+} EPR lines could be observed down to LHT only for samples with $x \leq 0.2$, while the lines disappeared much above LHT as the temperature was lowered for samples with $x \geq 0.3$. Further, for samples with x = 0.3, Gd^{3+} EPR lines could not be observed below 88 K, although they could be observed down to 4.2 K for samples with $x \leq 0.2$. Figure IV.3 displays the log-log plot of the experimentally observed Gd^{3+} EPR

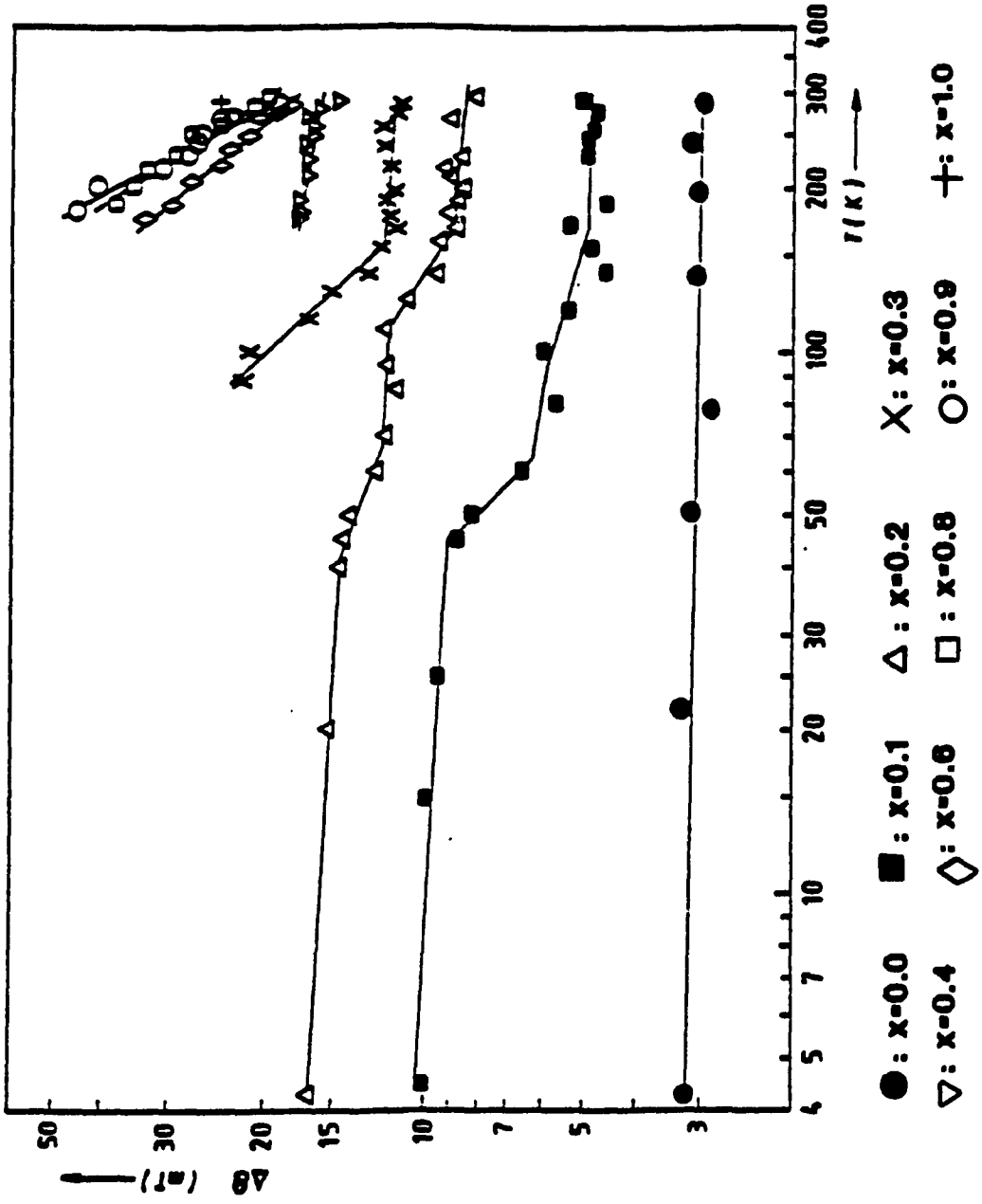

Figure IV.3 Log-log plot of the average experimentally observed Gd^{3+} EPR linewidth (FWHM), in $LiYb_xY_{1-x}F_4$, against the temperature, for various values of x.

linewidths versus the temperature in the various $LiYb_xY_{1-x}F_4$ single crystals.

The abrupt variation of EPR linewidth as a function of x cannot be explained by the increase of dipolar contribution by the paramagnetic Yb^{3+} host ions to Gd^{3+} EPR linewidth. This will be demonstrated below by means of the second moment, which is proportional to the EPR linewidth, as a function of x.

IV.3 Percolation model for $LiYb_xY_{1-x}F_4$

In order to explain the abrupt variation of Gd^{3+} linewidths, the process of percolation is described in this section. In the present calculations,, the sites occupied by the paramagnetic ions, Yb^{3+}, will represent the occupied sites, while those occupied by the diamagnetic ions, Y^{3+}, will represent the vacant sites. The process whose spread will be studied through the occupied sites is the relaxation process, in which the relaxation of a host spin (Yb^{3+}) is carried through the lattice by the mutual spin flips of other host ions. (Hereafter, spin-lattice relaxation refers to the relaxation of host Yb^{3+} spins by their mutual spin flips across the entire lattice.) It is noted that the presence of paramagnetic host ions and their spin-lattice relaxation does have a drastic influence on the EPR linewidth of the impurity ion in the present case (see Chapter III).

Before proceeding with the calculation of the percolation threshold in $LiYb_xY_{1-x}F_4$, the second moment, which is highly x dependent has to be calculated in order to show that the abrupt behaviour of the Gd^{3+} EPR linewidths as a function of x does not arise from the x dependence of the second moment.

IV.4. Crystal structure of $LiYb_xY_{1-x}F_4$

In order to calculate the second moment, and the percolation threshold, the details of the crystal structure are required. $LiYF_4$ nd $LiYbF_4$ crystals are characterized by the scheelite (tetragonal) structure.[28,29] The unit-cell parameters of $LiYF_4$ are a = 5.167 Å, c = 10.735 Å,[30] while those for $LiYbF_4$ are a = 5.134 Å and c = 10.588 Å.[28] There are three rare-earth ions in the unit cell, which are at the following locations:[31] (0.5,0,0), (0.5,0.5,0.5), and (0,0.5,1). The unit-cell parameters of the mixed $LiYb_xY_{1-x}F_4$ crystals can be estimated using Vegard's law.[32] In $LiYbF_4$ there are four nearest (r_n = 5.13 Å), and four next-nearest (r_{nn} = 5.88 Å), and four next-next-nearest (r_{nnn} = 7.26 Å) rare-earth neighbors to a rare-earth ion. Thus, the values of r_n and r_{nn} are very close to each other. Similar considerations apply to the mixed crystals $LiYb_xY_{1-x}F_4$. The Gd/(Yb+Y) ratio in the $LiYb_xY_{1-x}F_4$ samples, experimentally investigated, was 1/200, which is rather small; the present calculations take this value into account by considering

that no Gd^{3+} ion is sufficiently close to another Gd^{3+} ion to have any significant effect.

IV.5 Calculation of the second moment for $LiYb_xY_{1-x}F_4$

The contribution to the EPR linewidth of the impurity ion (Gd^{3+}) due to the paramagnetic host ions (Yb^{3+}) is determined by the second moment. The second moment of the impurity ion for crystals consisting of two kinds of paramagnetic ions, e.g., the impurity (Gd^{3+}) and the host (Yb^{3+}) ions in the present case, when the distance between the impurity ions is sufficiently large and the number of the neighbors considered is limited to N, was given by eq. (III.8) in Chapter III, as follows

$$<\Delta\nu^2> = \frac{1}{3}S'(S'+1)h^{-2}[NJ_p^2+(gg')^2\beta^2\mu_o^2\sum_{k'}^{N}(1-3\gamma_{jk'}^2)^2r_{jk'}^{-6}+$$

$$2J_pgg'\beta^2\mu_o\sum_{k'}^{N}(1-3\gamma_{jk'}^2)r_{jk'}^{-3}]. \qquad \text{(III.8)}$$

The various symbols appearing quantities in eq. (III.8) have already been defined in Chapter III.

The second moment, as given by eq. (III.8), does not itself depend significantly on temperature; its dependence on temperature is indirectly due to change in lattice spacings due to thermal expansion (contraction) affecting $r_{jk'}$ and $\gamma_{jk'}$. The sums in eq. (III.8) are expected to be continuous and convergent functions of x, determined by the

fraction (x) and locations of the Yb^{3+} ions. Thus, the second moment can not account for the abrupt disappearance of the Gd^{3+} EPR lines, i.e. the EPR linewidth approaching infinity, below certain temperatures for $x \geq 0.3$.

The calculation of the second moment for $x = 1$ is trivial, since for this case all rare-earth lattice sites surrounding an impurity ion (Gd^{3+}) are occupied by the paramagnetic Yb^{3+} ions, thus the calculation of the sums in eq. (III.8) is straightforward. However, when $x < 1$, then some of the sites surrounding the impurity ion are occupied by the diamagnetic Y^{3+} ions, which do not contribute to the second moment. Thus, when $x < 1$, the calculation of the sums in eq. (III.8) is complicated. For, one does not now know which particular sites have been occupied by the Yb^{3+} ions; an extremely large number of configurations are possible even in a relatively small lattice.

In order to calculate the second moment for $x < 1$ in mixed crystals, and to be able to perform calculations for larger values of N in eq. (III.8), a lattice-generating computer program was developed valid for any value of x. (See Appendix I for the program listing. This same program was also used to calculate the spin-lattice relaxation times given in Chapter III.)

A 40x40x40 array was utilized for the generation of the lattices considered presently. The positions of the rare-earth ion sites in the unit cell given in Sec. IV.4 for

$LiYb_xY_{1-x}F_4$ are the initial inputs required by the program. Next, each ion in the unit cell is assigned a set of array coordinates, by the user, corresponding to its position coordinates in the unit cell. Following this, for each rare-earth ion site, in the unit cell, the number of array-coordinate increments (s_{xj}, s_{yj}, s_{zj}), necessary to generate the same site in the next unit cell are entered for each axis. The correspondences between the unit cell parameters and the array increments, and between the unit cell position coordinates and the array coordinates are calculated as well. Thus, with all this information, the program generates the lattice by simply using a three dimensional loop with appropriate increments in each direction. After the generation of the lattice, the distance between any two sites can be calculated, by using the relation

$$r_{jk'} = [(r_{xj}-r_{xk'})^2+(r_{yj}-r_{yk'})^2+(r_{zj}-r_{zk'})^2]^{1/2} \qquad \text{(IV.1)}$$

where r_{xj}, r_{yj}, and r_{zj} are, respectively, x, y, and z components of r_j, the position vector of the site indexed by j. r_{xj} is calculated using

$$r_{xj} = [\mathrm{INT}(x_j/s_{xj})a_{xj}] + o_{xj}. \qquad \text{(IV.2)}$$

In eq. (IV.2), x_j is the array coordinate of the particular

site and a_{xj} is the distance between two equivalent sites, along the x axis. O_{xj} is the distance along the x axis between the origin and an equivalent site in the original unit cell. It should be noted, that in eq. (IV.2) INT stands for "the integer part of". r_{yj} and r_{zj} can be calculated in a similar way. The direction cosine of $r_{jk'}$ with respect to the z axis is calculated from the relation:

$$\gamma_{jk'} = \frac{(r_{zj}-r_{zk'})}{r_{jk'}} . \qquad \text{(IV.3)}$$

The $LiYb_xY_{1-x}F_4$ lattice was generated in the same manner described above. The generation of the lattice points of the $LiYb_xY_{1-x}F_4$ lattice along the x, y, and z axes is demonstrated in Figures. IV.4, IV.5, and IV.6 respectively. As seen from Figures IV.4-IV.6, the initial unit cell is represented by the elements of a 3x3x3 array segment, which have the following array coordinates: (1,0,0), (1,2,0), (1,1,1), (0,1,2), and (2,1,2). This set of the array coordinates corresponds to the position coordinates of the rare-earth ion sites in the unit cell, as given in Sec. IV.4. It should be noted, from Figures IV.4-IV.6, that three separate loops are needed to generate the three distinctly repeating kinds of ions. These different kinds of ions are depicted as differently filled circles in Figures IV.4-IV.6. While generating the $LiYb_xY_{1-x}F_4$ lattice, a random number

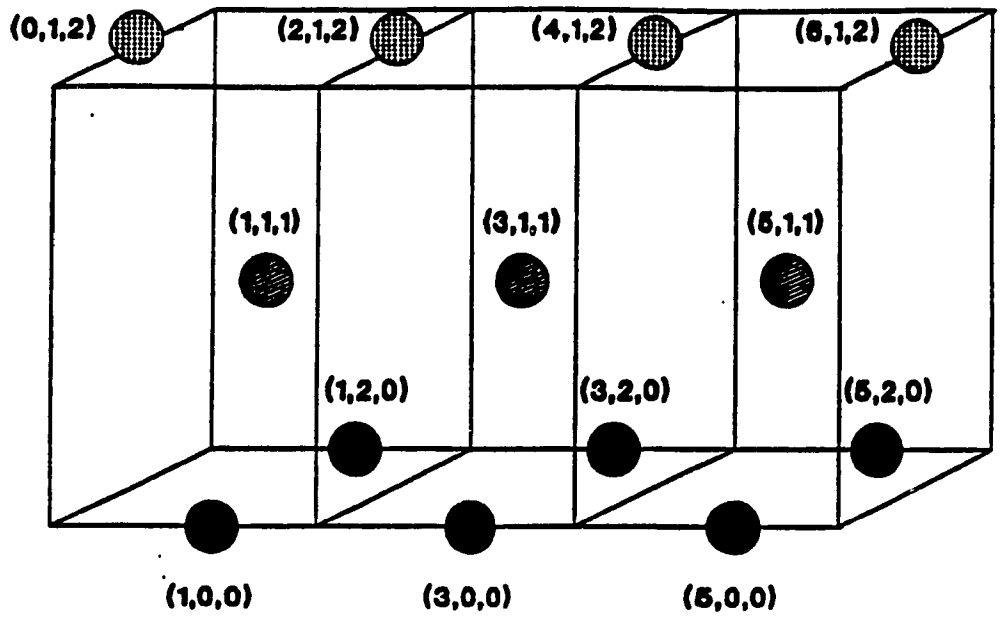

Figure IV.4 The generation of the $LiYb_xY_{1-x}F_4$ lattice along the x axis.

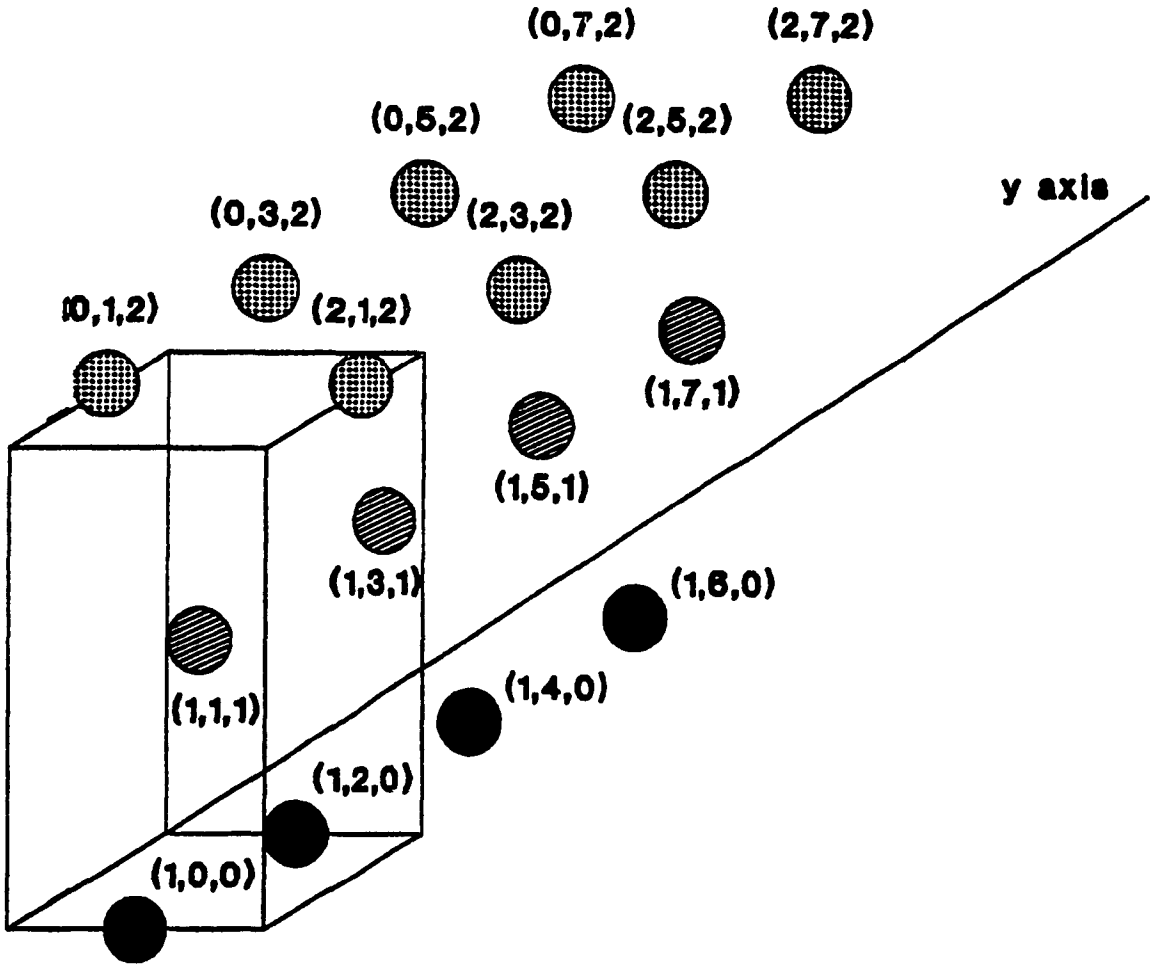

Figure IV.5 The generation of the $LiYb_xY_{1-x}F_4$ lattice along the y axis. The array-coordinate increments along the y-axis, for all sites, is 2.

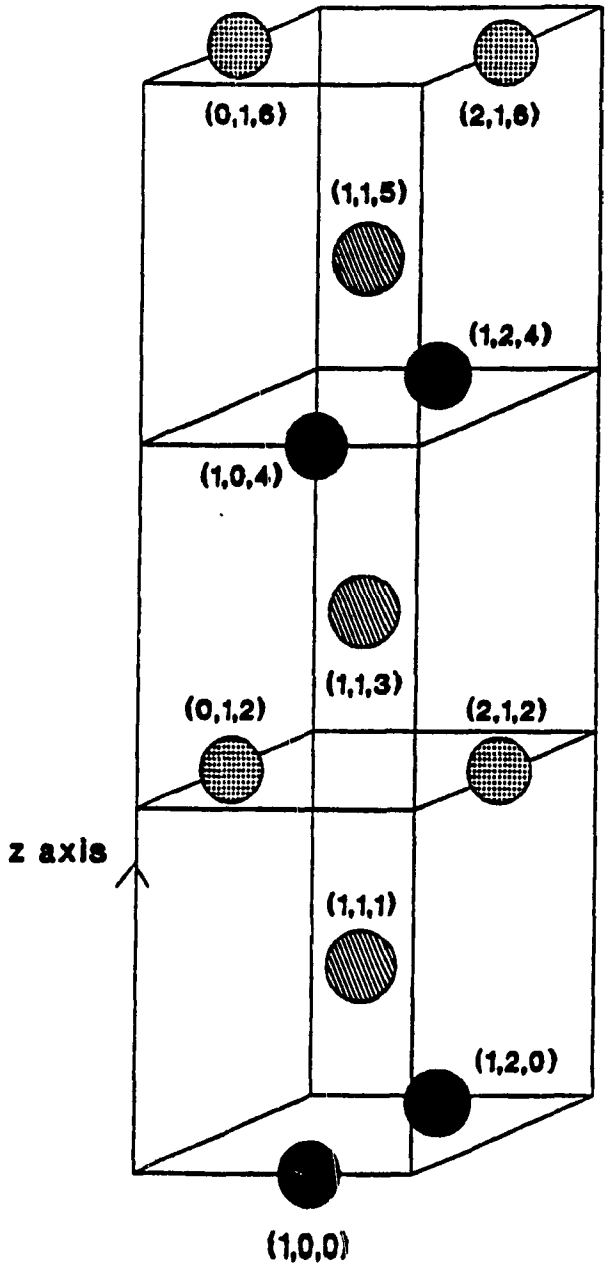

Figure IV.6 The generation of the $LiYb_xY_{1-x}F_4$ lattice along the z axis. The array-coordinate increment along the z axis, for solid and spotted circles is 4, and it is 2 for the sites represented by the hatched circles.

generator, between 0 and 1, was used to decide whether a site was occupied by a Yb^{3+} ion, according to x, the concentration of the Yb^{3+} ions. Thus, for example if x = 0.6, then for random numbers which are less than or equal to 0.6 a site was assumed to be occupied by a paramagnetic Yb^{3+} ion, otherwise considered to be occupied by a Y^{3+} ion.

Ideally, in order to calculate the second moment for a given value of x, for samples with $x < 1$, all possible configurations of the host ions (Yb^{3+} and Y^{3+}) around an impurity ion (Gd^{3+}) should be considered. Since this would have taken prohibitively long computer time, the second moment was calculated for 1000 randomly arranged configurations of the host ions around the impurity ion. Finally, the average of these second moments was computed. Up to next-next-nearest neighbors for each of these 1000 configurations were taken into account in the sums in eq. (III.8) to calculate the second moment for the various values of x. The interionic distances $r_{jk'}$ and the direction cosines $\gamma_{jk'}$ values were calculated using eqs. (IV.1) and (IV.3) respectively. It should be mentioned here, that, the second moment was calculated for $LiYb_xY_{1-x}F_4$ crystals for values of x in the range 0.1 - 1.0, in steps of 0.1.

Figure IV.7 exhibits the plot of the second moment $\langle \Delta\nu^2 \rangle$ versus x. It shows a linear continuous relation of $\langle \Delta\nu^2 \rangle$ to x, without exhibiting any abrupt behaviour as a function of x . This implies that the second moment can not account for

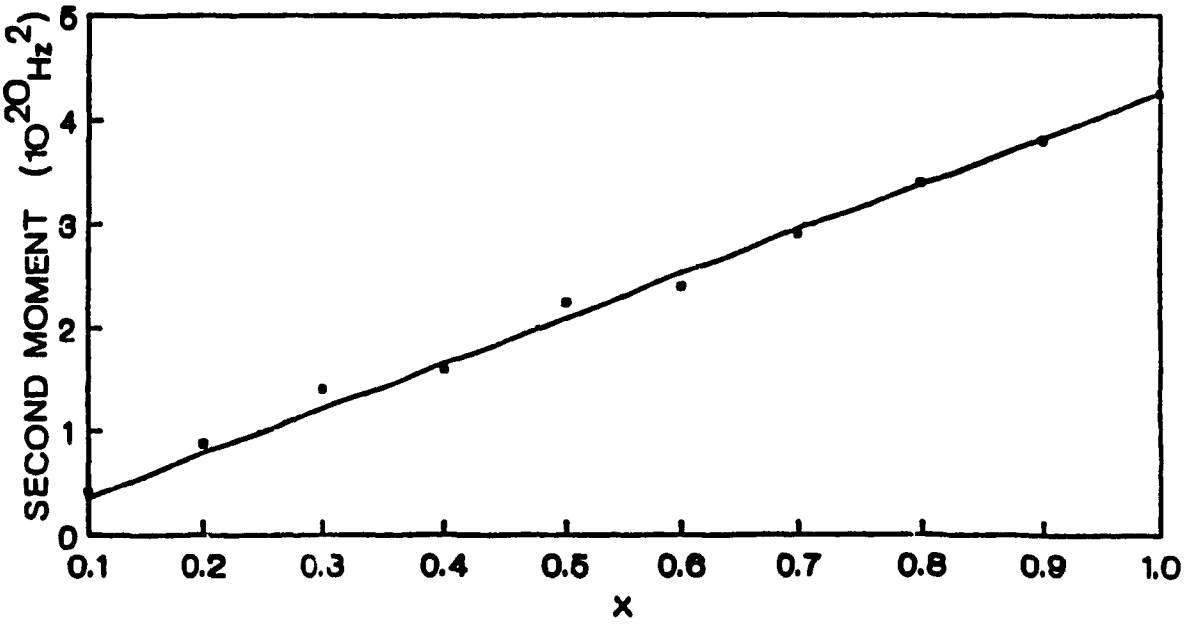

Figure IV.7. A plot of the calculated second moment, $\langle \Delta\nu^2 \rangle$, versus x in $LiYb_xY_{1-x}F_4$ single crystals.

the observed abrupt disappearance of EPR lines at low temperatures for samples as a function of x.

IV.6 Calculation of percolation threshold for $LiYb_xY_{1-x}F_4$

In order to explain the temperature variation of the impurity EPR linewidth, the spin-lattice relaxation process, a highly temperature-dependent phenomenon, of the host paramagnetic ions should be taken into account. The spin-lattice relaxation influences the impurity linewidth through the process of random-frequency modulation.[7-9] As discussed in Chapter III [see eq. (III.11)], the impurity-ion EPR linewidth, as influenced by spin-lattice relaxation , can be expressed as

$$\Delta B = 110hg'\langle\Delta\nu^2\rangle\tau/(3g^2\mu_B) \qquad \text{(IV.2)}$$

where τ is the spin-lattice relaxation time of the host ion; τ is, in general, highly temperature dependent. It is the variation of τ, as a function of x, the fraction of the paramagnetic host ions, that is responsible for the divergent behaviour of the linewidth ΔB as a function of temperature. It is seen from Figure IV.3, that the EPR lines broaden considerably for samples with $x \geq 0.3$, as the temperature is lowered from room temperature. However, the linewidths do not change significantly with temperature for

significantly with temperature for samples with $x < 0.3$; the EPR lines for them can be observed down to LHT. Finally, the spin-lattice relaxation due to the host paramagnetic ions, determines predominantly the temperature dependence of EPR linewidths; as seen below, it has a cutoff for $x < 0.3$.

It is suggested presently that the complete broadening of the EPR lines is caused by the existence of the site percolation of the paramagnetic host ions (Yb^{3+}) in the $LiYb_xY_{1-x}F_4$ lattices. A $LiYb_xY_{1-x}F_4$ lattice will be considered "percolating" if there exists a path from a Yb^{3+} site at one end of the lattice all the way to the other end of the lattice, through the Yb^{3+} ions, each of which lies within a distance of r_{nn}, the next-nearest neighbour distance, from a Yb^{3+} ion, i.e. when a percolating cluster exists. A paramagnetic site is considered to be able to percolate to both the nearest (n) and the next-nearest (nn) neighbors, since, as mentioned earlier, the difference between r_n and r_{nn} for the $LiYb_xY_{1-x}F_4$ hosts is very small. Figure IV.8 shows a Yb^{3+} ion and its neighbors (n and nn) to which percolation is allowed, along with their array coordinates in the lattice.

After the generation of the $LiYb_xY_{1-x}F_4$ lattice, as described in Sec. IV.6, the possible lattice sites in the array were filled randomly, using a random-number generator. When the random number generated was smaller than or equal to x, a site was made occupied by a paramagnetic Yb^{3+} ion by

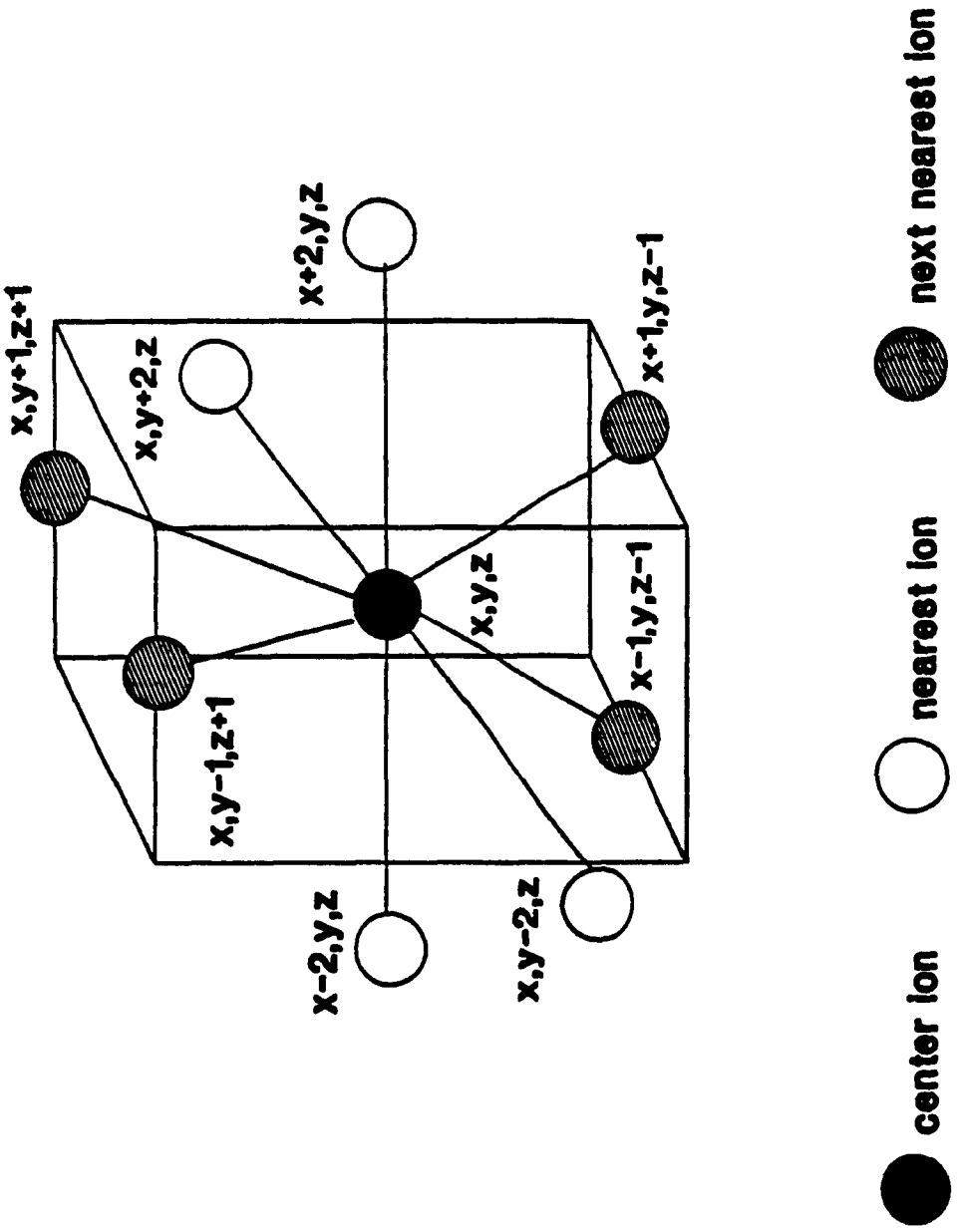

Figure IV.8. A Yb^{3+} ion in the unit cell of $LiYb_xY_{1-x}F_4$, along with its nearest and next-nearest neighbours to which the percolation is allowed.

assigning 1 to the appropriate array element. The array elements, for which the random number generated was greater than x, were assigned zeros, and considered to be occupied by the diamagnetic Y^{3+} ions.

To begin with, all sites occupied by the Yb^{3+} ions of the z = 0 plane (see Fig. IV.6) were assumed to belong to the percolation cluster. Next, all the occupied sites of the z = 1 plane (these are the center ions at 0.5c, see Figs. IV.4-IV.6), which are neighbours to the occupied sites of the z = 0 plane, i.e. they lie within the distance r_{nn}, were also included in the percolation cluster. In this manner, a sweep of the z = 1 plane was performed, in order to connect those occupied sites, which are within r_{nn} of the occupied and already connected sites, of the percolation cluster, i.e. the occupied sites in the z = 0 plane. In the same way, all the planes along the z axis were taken into account one by one, by considering z = 1, 2, 3,... planes in turn, attaching to the percolation cluster those occupied sites of the z = n plane under consideration, which lie within r_{nn} of an ion, located on the z = n-1 plane and belonging to the percolation cluster already constructed. In addition, a downward sweep, from the current z plane to the z = 0 plane, was performed in order to ascertain that no possible ions which should have been included, i.e., those within a distance of r_{nn} from a Yb^{3+} ion of the percolation cluster, were missed out in the percolation cluster already formed.

This sweep of the z planes continued, alternately, in the upward and downward directions. The computer program was terminated whenever, after two successive sweeps, a new site could not be attached to the cluster already formed. In this case, a percolating cluster did not exist. The execution of the program was also terminated whenever a site on the z = 39 plane became connected to the cluster, thus resulting in a percolating cluster. It should be mentioned, here, that whenever an occupied site, designated by 1, became connected to the cluster being formed, it was redesignated by 2. In this way, a distinction can be made between the occupied but not connected and the occupied plus connected sites. The listing of the computer program is given in Appendix I.

The calculation of the percolation threshold was performed for samples with x = 0.1 to 1 in steps of 0.1. It was found that x_c, the critical value of x at and above which a percolating cluster exists, but not below, lies between x = 0.2 and x = 0.3. Thereafter, the values of x between 0.2 and 0.3 were considered in steps of 0.01, using random integers in the range 1 to 100 to determine the occupied sites of the lattice in the similar way to that described in Sec. IV.6 for x between 0.0 and 1.0. This yielded the critical value of x to be $x_c = 0.27$. Thus, for x = 0.26 the lattice was not percolating, while it was percolating for $x \geq 0.27$. Better accuracy than this could not be achieved due to the limited size of the array used;

however, this value is eminently satisfactory to explain the experimental data considered here.

IV.7 Discussion of results for $LiYb_xY_{1-x}F_4$

The present results indicate that the spin-lattice relaxation threshold is directly linked to x_c. This is in accordance with the temperature behaviour of the observed EPR linewidths. The existence of a path for mutual spin flips for the transmission of energy of spins in the Zeeman field, via the host paramagnetic ions through the entire lattice, is necessary for the spin-lattice process to be effective. If a paramagnetic Yb^{3+} ion is completely surrounded by diamagnetic Y^{3+} ions, a spin flip of that Yb^{3+} ion will not be transmitted to the rest of the lattice because of diamagnetic shielding by the Y^{3+} ions. For the diamagnetic ions (Y^{3+}) develop net magnetic moments that tend to oppose any changes in the magnetic field. In fact, paramagnetic (Yb^{3+}) ions, situated sufficiently closely, are needed to transmit the magnetic energy to the rest of the lattice by mutual spin flips. Thus, the spin-lattice relaxation process is controlled by x, the concentration of the paramagnetic ions, which in turn controls the EPR linewidth and its temperature dependence.

It should be noted here, that when $x_c \leq x \leq (1-x_c)$, there exist both diamagnetic and paramagnetic percolating clusters in the lattice. In such a case, it is expected that

the existence of the diamagnetic percolating clusters would cause shortening of the host-ion spin-lattice relaxation time. In the case of $LiYb_xY_{1-x}F_4$ crystals, this mechanism is not clearly visible because of the particular temperature dependence of the impurity-ion EPR lines. The effect of the diamagnetic percolating clusters, on the EPR lines, will be discussed in Sec. IV.11, for $Pr_xLa_{1-x}F_3$, wherein this mechanism can easily be demonstrated.

The experimental Gd^{3+} EPR linewidth data in $LiYb_xY_{1-x}F_4$ hosts can be divided into following three temperature regions for a proper understanding (see Figure IV.3):

(i) High T, $x \geq 0.3$. In this region, the spin-lattice relaxation mechanism is fully effective because of the existence of percolating clusters. The linewidths become larger, as the temperature is lowered, because the spin-lattice relaxation time of the host ions becomes larger. Since $x > x_c$ (= 0.27), the energy released by the spin flip of a Yb^{3+} ion can be transmitted throughout the lattice by mutual spin flips of Yb^{3+} ions. The present percolation results suggest that, as long as $x > x_c$, there will be a path via the Yb^{3+} ions that spans the entire lattice even if there are more Y^{3+} ions present than Yb^{3+} ions in the lattice, i.e. for $0.5 > x > 0.27$.

(ii) Low T, $x \geq 0.3$. Here, the experimental data indicate that EPR lines could not be observed at temperatures below 85 K. Since $x \geq x_c$, broadening due to

spin-lattice relaxation is expected to be fully operative, and the EPR lines will be broadened since at low temperatures the spin-lattice relaxation time is much longer than that at high temperatures. It should be noted, here, that EPR lines can not be observed when they broaden beyond a certain value.

(iii) Any T, $x \leq 0.2$. For this case, the experimental EPR linewidths do not exhibit significant temperature dependence. Since $x < x_c$, the paramagnetic ions (Yb^{3+}) are not able to span a path all the way through the entire lattice for percolation; the transmission of energy given off by the flips of the Yb^{3+} ions will be shielded by the Y^{3+} ions, causing the effect of the flips of the Yb^{3+} ions to remain localized. Thus, the broadening due to the spin-lattice relaxation will not be effective for this case; and the Gd^{3+} EPR lines can be observed at all temperatures.

IV.8 $Pr_xLa_{1-x}F_3$ EPR data and percolation threshold

A variable-temperature EPR linewidth study of Gd^{3+}-doped $Pr_xLa_{1-x}F_3$ single crystals has recently been reported by Misra et al.[33] in the temperature range 4.2 - 295 K. The behavior of the reported Gd^{3+} EPR linewidth in $Pr_xLa_{1-x}F_3$ as a function of x, as exhibited in Fig. IV.9, is quite unusual. The experimental data can be divided, according to x, the fraction of the host paramagnetic ions, Pr^{3+}, into three categories:

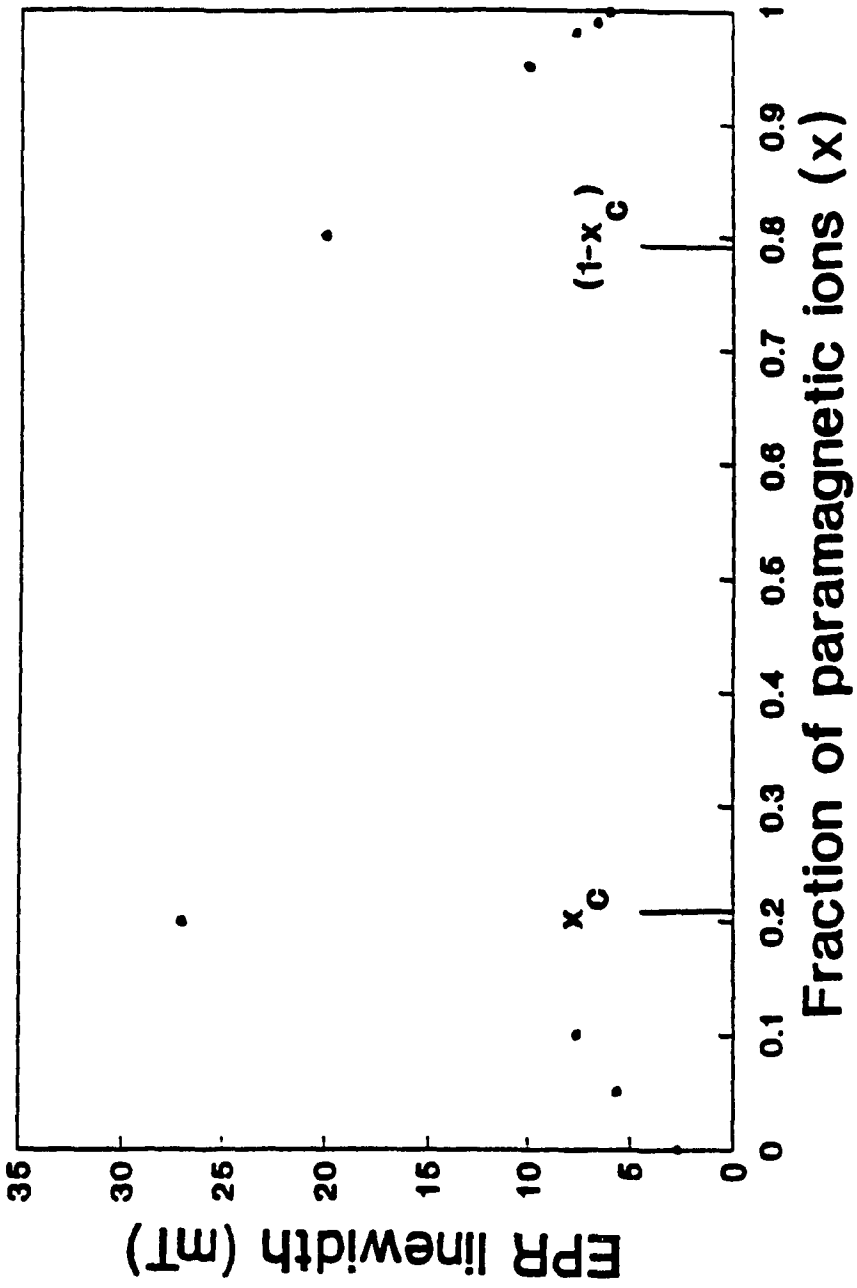

Figure IV.9. The averages of experimentally observed Gd^{3+} EPR linewidths plotted versus x, the concentration of the paramagnetic ions, Pr^{3+}, in $Pr_xLa_{1-x}F_3$ at room temperature.

(i) $0 \leq x \leq 0.2$. In this range, Gd^{3+} EPR lines are well resolved and temperature independent; they show increased broadening with increasing value of x.

(ii) $0.2 < x < 0.8$. The EPR lines are too broad to be observed for these concentrations.

(iii) $0.8 \leq x \leq 1$. For these values of x, the EPR lines are observable at room temperature, becoming narrower with increasing value of x. They are temperature dependent, broadening with increasing temperature, and are completely broadened out below certain temperatures.

The sudden disappearance of Gd^{3+} EPR lines in $Pr_xLa_{1-x}F_3$ at x = 0.3 as x increases from 0, suggests that a mechanism of EPR line broadening becomes effective somewhere between x = 0.2 and x = 0.3. As x is increased further, the sudden reappearance of EPR lines at x = 0.8 suggests that this mechanism of broadening apparently becomes weakened somewhere between x = 0.7 and 0.8. The particular dependences of the linewidths on these values of x between 0.2 and 0.3 and between 0.7 and 0.8 imply the existence of site-percolation phenomenon, which applies to both, the percolating clusters formed by the paramagnetic ions, Pr^{3+}, as well as those formed by the diamagnetic ions, La^{3+}. In other words, as x is increased to above a critical value, x_c, the formation of a paramagnetic site-percolation cluster is achieved. Using the same arguments, it can be seen that for $(1-x) \geq x_c$ the diamagnetic site-percolation occurs,

since the concentration of the diamagnetic ions is (1-x). The linewidth behavior observed in $Pr_xLa_{1-x}F_3$ suggests that if $x_c > 0.2$, the Gd^{3+} EPR lines disappear in $Pr_xLa_{1-x}F_3$ for $0.2 < x < 0.8$, because for these values of x there exist percolation clusters of both the paramagnetic ions, Pr^{3+}, and the diamagnetic ions, La^{3+}. On the other hand, for $x < x_c$ and for $x > (1-x_c)$ the Gd^{3+} line are not sufficiently broadened to disappear, because in these cases there exist only one type of percolation cluster: a paramagnetic percolation cluster for $x \geq x_c$ and a diamagnetic percolation cluster for $x \leq (1-x_c)$.

The calculation of x_c and an explanation of the linewidth behavior as governed by the formation of paramagnetic/diamagnetic clusters are provided in the following sections.

IV.9 The crystal structure of $Pr_xLa_{1-x}F_3$

For the present calculations one needs to know the positions of the rare-earth ions in $Pr_xLa_{1-x}F_3$ single crystals. Assuming that all these crystals have the same structure in accordance with Vegard's law,[32] $Pr_xLa_{1-x}F_3$ single crystals can be considered to be hexagonal with six molecules per unit cell.[34] The unit-cell parameters for PrF_3 are: a = 0.7061 nm, c = 0.7218 nm, while they are: a = 0.719 nm, c = 0.737 nm for LaF_3. The unit cell parameters for the various $Pr_xLa_{1-x}F_3$ crystals can be calculated from those for

LaF_3 and PrF_3 using Vegard's law.[32] The six rare-earth ion sites in the unit cell are located at (1/3, 1/3, 0), (0, 2/3, 0), (2/3, 0, 0), (2/3, 2/3, 1/2), (0, 1/3, 1/2), and (1/3, 0, 1/2), as displayed in Fig. IV.10. It is noted that different rare-earth sites in the unit cell have different surroundings. These sites are referred to as 1, 2, ...6, and their various neighbours are listed in Table IV.1.

IV.10 Calculation of x_c in $Pr_xLa_{1-x}F_3$

A $Pr_xLa_{1-x}F_3$ lattice was generated by using a 40x40x40 array. A random-number generator was used to fill the array elements by Pr^{3+} and La^{3+} ions, according to the particular value of x, representing the fraction of Pr^{3+} ions. The occupied paramagnetic sites were designated by the numbers 1-6, depending on to which particular site in the unit cell the occupied site corresponded, while the occupied diamagnetic sites were designated by 0. First, all the sites occupied by the paramagnetic ions in the z = 0 plane (the plane at one extremity of the array considered), parallel to the (001) plane in the $Pr_xLa_{1-x}F_3$ lattice, were assumed to be connected to the paramagnetic cluster by designating them by the numbers 7-12 by adding 6 to their original values. Next, the sites, in the z = 1 plane, lying within a distance r_L, defining the connectivity, to a paramagnetic ion in the z = 0 plane, were checked if they were occupied by paramagnetic ions. (The choice of the value of r_L is

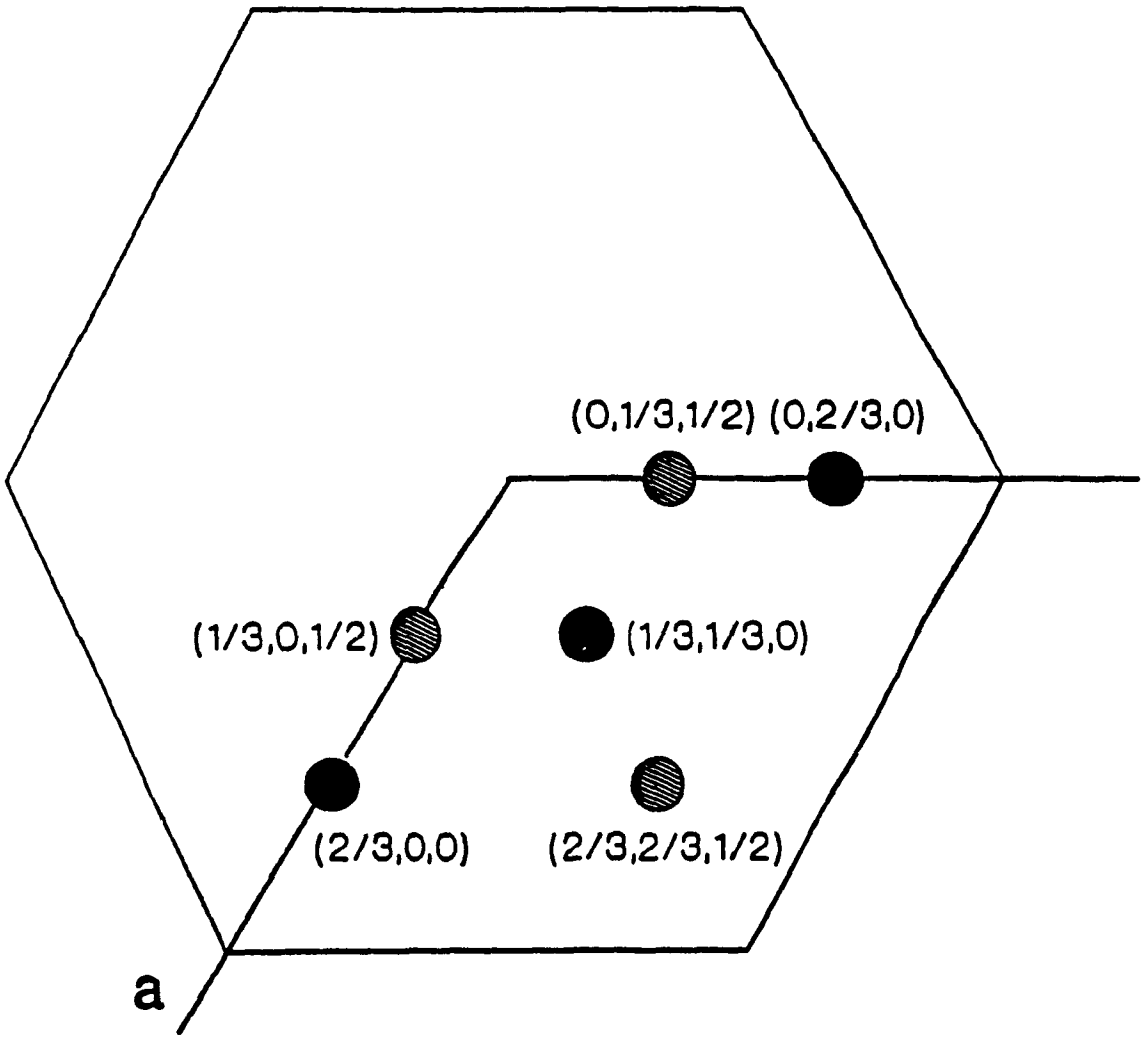

Figure IV.10. A $Pr_xLa_{1-x}F_3$ unit cell showing the rare-earth ion sites as projected on to the c = 0 plane. The solid circles represent the sites on the c = 0 plane, while the hatched ones represent those on the c = 0.5c plane.

Table IV.1. The distances (in nm) between the six rare-earth sites (see Figure IV.10) and their respective neighbors, in $Pr_xLa_{1-x}F_3$, which are included in the percolation process. The numbers in the brackets indicate the number of the neighbouring ions at that particular distance.

Site	1	2	3	4	5	6
r_1	0.408(1)	0.408(1)	0.406(1)	0.404(1)	0.404(1)	0.391(1)
r_2	0.414(1)	0.410(1)	0.408(1)	0.408(1)	0.410(1)	0.406(1)
r_3	0.429(2)	0.429(2)	0.428(2)	0.428(2)	0.430(2)	0.434(2)
r_4	0.589(2)	0.435(2)	0.430(2)	0.434(2)	0.589(2)	0.592(2)
r_5	0.714(2)	0.719(2)	0.435(2)	0.708(2)	0.592(2)	0.701(2)
r_6	0.722(2)	0.722(2)	0.722(2)	0.714(2)	0.722(2)	0.722(2)
r_7	0.741(2)	0.725(2)	0.797(1)	0.722(2)	0.791(1)	0.725(2)
r_8				0.793(1)		

described in the next paragraph.) The sites so occupied by paramagnetic ions were made a part of the paramagnetic cluster, and appropriately designated as 7-12. In this manner, all the sites in the various successive planes z = 1-39 were checked, and when qualified, were made a part of the cluster. The successive z = 1, 2, 3, ... planes were defined to be the planes which were located at 0.5c, c, 1.5c,... heights parallel to the z = 0 plane, because these are the planes in which the rare-earth ions are located. If, in the first sweep of z = 1 to 39 planes it was found that a site in the z = 39 plane was connected to the cluster, the program was terminated, and it was considered that a percolating cluster extended all the way from one end to the other end of the sample, i.e. the cluster was percolating. If this was not the case, a downward sweep from z = 39 to z = 0 plane, in a successive manner, was performed in order to include more sites to the cluster which were missed in the first upward sweep; thus, the cluster formed in the first sweep grew. After this, the sweep of successive z planes was repeated in the upward direction, then in the downward direction, and so on. These sweeps were continued until either a site in the z = 39 plane became connected to the cluster, in which case the cluster was considered to be percolating, or if the cluster did not at all grow after two successive sweeps: an upward sweep followed by a downward sweep. In the latter case it was considered that the cluster

did not extend all the way from one end to the other end of the sample, i.e. the cluster was not percolating.

The value of x_c depends on the limiting distance r_L, or the connectivity, around a paramagnetic ion, within which one includes the paramagnetic ions in the percolating cluster. In the present case, two different values of limiting distances, r_L, were employed: (i) r_L = 0.6 nm and (ii) r_L = 0.8 nm. The percolation threshold x_c was found to be 0.48 ± 0.01 for case (i), while for case (ii) the value of x_c was found to be 0.21 ± 0.01. The decrease in the value of x_c for case (ii), as compared to that for case (i), is due to the increase in the number of connectable neighbors for case (ii). Following similar considerations, it can be concluded that for $(1-x) \geq x_c$ a percolating diamagnetic cluster would exist. Specifically, corresponding to r_L = 0.6 nm and r_L = 0.8 nm a diamagnetic percolating cluster would exist for $x \leq 0.52$ and $x \leq 0.79$, respectively. Finally, the value of x_c = 0.21 as found for case (i) (r_L = 0.8 nm) appears to be in good agreement with the experimental data on Gd^{3+} EPR linewidths in $Pr_xLa_{1-x}F_3$ crystals as a function of x. The listing of the computer program is given in Appendix I.

IV.11 Discussion of results for $Pr_xLa_{1-x}F_3$

In the light of the presently-proposed percolation model, a possible explanation of the linewidth behavior can

be given as follows:

$0 \leq x \leq 0.2$. In this case, for r_L = 0.8 nm, there are present percolating clusters of diamagnetic ions only. Being diamagnetic, their presence does not broaden EPR lines too much. This is consistent with the experimental data that the EPR lines are well resolved and temperature independent in this range. The EPR lines, however, broaden with increasing x, because then the fraction of paramagnetic host spins increases, which increases the linewidth due to the dipole-dipole interaction with the impurity Gd^{3+} ion; however, since $x < x_c$, paramagnetic-site percolation does not exist, thereby having no dramatic broadening effect on EPR lines. Consequently, in analogy with the case of $LiYb_xY_{1-x}F_4$, it can be considered that in this range of x the host-ion spin-lattice relaxation process is not effective in broadening the EPR linewidth.

$0.2 < x < 0.8$. For this range, percolating clusters exist for both the paramagnetic and diamagnetic host spins, since $x_c < x < (1-x_c)$. Thus, their effect on the broadening of EPR linewidths is quite significant. The existence of a paramagnetic cluster has a profound effect on Gd^{3+} EPR linewidth. In addition, diamagnetic percolating clusters may further broaden EPR lines. This is because they respond to spin fluctuations of the paramagnetic ions by moving in such a way as to oppose any variation in the local magnetic field caused by the spin flip of a host paramagnetic ion in

accordance with Lenz's law. Accordingly, when a paramagnetic spin relaxes, the neighboring diamagnetic spins move, thus providing a wider energy spectrum to the lattice, which, in turn, enhances the host paramagnetic ion spin-lattice relaxation process. Thus, the host-ion spin-lattice relaxation time is further shortened, causing additional broadening of the EPR lines.

$0.8 \leq x \leq 1.0$. In this range, the diamagnetic-site percolation does not exist, because the fraction of diamagnetic ions is less than $(1 - x_c) = 0.21$. On the other hand, the paramagnetic-site percolation does exist, as the fraction of the paramagnetic ions is greater than $x_c = 0.21$. However, since no diamagnetic percolation cluster exists, the EPR lines are not too broadened to be unobservable. The narrowing of the lines, as compared to the case $0.2 < x < 0.8$, in the present case, is clearly due to the disappearance of the percolating diamagnetic clusters. Further, it should be noted that the broadening of lines with increasing temperature for samples with $x > 0.8$, suggests that for Gd^{3+}-doped $Pr_xLa_{1-x}F_3$ the spin-lattice relaxation time of the host Pr^{3+} ions is of the same order as that of the impurity ion, Gd^{3+}.[2,16]

It is noted that the presence of diamagnetic clusters in Gd^{3+}-doped $LiYb_xY_{1-x}F_4$ crystals does not have the same effect on EPR linewidth as in the case of Gd^{3+}-doped $Pr_xLa_{1-x}F_3$ crystals. This is because the experimental data

indicate that the impurity-ion linewidth, ΔB, is inversely proportional to the temperature ($\Delta B \propto T^{-1}$) in the former case, while it is proportional to T ($\Delta B \propto T$) in the latter case. Although, in both the cases the presence of diamagnetic clusters shortens the the host-ion spin-lattice relaxation time, resulting in larger linewidth, in the case of $LiYb_xY_{1-x}F_4$ crystals this effect is partially nullified by the decrease of the impurity-ion EPR linewidth with temperature, caused by the presence of other mechanisms, for all $x \geq x_c$.

IV.12 Concluding remarks

From the present calculations it can be concluded that the spin-lattice relaxation mechanism is closely tied to the percolation properties of the paramagnetic ions as demonstrated in both the $LiYb_xY_{1-x}F_4$ and $Pr_xLa_{1-x}F_3$ single crystals. The calculated paramagnetic percolation thresholds for the concentration x_c agree quite well with the observed EPR-linewidth behaviour. In other words, the spin-lattice relaxation due to paramagnetic host ions is not effective for concentrations of paramagnetic ions below x_c; whereas it is fully effective above x_c, for which concentrations there is a percolation path for mutual spin flips of paramagnetic ions throughout the entire lattice, i.e., a percolating cluster exists. In addition, the the effectiveness of the diamagnetic-site percolation, which shortens the

spin-lattice relaxation time, has also been demonstrated. Thus, the spin-lattice relaxation process is effective as long as $x \geq x_c$ due to paramagnetic site percolation, and the spin-lattice relaxation times are rendered shorter when $x \leq (1-x_c)$, due to the existence of diamagnetic site percolation. when $x \geq (1-x_c)$.

As seen above, the definition of a percolating cluster depends on the assumed connectivity of the sites, and one has to make a choice of the ions which should be considered "connected". In order to explain the experimental data, the connectivity was confined to distances < 0.6 nm in $LiYb_xY_{1-x}F_4$, while in $Pr_xLa_{1-x}F_3$ it was confined to distances < 0.8 nm.

Chapter V

Dual-probability percolation-limited diffusion on a square lattice

V.1 Introduction

Percolation, is a process which governs how a physical quantity spreads through a random medium. It has been used, mostly in the last several years, as a model to study diverse physical phenomena, such as conduction and phase transition. The fractal properties of the percolation clusters have been studied extensively; see, e.g., the reviews by Stauffer,[22] Essam,[23] and the article by Stanley[35] along with the references cited therein. These fractal properties include the cluster fractal dimension, cluster-backbone fractal dimension, and self similarity. A remarkable feature of a percolation process is the existence in many cases, of a threshold, below which the spread of the quantity of interest represented by the extent of the resulting cluster, remains confined to a finite region in the medium, thus not propagating all the way across the sample.

Diffusion processes, as described by random-walk, such as spreading of a solute in a solvent, or the motion of electrons in a semiconductor, have been well investigated.[36] In an ordinary diffusion process the sites of the sample

available for diffusion are occupied uniformly, and the quantity of interest propagates in a random-walk manner. Parts of the cluster, formed due to a diffusion process are also fractals, and are similar to that formed by a percolation process, a fact first pointed out by Sapoval et al.[37] In many aspects, diffusion and percolation processes are quite similar. The major difference between diffusion and percolation processes is that while the randomness in a diffusion process, which spreads infinitely, arises due to the randomness in the motion of particles, the randomness in a percolation process, for which there exists a critical threshold below which the percolation process is limited to a finite region, arises due to randomness in the medium itself. Figures V.1 and V.2 display clusters formed due to percolation and diffusion processes on a square lattice, respectively. The diffusion cluster, depicted in Figure V.2 is the result of random walkers, introduced at one end of the lattice. Each random walker makes an attempt, every t seconds, to jump to a randomly chosen nearest-neighbour site, if this site is already occupied by another walker, the attempt fails, and the walker waits in its original site for t seconds before it making another attempt.

The model, studied in this chapter, combines both percolation and diffusion processes, in order to be able to simulate the physical systems that can not be represented by percolation or diffusion processes alone. Basically, in this

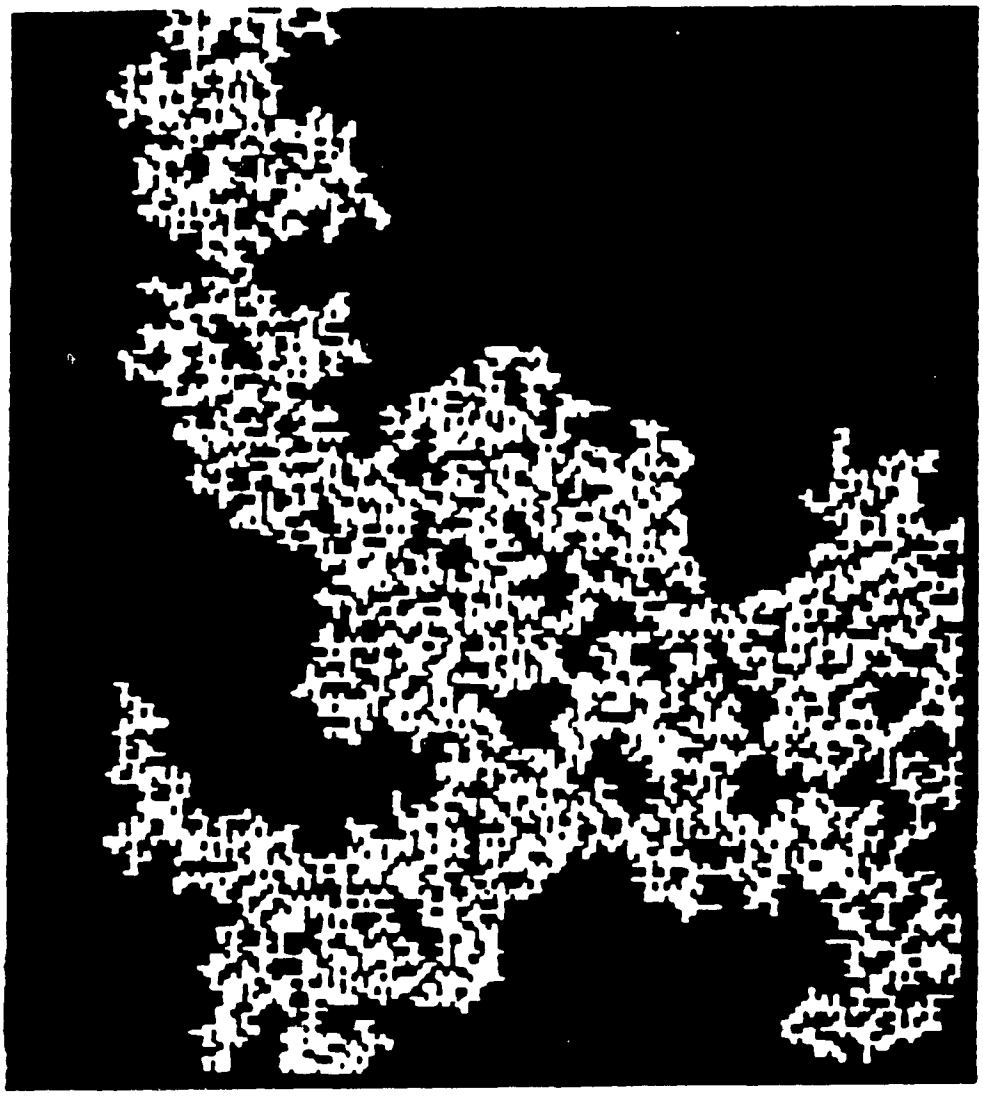

Figure V.1. A percolating cluster on a square lattice of size 200x200.

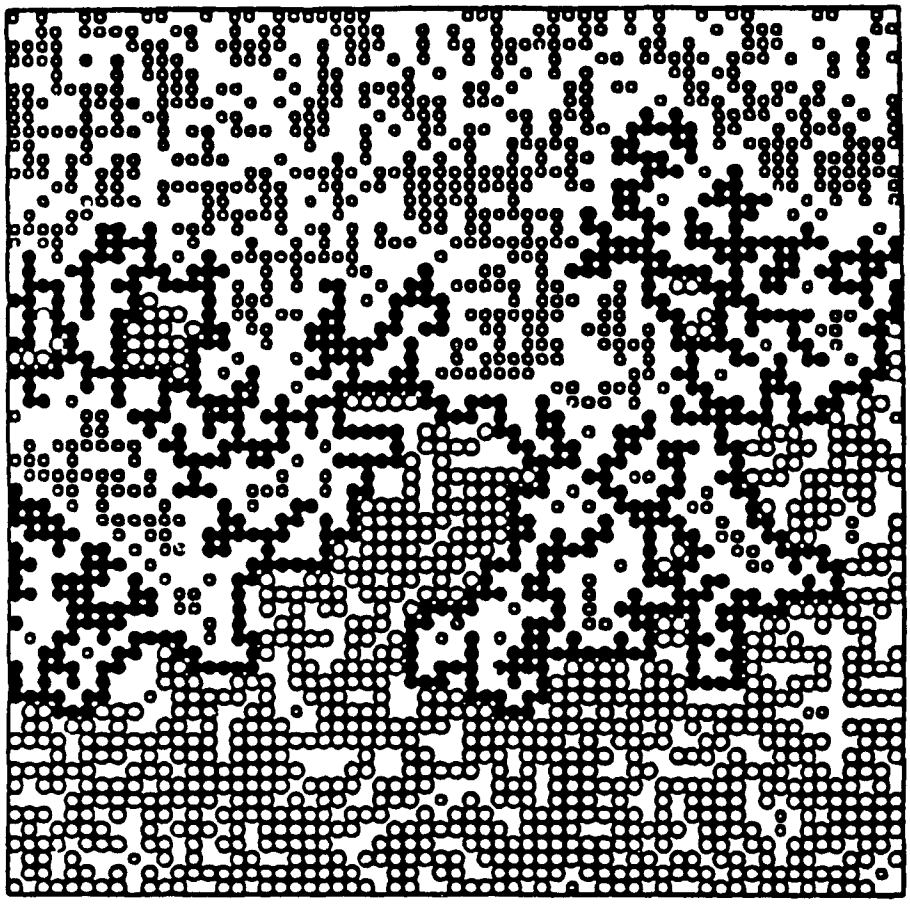

Figure V.2. Diffusion of particles injected from the bottom side of a square lattice. Solid circles represent the hull of the diffusion front.

model a random walk is performed on a randomly-occupied square lattice, to simulate random spreading of a quantity in a random medium. Since the otherwise-unrestricted random walk is now confined to a random medium, this model will, hereafter, be referred to as the percolation-limited diffusion model (PLD).

The particular PLD model, considered here, is governed by another probability (p_2) in addition to the regular site-occupation probability (p_1). Hereafter, p_2 will be associated with the orientation of a magnetic spin located at a lattice site. However, it should be noted here, that p_2 can be used to represent any other relevant quantity instead of the spin direction and, if desired it can also be neglected altogether. The criterion, chosen here, for a site to be "walkable", i.e. it is available for random-walk, is that it be occupied, and its spin orientation be down. (It is assumed, here, that the external Zeeman field is pointing in the upward direction and the magnetic moment of the spin is negative, so that the energy associated with the spin-down orientation is lower than that with the spin-up orientation.)

Three different variations of the PLD model are simulated and studied, these can be described as follows:

(i) The sites of the lattice are occupied randomly with p_1 and the spins of the occupied sites are set down with p_2, initially. This site-spin configuration does not change

during the simulation ,and therefore the random walk, for this case, is governed by a single probability $p = p_1 p_2$. This case is also known as "the ant in the labyrinth" problem, studied previously by several workers.[38-41] This variation of PLD may be used to simulate dilute magnets with frozen spins, e.g., spin glasses.

(ii) The site occupation configuration, as set initially with p_1, remains invariant, while the spin orientation configuration varies during the simulation. That is, the spin orientation of the occupied sites on the lattice are varied randomly with the same probability p_2, before each new step of the random walk is taken during the simulation. This case simulates a dynamic spin system of magnetically-dilute lattice. (iii) Both, the site occupation and the spin orientation vary during the simulation. At every step, each site can either be occupied or remain empty, regardless of the previous history of the site; the same is true for the spin orientation of an occupied site. This case may be used to simulate liquid crystals, where the molecules can slide by each other exchanging sites.

In each of the cases described above, clusters are formed by the random walker. These clusters are, hereafter, defined to be the complex of all those occupied sites connected by the random walk, which have their spins down just before the arrival of the random walk. As it will be

shown below, the PLD clusters are fractals at and above the PLD threshold, p_c. The PLD threshold, p_c, is defined here to be the critical threshold below which a PLD cluster will not reach the limits of the lattice. It should be noted here that in case (iii), the random walk, and therefore the PLD cluster formed, always reaches the limits of the lattice, thus, for this case, the PLD threshold does not exist.

The phenomenon of percolation-limited diffusion will be studied here, as applied to a 348x348 square lattice, for the three cases mentioned above, for various combinations of p_1 and p_2, each being in the range 0.01 to 1.00. Values of the critical exponents, fractal dimensions of the PLD clusters and those of random-walk, and PLD thresholds will be calculated. These will be compared with those reported previously for purely percolation, or for purely diffusion processes. An introduction to the random fractals is given in Sec. V.2. The details of computer simulations are described in Sec. V.3, while those of the quantities calculated in Sec. V.4, followed by the numerical results in Sec. V.5, and a discussion of the numerical values in Sec. V.6. An outline of the application of the present results to the phenomenon of spin-lattice relaxation is provided in Sec. V.7. The concluding remarks are made in Sec. V.8.

V.2 Random fractals

Fractals, which are the result of random phenomena are

called random fractals. It has been experimentally shown that aggregation and sedimentation of particles, as well as displacement of fluids in porous media result in random fractals. In addition, certain coastlines, landscapes, and clouds have also been classified as random fractals. In all these cases the use of fractal geometry has helped researchers to rationalize large sets of experimental results.[36] Like any fractal, the random fractals must have the following characteristics: (i) A fractal dimension, D_H, which is less than the Euclidian dimension, (ii) Self similarity, and (iii) Decreasing density with increasing size. The calculation of D_H will be discussed in detail below. As for the second characteristic, an object is said to be self similar, if parts of the object are similar to the whole object. The third characteristic is a consequence of the definition of D_H, which can also be seen below.

V.3 Details of Simulations

All the presently-described simulations were performed on an IBM-XT computer. VAX 2 and Cyber 835 computers were available, but could not be utilized because of the very limited memory available per user and the large memory requirements of the present programs used. A 348x348 array was used to represent the square lattice used in the present simulations. An array of this size requires 121104 bytes, if a site is represented by one byte. It should be mentioned

here, that bits can not be used to represent the sites, since more than two states are required to represent a site in the present calculations, i.e., 0: unoccupied, 1: occupied-spin up, 2: occupied-spin down, 3: occupied-spin down and visited by the random walk, while a bit has only two states. It is noted that, although a 348x348 lattice may be considered a rather small lattice to yield precise results, the phenomenon of PLD threshold can still be demonstrated reasonably well on a lattice of this size, as justified a posteriori by comparison of the present results with the previous results.

In the computer simulation, the array sites were initially set to be occupied with the probability p_1, using a uniform random-number generator between 0 and 1; if the number was less than or equal to p_1, the site was chosen to be occupied, otherwise not. Next, the spin orientations of the occupied sites were initially set pointing down with a probability p_2, using a random-number generator between 0 and 1. Finally, the empty sites on the array were designated by 0, those occupied with spin up by 1, and those occupied with spin down by 2. In the random-walk process only those sites designated as 2 (occupied and having spin down) were included in the path. The central site, at the location (174,174), was chosen to be the "source" of diffusion of the quantity of interest, i.e., the starting point of the random-walk process. A random integer, between 1 and 4, was

used to choose the direction of the random-walk; the choices 1, 2, 3, and 4 indicate walks along positive x, negative x, positive y, and negative y directions, respectively. In the present model, a site that is a part of the cluster can be revisited without limit, i.e., the random-walk is not restricted to self-avoiding paths.

The three cases described in Sec. V.1 for the formation of PLD clusters are simulated as follows:

Case (i). The site occupations and spin orientations chosen initially with the probabilities p_1 and p_2 respectively, using random-number generators between 0 and 1, remain the same at all steps of the random-walk. That is, the values assigned to the array elements do not change.

Case (ii). Here the occupied sites remain the same as those chosen initially with the probability p_1, while the spin orientations of the occupied sites are flipped completely randomly before a new step of the random-walk is taken, with the overall probability p_2. If the spin of an occupied site, as chosen by the random walk, was found to be pointing up, the choice was dropped and the step was not taken; however, the very same site could be connected to the cluster by the random walk later on in the simulation, if at that point its spin was found to be pointing down, and vice versa. Thus, the value of a certain array element representing a certain occupied site will vary, and can be 1 or 2 during the simulation.

Case (iii). Both, the site occupations and spin orientations of the occupied sites are changed randomly before every step of the random walk is taken, with the overall probabilities being p_1 and p_2, respectively. For all the three cases, the simulation was terminated either when the random walk had arrived at the boundary of the square lattice (equivalent to approaching infinity had the simulation been performed on an infinite lattice), or, when the random walk became confined to a finite cluster having no walkable sites adjacent to it. The simulation was terminated using these criteria, rather than by limiting the number of steps taken in each simulation. During the simulation the formation of the PLD cluster was monitored on a computer screen.

For all the three cases the simulations were made for a chosen value of p_1, while varying p_2 values ranging from 0.1 to 1.0 in steps of 0.1, as well as in steps of 0.01, when the values of p_1p_2 were in the range 0.50 to 0.65, since the percolation threshold, for a square lattice, falls in this range. This process was repeated such that the chosen p_1 values cover the range 0.1 to 1.0 in steps of 0.1. Thereafter, additional simulations were performed reversing the roles of p_1 and p_2.

For each simulation, the total number of steps taken and unsuccessful step attempts made were counted; this number (T) was used as a measure of the time it took to form the

particular cluster, while the number of connected sites was used as a measure of the mass of the cluster (M). It should be noted, that M ≤ T, since a site can be revisited. This increases T, but not M. The critical exponent γ was then calculated from the values of M (details in Sec. IV.4). The maximum linear dimension, as defined by the length (S) of the longer side of the smallest rectangle enclosing the cluster was also calculated. Using S, the critical exponent ν was calculated (details in Sec. IV.4). The average distance between 1000 randomly chosen pairs of visited sites was calculated as a measure of the r.m.s. distance, <s>, travelled by the random-walk. The effective interval of time, t, defined to be equal to T/M, was used to estimate the critical exponents μ, μ', as discussed in Sec. IV.4. In addition, the PLD threshold (when applicable) and the fractal dimension of PLD cluster and of random walk were estimated. For each case, a large number of simulations were performed to calculate average values; the standard deviation was used as the error bound in the calculated average values. The listings of the programs for all the three cases are given in Appendix I.

V.4 Quantities calculated

The details of the various quantities calculated, relevant to PLD clusters and random walk are described below.

A. PLD threshold (p_c). The percolation-limited diffusion threshold above which the diffusion spreads all the way across the sample, i.e. the cluster formed extends from one end to the other end of the crystal, only need to be calculated for cases (i) and (ii), since there is no percolation threshold for case (iii), as the process of diffusion will reach every site eventually, regardless of the choice of p_1, or p_2. In case (i), PLD threshold is controlled by the product of p_1 and p_2, while in case (ii), it is controlled by p_1.

B. Cluster-Fractal Dimension (D_H). The fractal dimension, D_H, of an incipient cluster was calculated from the value of M, using the following relation, derived in Appendix II:

$$D_H = 2 \log M/\log (ab), \qquad (V.1)$$

where a and b are the sides of the smallest rectangle that covers the cluster.

C. Random-Walk Fractal Dimension (d_{rw}). The random-walk fractal dimension, d_{rw}, relating the r.m.s distance travelled by random walk to time taken to form the cluster, was calculated, using the relation[42]

$$\langle s \rangle \propto T^{1/d_{rw}}. \qquad (V.2)$$

<s> was calculated to be the average of the distances between 1000 randomly chosen pairs of the visited sites.

D. Maximum linear dimension (S). The maximum linear dimension, S, exhibiting critical behaviour, can be calculated for cases (i) and (ii) only. For case (iii), the measure of S is meaningless since the random-walk, in this case, will always reach the limits of the lattice.

For case (i), S stretches all the way from one end of the lattice to the other (see the graphic picture of a PLD cluster in Fig. V.3) for all values of $p_1p_2 > (p_1p_2)_c$. The calculated results are investigated to exhibit the following dependence:

$$S \propto [(p_1p_2)-(p_1p_2)_c]^{-\nu};\ p_1p_2 > (p_1p_2)_c. \qquad (V.3)$$

For case (ii), S is independent of p_2. This is because an occupied site will have its spin pointing down sooner or later regardless of the value of p_2, since the spin orientations are varied before every step during the simulation; thus this site will be "walkable" eventually. S is, finally, found to be governed by

$$S \propto (p_1-p_{1c})^{-\nu},\ p_1 > p_{1c}. \qquad (V.4)$$

E. Mass of a cluster (M). The mass of a cluster, M,

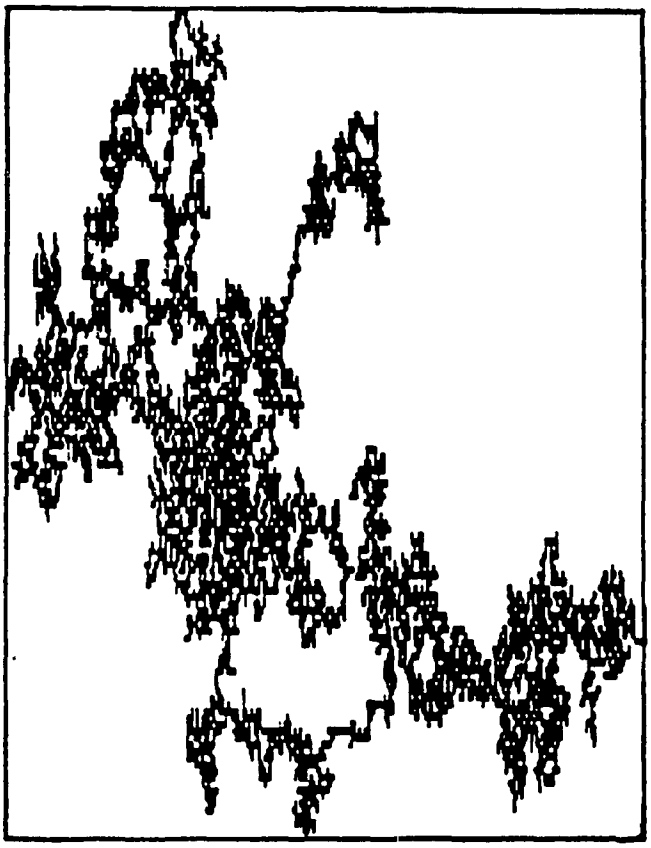

Figure V.3. The printout of a percolation limited diffusion cluster as displayed on the computer screen. The picture is somewhat elongated vertically by the printer.

which exhibits critical behavior in the same way as that exhibited by S. Likewise, it was calculated only for cases (i) and (ii). Specifically, for case (i)

$$M \propto [(p_1p_2)-(p_1p_2)_c]^{-\gamma},\ p_1p_2 > (p_1p_2)_c; \tag{V.5}$$

and, for case (ii)

$$M \propto (p_1-p_{1c})^{-\gamma},\ p_1 > p_{1c}. \tag{V.6}$$

For case (iii), no critical behavior was exhibited.

F. Effective time (t). For case (i), the behaviour of the effective time, t, exhibits a dependence on p_1p_2, which is similar to that of S, or M. Specifically,

$$t \propto [(p_1p_2)-(p_1p_2)_c]^{-\mu},\ p_1p_2 > (p_1p_2)_c. \tag{V.7}$$

As for case (ii), in addition to exhibiting critical dependence on p_1, it exhibits a p_2 power-law dependence in the following manner:

$$t \propto (p_1-p_{1c})^{-\mu}\ p_2^{-\mu'},\ p_1 > p_{1c}. \tag{V.8}$$

As for case (iii), t neither exhibits any critical dependence on p_1, nor on p_2. Instead, it exhibits a power-law dependence:

$$t \propto (p_1 p_2)^{-\mu'} . \qquad (V.9)$$

V.5 Numerical results

For both cases (i) and (ii), p_{1c} and $(p_1 p_2)_c$, as defined by eqs. (V.3)-(V.5) and (V.7), were all found to be $\cong 0.60$. The fractal dimension, D_H, as calculated using eq. (V.1), was found to be 1.70 ± 0.07 for all the three cases. The random-walk fractal dimension, d_{rw}, calculated using eq. (V.2) was found to be 2.86 ± 0.15. By fitting the calculated values of S, M, and t to eqs. (V.3), (V.4); (V.5), (V.6); and (V.7), (V.8), (V.9), respectively, the values of the exponents ν, γ, μ, μ', were estimated to be 1.20 ± 0.15, 2.050 ± 0.50, 1.80 ± 0.12, and 1.0 ± 0.01, respectively. The errors indicated in the various values are the calculated standard deviations.

V.6 Discussion

The values $p_{1c} = (p_1 p_2)_c \cong 0.60$ calculated here are in good agreement with $p_c = 0.59275 \pm 0.00003$, as determined by a computer simulation of the purely percolation process on a 450 x 450 lattice.[43]

The presently-calculated value of the fractal dimension (D_H) suggests that percolation-limited diffusion yields clusters whose fractal geometry is the same as that of the hulls of diffusion fronts. The hull, in a diffusion process,

consists of all those sites which are connected to the source, and are neighbors to the end part of the sample to which diffusion did not reach, i.e., the insulating end of the lattice. The hulls of diffusion fronts, have been reported to have the fractal dimension $D_H \cong 1.72\text{-}1.76$,[36,43,44] as calculated using computer simulations of diffusion processes on square lattices of various sizes, in agreement with the presently-estimated value of $D_H = 1.70 \pm 0.07$, calculated just above the threshold, p_c. On the other hand, all two-dimensional percolation clusters are characterized by $D_H \cong 1.89$,[36,45] estimated using several LxL square lattices from log-log plots of M versus L. However, these clusters are not the same as PLD clusters.

The present value of the random-walk fractal dimension, $d_{rw} = 2.86 \pm 0.15$, as defined by the exponent in eq. (V.2), is in good agreement with that based on a conjecture of Alexander and Orbach ($d_{rw} \cong 2.85$),[41] known as AO conjecture, according to which there exists the relation $d_{rw} = \frac{3}{2} D_H$ between the fractal dimension of the substrate (D_H) on which the walk takes place and that of the random-walk (d_{rw}). On the other hand, the conjecture given by Ahorony and Stauffer,[42] known as AS conjecture, proposes $d_{rw} = D_H + 1$. Both, AO and OS conjectures, have been tested not to hold exactly.[35,40]

The critical exponent (ν) for the maximum linear dimension (S), both, for the purely diffusion, and for the

purely percolation processes, have been reported to have the value of 4/3,[46] as calculated by the application of the variational method. This value is within the error bound of the the presently-calculated value $\nu = 1.2 \pm 0.15$. As for the critical exponent (γ) for the mass of clusters (M), the presently-calculated value of $\gamma = 2.05 \pm 0.50$ is also in agreement with that for the purely percolation process ($\gamma \cong 2.43$),[47] within error bounds, as estimated by a series expansion method, there being no corresponding exponent for the diffusion process.

V.7 Application to EPR

Percolation-limited diffusion, as proposed presently, can easily be applied to the study of EPR and spin-lattice relaxation in magnetically-dilute lattices, consisting of both paramagnetic and diamagnetic host ions, wherein one studies how the energy given off by an impurity or a host paramagnetic spin, as it relaxes by a mutual spin flip with another paramagnetic ion, spreads through the sample. The problem discussed in Chapter IV is, indeed, an application of case (ii) of PLD to EPR, as discussed in this chapter. It should be noted here, that in Chapter IV, p_2, the spin-orientation probability was not considered, since in Chapter IV only the percolation threshold was being calculated and this does not depend on p_2, the spin orientation probability, as seen previously for case (ii).

Relationship between the effective time (t) and the spin-lattice relaxation time τ. When the spin orientations are allowed to vary, as in cases (ii) and (iii), it is seen from eqs. (V.8) and (V.9) that, for a fixed value of p_1, $t \propto p_2^{-\mu'}$. The value of μ' was determined to be 1.0 ± 0.01. Assuming now that $\mu' = 1$, $t \propto 1/p_2$. Now, the spin-down probability, p_2, is directly proportional to the number of sites in the spin-down state, n_2. In thermal equilibrium, $n_2 \propto \exp(-1/kT)$,[1] where T is the temperature; thus $t^{-1} \propto \exp(-1/kT)$. Since in the case of the "direct" process,[21] the spin-lattice relaxation time τ has the temperature dependence $\tau^{-1} \propto \exp(-1/kT)$, it can be concluded that the effective time t, in PLD process, is proportional to the spin-lattice relaxation time, τ, as governed by the "direct" process. In the "direct" process, the spin-lattice relaxation process occurs between only two spin levels, the same as that considered presently in the PLD process.

V.8 Concluding remarks

The present results indicate that percolation-limited diffusion yields clusters that exhibit some properties of percolation clusters, such as thresholds and critical exponents. On the other hand, at and just above p_c, they exhibit the fractal behaviour of the hulls of diffusion fronts. In addition, the values of μ and μ', as estimated presently for clusters formed by percolation-limited

diffusion, are the first-ever reported. The critical exponents ν and γ for PLD clusters have been presently calculated to be in agreement, within error bounds, with those calculated previously using other techniques.

In addition to the application of the present results to the spin-lattice relaxation process, they can also be used to study other physical phenomena. To this end, the following examples may be cited:

(i) Travel of conduction electrons through a medium, consisting of a mixture of conducting and non-conducting atoms, the conduction electron belonging to the conducting atom. In this case, an "occupied" site is that occupied by the conducting atom, while p_2 represents the temperature distribution determining the probability of an electron being in the conduction band.

(ii) The spread, or diffusion, of particles, or molecules, e.g. that of a liquid through a porous medium.

(iii) Absorption and emission of photons, such that exists in laser materials, characterized by a triggering chain-reaction like process. The lasing action is controlled by a threshold, below which it does not occur.

Chapter VI

Conclusion

The main results of the calculations presented in this thesis can be summarized as follows:

Eq. (III.8) is the correct expression to calculate the second moment in crystals with two different kinds of paramagnetic ions, as is the typical EPR situation. Consequently, eq. (III.11) should be used, instead of the frequently-used incorrect eq. (III.4), to calculate the spin-lattice relaxation time of the host ions in crystals wherein the experimentally observed impurity-ion EPR lines become narrower with increasing temperature.

(ii) The host-ion spin-lattice relaxation process has a critical cut-off in diluted paramagnetic single crystals, below which it is not effective; the cut-off is governed by paramagnetic-site percolation threshold. In this way an explanation of the unusual temperature and paramagnetic-ion concentration (x) dependence of the Gd^{3+} EPR linewidths in $LiYb_xY_{1-x}F_4$ and $Pr_xLa_{1-x}F_3$ single crystals can be provided. In addition, it has been shown, that the diamagnetic-site percolation is responsible for the shortening of the host-ion spin-lattice relaxation time.

(iii) Percolation-limited diffusion process results in random fractal clusters, and has characteristics of both the

percolation and the diffusion processes. It is also suggested, that PLD can be used to simulate a number of physical systems and processes, e.g. the spin-lattice relaxation process. Specifically, it has been demonstrated, that case (ii) of PLD model can be used to simulate the Direct process in magnetically dilute crystals.

References

[1]G. E. Pake and T. L. Estle, The Physical Principles of Electron Paramagnetic Resonance, (W. A. Benjamin Inc., Reading, Massachusetts, 1973).

[2]S. K. Misra and U. Orhun, Phys. Rev. B38, 8683 (1988).

[3]I. Waller, Z. Phys. 79, 370 (1932).

[4]L. J. Broer, Physica 10, 801 (1943).

[5]J. H. Van Vleck, Phys. Rev. 74, 1168 (1948).

[6]P. W. Anderson and P. R. Weiss, Rev. Mod. Phys. 25, 269 (1953).

[7]P. W. Anderson, J. Phys. Soc. Jpn. 9, 316 (1954).

[8]T. Mitsuma, J. Phys. Soc. Jpn. 17, 128 (1962).

[9]V. M. Malhotra, H. A. Buckmaster, and J. M. Dixon, J. Phys. C13, 3921 (1980).

[10]V. M. Malhotra, J. M. Dixon, and H. A. Buckmaster, Physica, B101, 147 (1980).

[11]M. R. St. John, Ph. D. Thesis, University of California, Berkeley, 1975.

[12]R. S. Saraswat and G. C. Upreti, J. Chem. Phys. 67, 5428 (1977).

[13]V. K. Jain and S. K. Yadav, Phys. Rev. B33, 5034 (1986).

[14]V. K. Jain, N. V. Vugman, and V. S. Yadav, Phys. Rev. B37, 9716 (1988).

[15]S. A. Al'tshuler and B. M. Kozyrev, Electron Paramagnetic Resonance in Compounds of Transition Elements (Keter, Jerusalem, 1974).

[16]A. Abragam and B. Bleaney, Electron Paramagnetic Resonance of Transition Ions (Clarendon Press, Oxford, 1970).

[17]E. Eriksson, L. O. Larsson, L. Niinisto, and U. Skoglund, Inorg. Chem. 13, 290 (1974).

[18]H. A. Buckmaster, V. M. Malhotra, and H. D. Bist, Can. J. Phys. 58, 1667 (1980).

[19]S. K. Misra, U. Orhun, and J. Sun, Solid State Commun. 76, 949 (1990).

[20]H. A. Buckmaster, V. M. Malhotra and H. D. Bist, Can. J. Phys. 59, 596 (1981).

[21]K. N. Shrivastava, Phys. Stat. Sol. (b) 117, 437 (1983).

[22]D. Stauffer, Phys. Rep. 54, 1(1979).

[23]J. W. Essam, Rep. Prog. Phys. 43, 833(1980).

[24]Y. Vaills, J. Y. Buzaré, and J. Y. Gesland, Solid State Commun. 45, 1093 (1983).

[25]S. K. Misra, M. Kahrizi, P. Mikolajczak, and L. Misiak, Phys. Rev. B32, 4738(1985).

[26]L. E. Misiak, S. K. Misra, and P.Mikolajczak, Phys. Rev.B38, 8673(1988).

[27]L. E. Misiak, S. K. Misra, and U. Orhun, Phys. Status Solidi (B) 154, 249 (1989).

[28]R. E. Thoma, C. F. Weaver, H. A. Friedman, H. Insley, L. A. Harris, and H. A. Yakel, Jr., J. Phys. Chem 65, 1096 (1961).

[29]R. E. Thoma, G. D. Brunton, R. A. Penneman, and T. K. Keenan, Inorg. Chem. 9, 1096 (1970).

[30]L. E. Misiak, P.Mikolajczak, and M. Subotowicz, Phys. Status Solidi (A) 97, 353 (1986).

[31]L. M. Holmes, T. Johansson, and H. J. Guggenheim, Solis State Commun. 12, 993 (1973).

[32]L. Vegard, Z. Cryst. 67, 239 (1928).

[33]S. K. Misra, W. Korczak, S. Z. Korczak and M. Subotowicz, Solid State Commun. 76, 1055 (1990).

[34]J. D. H. Donnay and G. Donnay, Crystal Data Determinative Determinative Table, 2nd ed. (American Crystallographic Association, New York, 1962).

[35]H. E. Stanley in, On Growth and Form, H. E. Stanley and N. Ostrowsky, Eds., (Maritus Nijhoff, Dordrecht, 1986).

[36]J. Feder, Fractals (Plenum Press, New York, 1988).

[37]B. Sapoval, M. Rosso, J. F. Gouyet, J. Phys. Lett. 46, L149(1985).

[38]P. G. de Gennes, La Recherche 7, 919(1976).

[39]C. Mitescu and R. Roussenq in, Percolation Structures and Processes, G. Deutscher, R. Zallen and J. Adles, Eds., Ann. Israel Phys. Soc. volume 5 (Adam Hilger, Bristol, 1983).

[40]Y. Gefen, A. Ahorany and S. Alexander, Phys. Rev. Lett. 50, 77(1983).

[41]S. Alexander and R. Orbach, J. Physique (Paris) 43, L625(1982).

[42]A. Ahorany and D. Stauffer, Phys. Rev. Lett. 52, 2368(1984).

[43]R. M. Ziff, Phys. Rev. Lett. 56, 545(1986).

[44]R. F. Voss, J. Phys. A17, L373(1984).

[45]D. Stauffer, Introduction to Percolation Theory, (Taylor and Francis, London, 1985).

[46]M. P. M. Den Nijs, J. Phys. A12, 1857(1979).

[47]M. F. Sykes, D. S. Gaunt, and M. Glen, J. Phys. A9, 97(1976).

APPENDIX I

Algorithms and listings of the computer programs

The computer programs used in this thesis are written in Pascal programming language, using the Turbo Pascal compiler for IBM PC/XT/AT and compatible computers. Monographic (TTL) display is adapted in the following listings, however, modifications to the programs can be made for use with other graphics adaptors. In addition, the lattice sizes may be increased, if the particular compiler and the computer used allow such a change.

A typical Pascal program has the following structure:

1. Program name;
2. Definition of global variables;
3. Procedures and functions
4. Main body of the program, which calls the procedures and functions above.

The programs listed here have the form given above. Algorithms for all program are given prior to their listings.

Program I

Purpose: To generate lattices, calculate the second moment, and the spin-lattice relaxation time.

Algorithm I

```
read ( unit cell parameters,
       number of ions in unit cell,
       unit cell coordinates of ions,
       array steps along x, y, z for each site,
       distances between equivalent sites )

read ( EPR data )

do 3D loop for each ion in the unit cell to generate
       the lattice

       choose an occupied site near the center of array
            and calculate the distances of other
                occupied sites around it

            calculate the direction cosines

                calculate the second moment

                    calculate τ

write ( distances of neighbours, second moment, τ )

       end.
```

Listing I

```
program Lattice_Generator;
   const
    beta=9.27;
     h=6.63;
      mu=1.26;
   var
     filename:string[8];
          crint:file of integer;
               creal:file of real;
          points : array [0..36,0..36,0..36] of byte;
  distx:array  [1..6] of real;
  disty:array  [1..6] of real;
  distz:array  [1..6] of real;
  locx:array   [1..6] of real;
  locy:array   [1..6] of real;
```

```
   locz:array   [1..6] of real;
       stepx: array [1..6] of integer;
       stepy: array [1..6] of integer;
       stepz: array [1..6] of integer;
   xlim, ylim, zlim, nk, fm, ran : byte;
   along, counter, px, py, pz, cx, cy, cz, n, rmin, sx, sy,
   sz, m, x, y, z, i, j, k, xo, yo, zo, inx :integer;
   jp, second, third, sum1, sum2, gam, s, g,
   supersum, slrt, lw, gp, pro, r3, r6, rx, ry, rz, rad,
   rx1, ry1, rz1, a, b, c, alpha, bheta, gamma, cosgamma,
   alphar, betar, gammar : real;
           key,dim :char;

   procedure zero;
{Initialize the array elements}
      begin
           for sz:=0 to 36 do begin
              for sy:=0 to 36 do begin
                   for sx:=0 to 36 do begin
   points [sx,sy,sz]:=0;
                   end;
               end;
           end;
   end;

   procedure zero1;
{Input of values for a new crystal}
 begin
   write ('enter # of master ions:');
   readln (n);
                write(crint,n);
   write ('enter unit-cell parameters in nm: a=');
   readln (a);
                write(creal,a);
   write ('                                  b=');
   readln (b);
                write(creal,b);
   write ('                                  c=');
   readln (c);
                write(creal,c);
   write ('external field along alpha ? ');
   readln (alpha);
                write(creal,alpha);
   write ('beta ?');
   readln(bheta);
                write (creal,bheta);
   write ('gamma ?');
   readln(gamma);
                write (creal,gamma);
   write ('effective spin of host ? ');
   readln (s);
```

```
                write(creal,s);
   write ('g-host ? ');
   readln (gp);
                write(creal,gp);
   write ('g-impurity ? ');
   readln (g);
                write(creal,g);
   write ('avg. J-pair in GHz ? ');
   readln (jp);
                write(creal,jp);
   alpha:=(alpha*3.14159)/180;
      bheta:=(bheta*3.14159)/180;
         gamma:=(gamma*3.14159)/180;
   end;

      procedure creator;
  {Occupy the proper sites in the array}
    begin
      i:=(36-xo) div stepx[m];
           j:=(36-yo) div stepy[m];
                k:=(36-zo) div stepz[m];
      for sz:=0 to k do begin
            for sy:=0 to j do begin
                 for sx:=0 to i do begin
   if random(10)+1<=ran then
points[xo+(sx*stepx[m]),yo+(sy*stepy[m]),zo+(sz*stepz[m])]:=m;
                                    end;
                               end;
                          end;
      end;

   procedure origin;

{More input about the new crystal}

    begin
    writeln ('enter array-coordinates of master ion: #',m);
    write ('a=');    readln (xo);
      write(crint,xo);
    write ('b=');    readln (yo);
      write(crint,yo);
    write ('c=');    readln(zo);
      write(crint,zo);
   write ('enter # of array steps along a :');
   readln(stepx[m]);
      write(crint,stepx[m]);
   write ('                          along b :');
   readln (stepy[m]);
      write(crint,stepy[m]);
   write ('                          along c :');
   readln (stepz[m]);
      write(crint,stepz[m]);
                          creator;
```

```
   write('enter distance between master ions along a in a:');
   readln (distx[m]);
    distx[m]:=distx[m]*a;
       write(creal,distx[m]);
    write('                                        along b in b:');
    readln (disty[m]);
    disty[m]:=disty[m]*b;
       write(creal,disty[m]);
    write('                                        along c in c:');
    readln (distz[m]);
    distz[m]:=distz[m]*c;
        write(creal,distz[m]);
    write ('enter location of master ion along a in a:');
    readln (locx[m]);
    locx[m]:=locx[m]*a;
        write(creal,locx[m]);
    write ('                                  along b in b:');
    readln (locy[m]);
    locy[m]:=locy[m]*b;
        write(creal,locy[m]);
    write ('                                  along c in c:');
    readln (locz[m]);
    locz[m]:=locz[m]*c;
        write(creal,locz[m]);
      end;

   procedure findcenter;

   {Make note of the central ion in the array}

      begin
           repeat
    write ('enter array-coordinates of near-center ion : x=');
       readln (cx);
    write ('                                           : y=');
       readln (cy);
    write ('                                           : z=');
       readln (cz);
             until points[cx,cy,cz]<>0;
    write(crint,cx);
    write(crint,cy);
    write(crint,cz);
     end;

   procedure distance;

{Find components of r vector}

   begin
   rx:=((sx div stepx[inx])*distx[inx])+locx[inx];
    ry:=((sy div stepy[inx])*disty[inx])+locy[inx];
     rz:=((sz div stepz[inx])*distz[inx])+locz[inx];
   end;

   procedure sums;
```

```
{Calculate the sums of the second moment}
    begin
     nk:=nk+1;
      gam:=(1-(3*sqr(cosgamma)));
        r3:=rad*rad*rad; r6:=sqr(r3);
   sum1:=sum1+(sqr(gam)*(1/r6));
    sum2:=sum2+(gam*(1/r3))    ;
   end;
   procedure nearest;
{Find neighbours}
   begin
      sx:=cx;
           sy:=cy;
                sz:=cz;
   inx:=points[sx,sy,sz];
                     distance;
   rx1:=rx;
      ry1:=ry;
           rz1:=rz;
 for sz:=cz-(stepz[inx]*3) to cz+(stepz[inx]*3) do begin
   for sy:=cy-(stepy[inx]*3) to cy+(stepy[inx]*3) do begin
    for sx:=cx-(stepx[inx]*3) to cx+(stepx[inx]*3) do begin
   if points [sx,sy,sz]<>0 then begin
      inx:=points[sx,sy,sz];
           distance;
   rad:=sqrt(sqr(rx1-rx)+sqr(ry1-ry)+sqr(rz1-rz));
       if round(1000*rad)=rmin then begin
    writeln (rad:5:3,'nm  at ',sx,',',sy,',',sz);
   alphar:=(rx-rx1)/rad;
      betar:=(ry-ry1)/rad;
           gammar:=(rz-rz1)/rad;
cosgamma:=(cos(alpha)*alphar)+(cos(bheta)*betar)
           +(cos(gamma)*gammar);
                                  sums;
           points[sx,sy,sz]:=0;
                     end;
                end;
               end;
           end;
            end;
        end;
   procedure neighbors;
{Locate surrounding ions}
  begin
   sx:=cx;
      sy:=cy;
           sz:=cz;
                rmin:=10000;
```

```
   inx:=points[sx,sy,sz];
      distance;
   rx1:=rx;
      ry1:=ry;
           rz1:=rz;
   for sz:=cz-(stepz[inx]*3) to cz+(stepz[inx]*3)do begin
   for sy:=cy-(stepy[inx]*3) to cy+(stepy[inx]*3)do begin
   for sx:=cx-(stepx[inx]*3) to cx+(stepx[inx]*3)do begin
      if points [sx,sy,sz]<>0 then begin
   inx:=points[sx,sy,sz];
      distance;
   rad:=sqrt(sqr(rx1-rx)+sqr(ry1-ry)+sqr(rz1-rz));
  if (round(1000*rad)<rmin) and
      (rad<>0) then rmin:=round(1000*rad);
   end;
      end;
           end;
                end;
                     end;
   procedure neighbors1;
{Calculation of direction cosines}
    begin
   sx:=i;
      sy:=j;
           sz:=k;
   inx:=points[sx,sy,sz];
   distance;
   rx1:=rx;
      ry1:=ry;
           rz1:=rz;
   for sz:=k-zlim to k+zlim do begin
      for sy:=j-ylim to j+ylim do begin
           for sx:=i-xlim to i+xlim do begin
                if points [sx,sy,sz]<>0 then begin
   inx:=points[sx,sy,sz];
           distance;
   rad:=sqrt(sqr(rx1-rx)+sqr(ry1-ry)+sqr(rz1-rz));
      alphar:=(rx-rx1)/rad;
   betar:=(ry-ry1)/rad;
      gammar:=(rz-rz1)/rad;
   cosgamma:=(cos(alpha)*alphar)+(cos(bheta)*betar)
                +(cos(gamma)*gammar);
   if (rad<>0) and (round(rad*1000)<=rmin) then sums;
    end   ;
          end;
           end;
                end;
    end;
   procedure moment;
```

```
{Final calculations of the second moment}
   begin
second:=(1/3)*s*(s+1);
 third:=(nk*sqr(jp)*1e18)+((1/sqr(h))*1e14*sqr(g*gp)*sqr(sqr(
  beta))*sqr(mu)*sum1)+((1/h)*1e16*2*jp*g*gp*sqr(beta)*mu*sum2);
   second:=second*third;
   supersum:=supersum+second;
   end;
  {****    Main Program    ****}
   begin
     randomize;
      ran:=10;
   clrscr;
      write ('Enter 1 for new file, 2 for disk-file :');
   readln (fm);
      write ('Filename :');
           readln(filename);
    assign (crint,'b:'+filename+'.int');
    assign (creal,'b:'+filename+'.rel');
   zero   ;
   if fm=1 then begin
                rewrite (crint);
                rewrite (creal);  clrscr;
   zero1;
     for m:=1 to n do
     origin;
     findcenter;
   close(creal);
      close(crint);
    end   ;
     if fm=2 then begin
   clrscr; writeln ('Reading crystal data ......');
   reset (crint);
      reset (creal);
   read(crint,n);
      read(creal,a);
           read(creal,b);
                read(creal,c);
   read(creal,alpha);
      read(creal,bheta);
           read(creal,gamma);
   read(creal,s);
      read(creal,gp);
   read(creal,g);
      read(creal,jp);
   for m:=1 to n do begin
   read(crint,xo);
      read(crint,yo);
           read(crint,zo);
   read (crint,stepx[m]);
      read(crint,stepy[m]);
```

```
            read(crint,stepz[m]);
   creator;
   read (creal,distx[m]);
      read(creal,disty[m]);
            read(creal,distz[m]);
   read (creal,locx[m]);
      read(creal,locy[m]);
            read(creal,locz[m]);
    end   ;
    read (crint,cx);
      read(crint,cy);
            read(crint,cz);
   close(creal);
close(crint);
   clrscr;
   write ('Alpha      :',alpha,' ?');
readln(alpha);
   write ('Beta       :',bheta,' ?');
readln(bheta);
   write ('Gamma      :',gamma,' ?');
readln(gamma);
   alpha:=(alpha*3.14159)/180;
   bheta:=(bheta*3.14159)/180;
   gamma:=(gamma*3.14159)/180;
writeln ('Number of master ions = ',n);
writeln ('Unit cell a:',a:5:3,' b:',b:5:3,' c:',c:5:3,' nm.');
writeln ('Exchange constant     :',jp:5:3,' Ghz.');
writeln ('Effective nost spin   :',s:5:3);
writeln ('g-host :',gp:5:3,' g-guest :',g:5:3);
     end;
   writeln ('change J to ? ');readln(jp);
   writeln ('change g-host to ? '); readln(gp);
   writeln ('change host spin to ?'); readln(s);
   randomize;  ran:=10;
   nk:=0;   sum1:=0; sum2:=0;
   write   ('Upto ?-nearest        :'); readln(fm);
   for m:=1 to fm do begin
   neighbors;
   writeln(m,'-nearest= ',rmin);
   nearest;              end;
   repeat
   second:=(1/3)*s*(s+1);
   writeln('Total ions :',nk);
   write ('change J to:');
      readln(jp);
   write ('change g-host to:');
      readln(gp);
   third:=(nk*sqr(jp)*1e18)+((1/sqr(h))*1e14*sqr(g*gp)
         *sqr(sqr( beta))*sqr(mu)*sum1)
          +((1/h)*1e16*2*jp*g*gp*sqr(beta)*mu*sum2);
   second:=second*third;
   writeln ('second moment = ',second:9,' Hz^2');
```

```
write ('observed LW along ',along,'-axis in T ? ');
readln (lw);
slrt:=(3*lw*sqr(g)*beta*1e-24)/(110*h*1e-34*gp*second);
writeln (lst,'j=',jp,' g=',gp,' tau=',slrt:9);
second:=0;
until jp=0;
end.
```

Program II

Purpose: To find the percolation threshold value x_c in $LiYb_xY_{1-x}F_4$.

Algorithm II

generate the lattice sites

occupy proper sites randomly,
occupied=1, unoccupied=0

connect all sites in z=0 to cluster,
site=2

connect all occupied sites
negihbouring percolating sites to
the cluster

sweep { in ±x, ±y, and ±z directions }

until a site in last plane becomes connected
or
no new site can be connected

repeat for various values of x

end.

Listing II

```
program 3_D_percolation {for LiYb_xY_1-xF_4}

var
   points : array [-2..47,-2..47,-2..47] of byte;
   sx, sy, sz, h, m, a, b, c, d, e, f, g, l, i, j, k,
```

```
   x, y, z, s:integer;
      ia, ja, ka, ir, jr, kr, r:real;
           key,dim:char;

   procedure first;  {on z = 0 plane all occupied neighbors
                      are connected, all assumed percolating}
begin
    k:=0;
  for j:=0 to 17 do begin
      for i:=0 to 18 do begin
            if points[i*2,(2*j)+1,k]=1 then begin
                  points[i*2,(2*j)+1,k]:=2;
               if points[(i*2)+2,(2*j)+1,k]=1
                   then points[(i*2)+2,(2*j)+1,k]:=2;
               if points[(i*2)-2,(2*j)+1,k]=1
                   then points[(i*2)-2,(2*j)+1,k]:=2;
               if points[(i*2),(2*j)+3,k]=1
                   then points[(i*2),(2*j)+3,k]:=2;
               if points[(i*2),(2*j)-1,k]=1
                   then points[(i*2),(2*j)-1,k]:=2;
               if points[(i*2)+1,(2*j)+1,k+1]=1
                   then points[(i*2)+1,(2*j)+1,k+1]:=2;
               if points[(i*2)-1,(2*j)+1,k+1]=1
                   then points[(i*2)-1,(2*j)+1,k+1]:=2;
               if points[(i*2)-1,(2*j)+1,k+1]=1
                   then points[(i*2)-1,(2*j)+1,k-1]:=2;
              if points[(i*2)+1,(2*j)+1,k+1]=1
                   then points[(i*2)+1,(2*j)+1,k-1]:=2;
            end;
      end;
  end;
end;

   procedure second;
{connect sites on the next plane}
   begin
for i:=0 to 18 do begin
    if points[i*2,j,k]=2
       then
  begin
      if points[(i*2)+2,j,k]=1
         then points[(i*2)+2,j,k]:=2;
      if points[(i*2)-2,j,k]=1
         then points[(i*2)-2,j,k]:=2;
      if points[(i*2),j+2,k]=1
         then  points[(i*2),j+2,k]:=2;
      if points[(i*2),j-2,k]=1
         then  points[(i*2),j-2,k]:=2;
      if points[(i*2)+1,j,k+1]=1
         then points[(i*2)+1,j,k+1]:=2;
      if points[(i*2)-1,j,k+1]=1
         then points[(i*2)-1,j,k+1]:=2;
```

```
      if points[(i*2)-1,j,k-1]=1
         then points[(i*2)-1,j,k-1]:=2;
      if points[(i*2)+1,j,k-1]=1
         then points[(i*2)+1,j,k-1]:=2;
  end;
end;
     for i:=18 downto 0 do begin
           if points[i*2,j,k]=2
              then
        begin
            if points[(i*2)+2,j,k]=1
               then points[(i*2)+2,j,k]:=2;
            if points[(i*2)-2,j,k]=1
               then points[(i*2)-2,j,k]:=2;
            if points[(i*2),j+2,k]=1
               then points[(i*2),j+2,k]:=2;
            if points[(i*2),j-2,k]=1
               then points[(i*2),j-2,k]:=2;
            if points[(i*2)+1,j,k+1]=1
               then points[(i*2)+1,j,k+1]:=2;
            if points[(i*2)-1,j,k+1]=1
                then points[(i*2)-1,j,k+1]:=2;
            if points[(i*2)-1,j,k-1]=1
                then points[(i*2)-1,j,k-1]:=2;
            if points[(i*2)+1,j,k-1]=1
                then points[(i*2)+1,j,k-1]:=2;
        end;
     end;
end;

  procedure third;
  begin
    for i:=0 to 17 do begin
     if points[(i*2)+1,j,k]=2
          then
     begin
        if points[(i*2)+3,j,k]=1
              then points[(i*2)+3,j,k]:=2;
        if points[(i*2)-1,j,k]=1
              then points[(i*2)-1,j,k]:=2;
        if points[(i*2)+1,j+2,k]=1
              then  points[(i*2)+1,j+2,k]:=2;
        if points[(i*2)+1,j-2,k]=1
              then  points[(i*2)+1,j-2,k]:=2;
        if points[(i*2)+1,j+1,k+m]=1
              then points[(i*2)+1,j+1,k+m]:=2;
        if points[(i*2)+1,j-1,k+m]=1
              then points[(i*2)+1,j-1,k+m]:=2;
        if points[(i*2)+2,j,k-m]=1
              then points[(i*2)+2,j,k-m]:=2;
        if points[(i*2),j,k-m]=1
              then points[(i*2),j,k-m]:=2;
     end;
```

```
      end;
       for i:=17 downto 0 do begin
        if points[(i*2)+1,j,k]=2 then begin
            if points[(i*2)+3,j,k]=1
                  then points[(i*2)+3,j,k]:=2;
            if points[(i*2)-1,j,k]=1
                  then points[(i*2)-1,j,k]:=2;
            if points[(i*2)+1,j+2,k]=1
                  then points[(i*2)+1,j+2,k]:=2;
            if points[(i*2)+1,j-2,k]=1
                  then  points[(i*2)+1,j-2,k]:=2;
            if points[(i*2)+1,j+1,k+m]=1
                  then points[(i*2)+1,j+1,k+m]:=2;
            if points[(i*2)+1,j-1,k+m]=1
                  then points[(i*2)+1,j-1,k+m]:=2;
            if points[(i*2)+2,j,k-m]=1
                  then points[(i*2)+2,j,k-m]:=2;
            if points[(i*2),j,k-m]=1
                  then points[(i*2),j,k-m]:=2;
          end;
       end;
      end;
procedure fourth;
   begin
     for i:=0 to 17 do begin
      if points[(i*2)+1,j,k]=2
           then
       begin
          if points[(i*2)+3,j,k]=1
                then points[(i*2)+3,j,k]:=2;
        if points[(i*2)-1,j,k]=1
                then points[(i*2)-1,j,k]:=2;
      if points[(i*2)+1,j+2,k]=1
                then  points[(i*2)+1,j+2,k]:=2;
       if points[(i*2)+1,j-2,k]=1
                then  points[(i*2)+1,j-2,k]:=2;
          if points[(i*2)+1,j+1,k-1]=1
                then points[(i*2)+1,j+1,k-1]:=2;
        if points[(i*2)+1,j-1,k-1]=1
                then points[(i*2)+1,j-1,k-1]:=2;
          if points[(i*2)+1,j+1,k+1]=1
                then points[(i*2)+1,j+1,k+1]:=2;
        if points[(i*2)+1,j-1,k+1]=1
                then points[(i*2)+1,j-1,k+1]:=2;
      end;
     end;
      for i:=17 downto 0 do begin
         if points[(i*2)+1,j,k]=2
                then
           begin
          if points[(i*2)+3,j,k]=1
                then points[(i*2)+3,j,k]:=2;
```

```
          if points[(i*2)-1,j,k]=1
                then points[(i*2)-1,j,k]:=2;
       if points[(i*2)+1,j+2,k]=1
                then  points[(i*2)+1,j+2,k]:=2;
        if points[(i*2)+1,j-2,k]=1
                then  points[(i*2)+1,j-2,k]:=2;
          if points[(i*2)+1,j+1,k-1]=1
                then points[(i*2)+1,j+1,k-1]:=2;
         if points[(i*2)+1,j-1,k-1]=1
                then points[(i*2)+1,j-1,k-1]:=2;
          if points[(i*2)+1,j+1,k+1]=1
                then points[(i*2)+1,j+1,k+1]:=2;
         if points[(i*2)+1,j-1,k+1]=1
                then points[(i*2)+1,j-1,k+1]:=2;
        end;
      end;
    end;
    procedure threed;
       begin
            draw(119,187,338,187,1);
              draw(338,187,517,149,1);
                draw(517,149,298,149,1);
                  draw(298,149,119,187,1);
                draw(119,76,338,76,1);
            draw(338,76,517,38,1);
              draw(517,38,298,38,1);
                draw(298,38,119,76,1);
                  draw(119,76,119,187,1);
                     draw(338,187,338,76,1);
                  draw(517,149,517,38,1);
                draw(298,149,298,38,1);
    sx:=300;sy:=150;
       for c:=0 to 36 do begin
             for b:=0 to 36 do begin
                   for a:=0 to 36 do begin
     if points[a,b,c]=2
       then plot((a*6)+sx,b+sy,1);
                                        end;
       sx:=sx-5
                                   end;
       sx:=300;
       sy:=sy-3;
                              end;
end;
   procedure twod;
       begin
       sx:=0;
            sy:=0;
       for c:=0 to 36 do begin
             for b:=0 to 36 do begin
                   for a:=0 to 36 do begin
```

```
        if points[a,b,c]=2
            then
                 plot(a+sx,b+sy,1);
                                      end;
                                  end;
       sx:=sx+60;
            if sx>602 then begin
                       sy:=sy+40;
                            sx:=0;
                             end;
                                    end;
 end;
procedure occupier;
   begin
              for k:= -2 to 47 do begin
                for j:=-2 to 47 do begin
                   for i:=-2 to 47 do
                       points[i,j,k]:=0;
                   end;
             end;
         for k:=0 to 9 do begin
             for j:=0 to 17 do begin
                for i:=0 to 18 do begin
         if random (1000)+1<=265
             then points [i*2,(2*j)+1,k*4]:=1;
                                    end;
                               end;
                          end;
             for k:=0 to 8 do begin
                  for j:=0 to 18 do begin
                             for i:=0 to 17 do begin
           if random (1000)+1<=265
             then points [(i*2)+1,j*2,(k*4)+2]:=1;
                                          end;
                                      end;
                               end;
                  for k:=0 to 17 do begin
                            for j:=0 to 17 do begin
                                    for i:=0 to 17 do begin
           if random (1000)+1<=265
             then points [(i*2)+1,(j*2)+1,(k*2)+1]:=1;
                                                        end;
                                                  end;
                                        end;
 end;
{*********              Main Program           *********}
   begin
      randomize;
           occupier;
        1:=0;
              write('dimension ?');
                      read (kbd,dim);
```

```
   hires;
first;
        repeat
             k:=0;
                  for y:=0 to 16  do begin
                       j:=(2*y)+1;
                        second;
                                        end;
                  for y:=16 downto 0 do begin
                       j:=(2*y)+1;
                        second;
                                          end;
                            k:=1;
                               m:=1;
                       for y:=0 to 16  do begin
                            j:=(2*y)+1;
                                 third;
                                        end;
                        for y:=16 downto 0 do begin
                             j:=(2*y)+1;
                                    third;
                                             end;
                          k:=2;
                        for y:=0 to 17  do begin
                             j:=(2*y);
                                  fourth;
                                        end;
                   for y:=17 downto 0 do begin
                        j:=(2*y);
                   fourth;
                                     end;
                      k:=3;
              m:=-1;
                        for y:=0 to 16  do begin
                             j:=(2*y)+1;
                                  third;
                                        end;
                        for y:=16 downto 0 do begin
                                  j:=(2*y)+1;
                             third;
                                          end;
                          k:=4;
                        for y:=0 to 16  do begin
                             j:=(2*y)+1;
                        second;
                                        end;
for y:=16 downto 0 do begin
   j:=(2*y)+1;
        second;
                        end;
   k:=5;
        m:=1;
```

```
for y:=0 to 16  do begin
     j:=(2*y)+1;
               third;
                    end;
          for y:=16 downto 0 do begin
                    j:=(2*y)+1;
                         third;
                                   end;
            k:=k+1;
               for y:=0 to 17  do begin
                    j:=(2*y);
                    fourth;
                                        end;
     for y:=17 downto 0 do begin
          j:=(2*y);
               fourth;
                                  end;
            k:=k+1;
               m:=-1;
          for y:=0 to 16  do begin
     j:=(2*y)+1;
               third;
                                  end;
     for y:=16 downto 0 do begin
          j:=(2*y)+1;
               third;
                    end;
      k:=k+1;
          for y:=0 to 16  do begin
               j:=(2*y)+1;
          second;
                              end;
     for y:=16 downto 0 do begin
               j:=(2*y)+1;
     second;
               end;
            k:=k+1;
        m:=1;
     for y:=0 to 16  do begin
          j:=(2*y)+1;
     third;
                              end;
     for y:=16 downto 0 do begin
          j:=(2*y)+1;third;
                                  end;
                k:=k+1;
for y:=0 to 17  do begin
          j:=(2*y);
     fourth;
               end;
     for y:=17 downto 0 do begin
          j:=(2*y);
```

```
                        fourth;
                                              end;
  k:=k+1;
       m:=-1;
      for y:=0 to 16  do begin
      j:=(2*y)+1;
third;
      end;
        for y:=16 downto 0 do begin
      j:=(2*y)+1;
third;
      end;
       k:=k+1;
         for y:=0 to 16  do begin
           j:=(2*y)+1;
second;
      end;
        for y:=16 downto 0 do begin
          j:=(2*y)+1;
second;
      end;
        k:=k+1;
   m:=1;
      for y:=0 to 16  do begin
          j:=(2*y)+1;
third;
      end;
        for y:=16 downto 0 do begin
         j:=(2*y)+1;
third;
      end;
      k:=k+1;
      for y:=0 to 17  do begin
         j:=(2*y);
fourth;
      end;
      for y:=17 downto 0 do begin
      j:=(2*y);
fourth;
      end;
         k:=k+1;
m:=-1;
      for y:=0 to 16  do begin
        j:=(2*y)+1;
third;
      end;
        for y:=16 downto 0 do begin
          j:=(2*y)+1;
third;
      end;
```

```
 k:=k+1;
       for y:=0 to 16  do begin
         j:=(2*y)+1;
second;
       end;
         for y:=16 downto 0 do begin
       j:=(2*y)+1;
second;
       end;
  k:=k+1;
    m:=1;
       for y:=0 to 16  do begin
         j:=(2*y)+1;
third;
       end;
         for y:=16 downto 0 do begin
       j:=(2*y)+1;
third;
       end;
  k:=k+1;
       for y:=0 to 17  do begin
          j:=(2*y);
fourth;
       end;
          for y:=17 downto 0 do begin
              j:=(2*y);
fourth;
       end;
k:=k+1;
     m:=-1;
          for y:=0 to 16  do begin
       j:=(2*y)+1;
third;
          end;
       for y:=16 downto 0 do begin
              j:=(2*y)+1;
third;
       end;   k:=k+1;
         for y:=0 to 16  do begin
          j:=(2*y)+1;
second;
       end;
          for y:=16 downto 0 do begin
               j:=(2*y)+1;
second;
       end;
   k:=k+1;
       m:=1;
           for y:=0 to 16  do begin
       j:=(2*y)+1;
third;
       end;
```

```
      for y:=16 downto 0 do begin
        j:=(2*y)+1;
third;
      end;
  k:=k+1;
      for y:=0 to 17  do begin
         j:=(2*y);
fourth;
      end;
        for y:=17 downto 0 do begin
           j:=(2*y);
fourth;
      end;
  k:=k+1;
     m:=-1;
         for y:=0 to 16  do begin
               j:=(2*y)+1;
third;
      end;
        for y:=16 downto 0 do begin
           j:=(2*y)+1;
third;
      end;
  k:=k+1;
      for y:=0 to 16  do begin
         j:=(2*y)+1;
second;
      end;
        for y:=16 downto 0 do begin
           j:=(2*y)+1;
second;
      end;
  k:=k+1;
m:=1;
      for y:=0 to 16  do begin
         j:=(2*y)+1;
third;
      end;
        for y:=16 downto 0 do begin
      j:=(2*y)+1;
third;
      end;
 k:=k+1;
      for y:=0 to 17  do begin
         j:=(2*y);
fourth;
      end;
        for y:=17 downto 0 do begin
      j:=(2*y);
fourth;
      end;
 k:=k+1;
```

```
    m:=-1;
      for y:=0 to 16  do begin
        j:=(2*y)+1;
third;
      end;
        for y:=16 downto 0 do begin
      j:=(2*y)+1;
third;
      end;
  k:=k+1;
      for y:=0 to 16  do begin
      j:=(2*y)+1;
second;
      end;
         for y:=16 downto 0 do begin
      j:=(2*y)+1;
second;
      end;
k:=k+1;
     m:=1;
      for y:=0 to 16  do begin
        j:=(2*y)+1;
third;
      end;
        for y:=16 downto 0 do begin
      j:=(2*y)+1;
third;
      end;
  k:=k+1;
      for y:=0 to 17  do begin
         j:=(2*y);
fourth;
      end;
        for y:=17 downto 0 do begin
          j:=(2*y);
fourth;
      end;
 k:=k+1;
   m:=-1;
      for y:=0 to 16  do begin
        j:=(2*y)+1;
third;
      end;
      for y:=16 downto 0 do begin
         j:=(2*y)+1;
third;
      end;
   k:=k+1;
      for y:=0 to 16  do begin
         j:=(2*y)+1;
second;
      end;
```

```
        for y:=16 downto 0 do begin
         j:=(2*y)+1;
second;
      end;
  k:=k+1;
    m:=1;
       for y:=0 to 16  do begin
         j:=(2*y)+1;
third;
      end;
        for y:=16 downto 0 do begin
            j:=(2*y)+1;
third;
      end;
 k:=k+1;
      for y:=0 to 17  do begin
         j:=(2*y);
fourth;
      end;
      for y:=17 downto 0 do begin
             j:=(2*y);
fourth;
      end;
          if dim='3' then threed else twod;
      k:=36;
           for y:=0 to 16  do begin
      j:=(2*y)+1;
second;
           end;
      for y:=16 downto 0 do begin
          j:=(2*y)+1;second;
      end;
      k:=35;
 m:=-1;
      for y:=0 to 16  do begin
      j:=(2*y)+1;
third;
      end;
      for y:=16 downto 0 do begin
      j:=(2*y)+1;
third;
      end;
        k:=34;
      for y:=0 to 17  do begin
      j:=(2*y);
fourth;
      end;
      for y:=17 downto 0 do begin
      j:=(2*y);
fourth;
      end;
         k:=33;
```

```
m:=1;
      for y:=0 to 16  do begin
      j:=(2*y)+1;
third;
      end;
      for y:=16 downto 0 do begin
      j:=(2*y)+1;
third;
      end;
        k:=32;
      for y:=0 to 16  do begin
      j:=(2*y)+1;
second;
      end;
      for y:=16 downto 0 do begin
      j:=(2*y)+1;
second;
      end;
      k:=31;
m:=-1;
      for y:=0 to 16  do begin
      j:=(2*y)+1;
third;
      end;
        for y:=16 downto 0 do begin
          j:=(2*y)+1;
third;
      end;
       k:=k-1;
      for y:=0 to 17  do begin
      j:=(2*y);
fourth;
      end;
       for y:=17 downto 0 do begin
        j:=(2*y);
fourth;
      end;
        k:=k-1;
  m:=1;
      for y:=0 to 16  do begin
      j:=(2*y)+1;
third;
      end;
      for y:=16 downto 0 do begin
      j:=(2*y)+1;
third;
      end;
      k:=k-1;
         for y:=0 to 16  do begin
      j:=(2*y)+1;
second;
      end;
```

```
          for y:=16 downto 0 do begin
           j:=(2*y)+1;
second;
       end;
        k:=k-1;
         m:=-1;
       for y:=0 to 16  do begin
         j:=(2*y)+1;
third;
       end;
         for y:=16 downto 0 do begin
       j:=(2*y)+1;
third;
       end;
        k:=k-1;
         for y:=0 to 17  do begin
       j:=(2*y);
fourth;
       end;
        for y:=17 downto 0 do begin
       j:=(2*y);
fourth;
       end;
         k:=k-1;
 m:=1;
        for y:=0 to 16  do begin
       j:=(2*y)+1;
 third;
       end;
       for y:=16 downto 0 do begin
         j:=(2*y)+1;
third;
       end;
         k:=k-1;
         for y:=0 to 16  do begin
       j:=(2*y)+1;
second;
       end;
         for y:=16 downto 0 do begin
           j:=(2*y)+1;
second;
       end;
         k:=k-1;
  m:=-1;
        for y:=0 to 16  do begin
          j:=(2*y)+1;
 third;
       end;
         for y:=16 downto 0 do begin
               j:=(2*y)+1;
third;
       end;
```

```
        k:=k-1;
            for y:=0 to 17  do begin
             j:=(2*y);
fourth;
       end;
          for y:=17 downto 0 do begin
             j:=(2*y);
fourth;
       end;
          k:=k-1;
m:=1;
       for y:=0 to 16  do begin
           j:=(2*y)+1;
third;
       end;
        for y:=16 downto 0 do begin
          j:=(2*y)+1;
third;
       end;
 k:=k-1;
        for y:=0 to 16  do begin
          j:=(2*y)+1;
second;
       end;
        for y:=16 downto 0 do begin
         j:=(2*y)+1;
second;
       end;
  k:=k-1;
 m:=-1;
        for y:=0 to 16  do begin
           j:=(2*y)+1;
third;
       end;
         for y:=16 downto 0 do begin
      j:=(2*y)+1;
third;
       end;
   k:=k-1;
        for y:=0 to 17  do begin
          j:=(2*y);
 fourth;
       end;
        for y:=17 downto 0 do begin
         j:=(2*y);
fourth;
       end;
  k:=k-1;
     m:=1;
      for y:=0 to 16  do begin
         j:=(2*y)+1;
third;
```

```
      end;
        for y:=16 downto 0 do begin
           j:=(2*y)+1;
third;
      end;
 k:=k-1;
      for y:=0 to 16  do begin
           j:=(2*y)+1;
second;
      end;
         for y:=16 downto 0 do begin
            j:=(2*y)+1;
second;
      end;
k:=k-1;
     m:=-1;
      for y:=0 to 16  do begin
         j:=(2*y)+1;
third;
      end;
        for y:=16 downto 0 do begin
           j:=(2*y)+1;
third;
      end;
k:=k-1;
      for y:=0 to 17  do begin
         j:=(2*y);
    fourth;
      end;
        for y:=17 downto 0 do begin
           j:=(2*y);
fourth;
       end;   k
:=k-1;
   m:=1;
      for y:=0 to 16  do begin
         j:=(2*y)+1;
third;
      end;
         for y:=16 downto 0 do begin
            j:=(2*y)+1;
third;
      end;
k:=k-1;
      for y:=0 to 16  do begin
         j:=(2*y)+1;
second;
      end;
         for y:=16 downto 0 do begin
            j:=(2*y)+1;
second;
       end;
```

```
 k:=k-1;
   m:=-1;
       for y:=0 to 16  do begin
         j:=(2*y)+1;
third;
       end;
         for y:=16 downto 0 do begin
            j:=(2*y)+1;
third;
       end;
         k:=k-1;
              for y:=0 to 17  do begin
       j:=(2*y);
fourth;
       end;
          for y:=17 downto 0 do begin
             j:=(2*y);
fourth;
       end;
  k:=k-1;
   m:=1;
       for y:=0 to 16  do begin
          j:=(2*y)+1;
third;
       end;
          for y:=16 downto 0 do begin
       j:=(2*y)+1;
third;
       end;
  k:=k-1;
       for y:=0 to 16  do begin
          j:=(2*y)+1;
second;
       end;
         for y:=16 downto 0 do begin
            j:=(2*y)+1;
second;
         end;
 k:=k-1;
   m:=-1;
       for y:=0 to 16  do begin
       j:=(2*y)+1;
third;
       end;
         for y:=16 downto 0 do begin
       j:=(2*y)+1;
third;
       end;
   k:=k-1;
       for y:=0 to 17  do begin
         j:=(2*y);
fourth;
```

```
      end;
         for y:=17 downto 0 do begin
      j:=(2*y);
fourth;
      end;
 k:=k-1;
    m:=1;
      for y:=0 to 16  do begin
         j:=(2*y)+1;
third;
      end;
       for y:=16 downto 0 do begin
         j:=(2*y)+1;
third;
      end;
 k:=k-1;
      for y:=0 to 16  do begin
          j:=(2*y)+1;
second;
      end;
        for y:=16 downto 0 do begin
          j:=(2*y)+1;
second;
      end;
  k:=k-1;
     m:=-1;
        for y:=0 to 16  do begin
          j:=(2*y)+1;
third;
      end;
        for y:=16 downto 0 do begin
           j:=(2*y)+1;
third;
       end;
  k:=k-1;
      for y:=0 to 17  do begin
          j:=(2*y);
fourth;
      end;
        for y:=17 downto 0 do begin
          j:=(2*y);
fourth;
      end;
         if dim='3' then threed else twod;
             until keypressed;
       read (kbd,dim);
         if dim='2' then begin hires; twod; end;
   if dim='3' then begin hires; threed;end;
  end.
```

Program III

Purpose: To calculate the percolation threshold value x_c in $Pr_xLa_{1-x}F_3$.

Algorithm III

.Similar to Algorithm II.

Listing III

```
program 3D_percolation (for PrxLa1-xF3);
uses graph,crt;
 var
  site:array [0..38,0..38,0..38] of byte;
   mode,driver,yes,y,p,x,z,i,j,k,l,m,n:integer;
    path:string[15];
     yc:char;
procedure graphics;
  begin
  mode:=1; driver:=1; path:='cga.bgi';
  initgraph (driver,mode,path);
  end;
  procedure connector;
  begin
     case site [x,y,z] of
7: begin                                {master # + 6}
  if site[x+3,y+2,z-1]<>0 then site[x+3,y+2,z-1]:=10;
  if site[x+3,y+2,z+1]<>0 then site[x+3,y+2,z+1]:=10;
  if site[x,y,z-2]<>0 then site[x,y,z-2]:=7;
  if site[x,y,z+2]<>0 then site[x,y,z+2]:=7;
  if site[x-2,y-1,z-1]<>0 then site[x-2,y-1,z-1]:=10;
  if site[x-2,y-1,z+1]<>0 then site[x-2,y-1,z+1]:=10;
  if site[x+3,y,z-1]<>0 then site[x+3,y,z-1]:=11;
  if site[x+3,y,z+1]<>0 then site[x+3,y,z+1]:=11;
  if site[x+2,y+1,z]<>0 then site[x+2,y+1,z]:=9;
  if site[x-1,y-1,z]<>0 then site[x-1,y-1,z]:=12;
  if site[x+1,y+1,z-1]<>0 then site[x+1,y+1,z-1]:=8;
  if site[x+1,y+1,z+1]<>0 then site[x+1,y+1,z+1]:=8;
           end;
8: begin
  if site[x-2,y-2,z-1]<>0 then   site[x-2,y-2,z-1]:=12;
  if site[x-2,y-2,z+1]<>0 then   site[x-2,y-2,z+1]:=12;
  if site[x,y,z-2]<>0 then site[x,y,z-2]:=8;
  if site[x,y,z+2]<>0 then site[x,y,z+2]:=8;
  if site[x+3,y+1,z-1]<>0 then   site[x+3,y+1,z-1]:=12;
  if site[x+3,y+1,z+1]<>0 then   site[x+3,y+1,z+1]:=12;
  if site[x+2,y+1,z]<>0 then   site[x+2,y+1,z]:=10;
  if site[x+2,y-1,z]<>0 then   site[x+2,y-1,z]:=11;
  if site[x-1,y-1,z-1]<>0 then site[x-1,y-1,z-1]:=7;
```

```
   if site[x-1,y-1,z+1]<>0 then site[x-1,y-1,z+1]:=7;
   if site[x+1,y,z-1]<>0 then   site[x+1,y,z-1]:=9;
   if site[x+1,y,z+1]<>0 then   site[x+1,y,z+1]:=9;
              end;
9: begin
 if site[x,y,z-2]<>0 then   site[x,y,z-2]:=9;
 if site[x,y,z+2]<>0 then   site[x,y,z+2]:=9;
 if site[x+3,y+2,z]<>0 then site[x+3,y+2,z]:=7;
 if site[x+2,y+1,z]<>0 then   site[x+2,y+1,z]:=12;
 if site[x-2,y-1,z]<>0 then   site[x-2,y-1,z]:=7;
 if site[x+1,y+1,z-1]<>0 then site[x+1,y+1,z-1]:=10;
 if site[x+1,y+1,z+1]<>0 then site[x+1,y+1,z+1]:=10;
 if site[x+1,y-1,z-1]<>0 then   site[x+1,y-1,z-1]:=11;
 if site[x+1,y-1,z+1]<>0 then   site[x+1,y-1,z+1]:=11;
 if site[x-1,y,z-1]<>0 then   site[x-1,y,z-1]:=8;
 if site[x-1,y,z+1]<>0 then   site[x-1,y,z+1]:=8;
      end;
10: begin
 if site[x+2,y+1,z-1]<>0 then  site[x+2,y+1,z-1]:=7;
 if site[x+2,y+1,z+1]<>0 then  site[x+2,y+1,z+1]:=7;
 if site[x-3,y-2,z-1]<>0 then site[x-3,y-2,z-1]:=7;
 if site[x-3,y-2,z+1]<>0 then site[x-3,y-2,z+1]:=7;
 if site[x,y,z-2]<>0 then site[x,y,z-2]:=10;
 if site[x,y,z+2]<>0 then site[x,y,z+2]:=10;
 if site[x+3,y+2,z]<>0 then site[x+3,y+2,z]:=8;
 if site[x,y-2,z]<>0 then   site[x,y-2,z]:=11;
 if site[x-2,y-1,z]<>0 then  site[x-2,y-1,z]:=8;
 if site[x-1,y-1,z-1]<>0 then   site[x-1,y-1,z-1]:=9;
 if site[x-1,y-1,z+1]<>0 then   site[x-1,y-1,z+1]:=9;
 if site[x+1,y,z-1]<>0 then   site[x+1,y,z-1]:=12;
 if site[x+1,y,z+1]<>0 then   site[x+1,y,z+1]:=12;
  end;
11: begin
   if site[x,y,z-2]<>0 then site[x,y,z-2]:=11;
   if site[x,y,z+2]<>0 then site[x,y,z+2]:=11;
   if site[x+3,y-2,z]<>0 then site[x+3,y-2,z]:=8;
   if site[x-3,y,z-1]<>0 then site[x-3,y,z-1]:=7;
   if site[x-3,y,z+1]<>0 then site[x-3,y,z+1]:=7;
   if site[x+1,y+2,z-1]<>0 then site[x+1,y+2,z-1]:=12;
   if site[x+1,y+2,z+1]<>0 then site[x+1,y+2,z+1]:=12;
   if site[x,y+2,z]<>0 then   site[x,y+2,z]:=10;
   if site[x-2,y+1,z]<>0 then  site[x-2,y+1,z]:=8;
   if site[x-1,y+1,z-1]<>0 then   site[x-1,y+1,z-1]:=9;
   if site[x-1,y+1,z+1]<>0 then  site[x-1,y+1,z+1]:=9;
        end;
12: begin
 if site[x+2,y+2,z-1]<>0 then site[x+2,y+2,z-1]:=8;
 if site[x+2,y+2,z+1]<>0 then site[x+2,y+2,z+1]:=8;
 if site[x,y,z-2]<>0 then   site[x,y,z-2]:=12;
 if site[x,y,z+2]<>0 then  site[x,y,z+2]:=12;
 if site[x-3,y-1,z-1]<>0 then   site[x-3,y-1,z-1]:=8;
 if site[x-3,y-1,z+1]<>0 then  site[x-3,y-1,z+1]:=8;
```

```
 if site[x-1,y-2,z-1]<>0 then site[x-1,y-2,z-1]:=11;
 if site[x-1,y-2,z+1]<>0 then site[x-1,y-2,z+1]:=11;
 if site[x+1,y+1,z]<>0 then   site[x+1,y+1,z]:=7;
 if site[x-2,y-1,z]<>0 then  site[x-2,y-1,z]:=9;
 if site[x-1,y,z-1]<>0 then   site[x-1,y,z-1]:=10;
 if site[x-1,y,z+1]<>0 then  site[x-1,y,z+1]:=10;
      end;
         end;
              end;
    procedure major_down;
    begin
       case site [x,y,z] of
1: begin                                  {master # + 6}
   if site[x+3,y+2,z-1]>6 then site[x,y,z]:=7;
   if site[x+3,y+2,z+1]>6 then site[x,y,z]:=7;
   if site[x,y,z-2]>6 then site[x,y,z]:=7;
   if site[x,y,z+2]>6 then site[x,y,z]:=7;
   if site[x-2,y-1,z-1]>6 then site[x,y,z]:=7;
   if site[x-2,y-1,z+1]>6 then site[x,y,z]:=7;
   if site[x+3,y,z-1]=11 then site[x,y,z]:=7;
   if site[x+3,y,z+1]=11 then site[x,y,z]:=7;
   if site[x+2,y+1,z]=9 then site[x,y,z]:=7;
  if site[x-1,y-1,z]=12 then site[x,y,z]:=7;
  if site[x+1,y+1,z-1]=8 then site[x,y,z]:=7;
  if site[x+1,y+1,z+1]=8 then site[x,y,z]:=7;
       end;
2: begin
 if site[x-2,y-2,z-1]>6 then   site[x,y,z]:=8;
 if site[x-2,y-2,z+1]>6 then   site[x,y,z]:=8;
 if site[x,y,z-2]>6 then site[x,y,z]:=8;
 if site[x,y,z+2]>6 then site[x,y,z]:=8;
 if site[x+3,y+1,z-1]>6 then   site[x,y,z]:=8;
 if site[x+3,y+1,z+1]>6 then   site[x,y,z]:=8;
 if site[x+2,y+1,z]=10 then   site[x,y,z]:=8;
 if site[x+2,y-1,z]=11 then   site[x,y,z]:=8;
 if site[x-1,y-1,z-1]=7  then site[x,y,z]:=8;
 if site[x-1,y-1,z+1]=7  then site[x,y,z]:=8;
 if site[x+1,y,z-1]=9  then   site[x,y,z]:=8;
 if site[x+1,y,z+1]=9  then   site[x,y,z]:=8;
          end;
3: begin
       if site[x,y,z-2]>6 then   site[x,y,z]:=9;
       if site[x,y,z+2]>6 then   site[x,y,z]:=9;
       if site[x+3,y+2,z]>6 then site[x,y,z]:=9;
       if site[x+2,y+1,z]=12 then   site[x,y,z]:=9;
       if site[x-2,y-1,z]=7 then   site[x,y,z]:=9;
       if site[x+1,y+1,z-1]=10 then site[x,y,z]:=9;
       if site[x+1,y+1,z+1]=10 then site[x,y,z]:=9;
       if site[x+1,y-1,z-1]=11 then   site[x,y,z]:=9;
       if site[x+1,y-1,z+1]=11 then   site[x,y,z]:=9;
       if site[x-1,y,z-1]=8 then   site[x,y,z]:=9;
       if site[x-1,y,z+1]=8 then   site[x,y,z]:=9;
```

```
            end;
4: begin
 if site[x+2,y+1,z-1]>6 then  site[x,y,z]:=10;
 if site[x+2,y+1,z+1]>6 then  site[x,y,z]:=10;
 if site[x-3,y-2,z-1]>6 then site[x,y,z]:=10;
 if site[x-3,y-2,z+1]>6 then site[x,y,z]:=10;
 if site[x,y,z-2]>6 then site[x,y,z]:=10;
 if site[x,y,z+2]>6 then site[x,y,z]:=10;
 if site[x+3,y+2,z]>6 then site[x,y,z]:=10;
 if site[x,y-2,z]=11 then   site[x,y,z]:=10;
 if site[x-2,y-1,z]=8 then  site[x,y,z]:=10;
 if site[x-1,y-1,z-1]=9 then   site[x,y,z]:=10;
 if site[x-1,y-1,z+1]=9 then   site[x,y,z]:=10;
 if site[x+1,y,z-1]=12 then   site[x,y,z]:=10;
 if site[x+1,y,z+1]=12 then   site[x,y,z]:=10;
         end;
5: begin
   if site[x,y,z-2]>6 then site[x,y,z]:=11;
   if site[x,y,z+2]>6 then site[x,y,z]:=11;
   if site[x+3,y-2,z]>6 then site[x,y,z]:=11;
   if site[x-3,y,z-1]=7 then site[x,y,z]:=11;
   if site[x-3,y,z+1]=7 then site[x,y,z]:=11;
   if site[x+1,y+2,z-1]=13 then site[x,y,z]:=11;
   if site[x+1,y+2,z+1]=13 then site[x,y,z]:=11;
   if site[x,y+2,z]=10 then   site[x,y,z]:=11;
   if site[x-2,y+1,z]=8 then  site[x,y,z]:=11;
   if site[x-1,y+1,z-1]=9 then   site[x,y,z]:=11;
   if site[x-1,y+1,z+1]=9 then  site[x,y,z]:=11;
        end;
6: begin
 if site[x+2,y+2,z-1]>6 then site[x,y,z]:=12;
 if site[x+2,y+2,z+1]>6 then site[x,y,z]:=12;
 if site[x,y,z-2]>6 then   site[x,y,z]:=12;
 if site[x,y,z+2]>6 then  site[x,y,z]:=12;
 if site[x-3,y-1,z-1]>6 then   site[x,y,z]:=12;
 if site[x-3,y-1,z+1]>6 then  site[x,y,z]:=12;
 if site[x-1,y-2,z-1]=11 then site[x,y,z]:=12;
 if site[x-1,y-2,z+1]=11 then site[x,y,z]:=12;
 if site[x+1,y+1,z]=7  then   site[x,y,z]:=12;
 if site[x-2,y-1,z]=9  then  site[x,y,z]:=12;
 if site[x-1,y,z-1]=10 then   site[x,y,z]:=12;
 if site[x-1,y,z+1]=10 then  site[x,y,z]:=12;
       end;
          end;
               end;
  procedure generator;
                begin
      for z:=0 to 18 do begin
        for y:=0 to 5 do begin
           for x:=0 to 3 do begin
  if random (1000)+1 <=p
    then site [(x*10),(y*6)+3,(z*2)]:=1;
```

```
if random (1000)+1 <=p
  then site [(x*10)+1,(y*6)+4,(z*2)+1]:=2;
if random (1000)+1 <=p
  then site [(x*10)+2,(y*6)+4,(z*2)]:=3;
if random (1000)+1 <=p
  then site [(x*10)+3,(y*6)+5,(z*2)+1]:=4;
if random (1000)+1 <=p
  then site [(x*10)+3,(y*6)+3,(z*2)+1]:=5;
if random (1000)+1 <=p
  then site [(x*10)+4,(y*6)+5,(z*2)]:=6;
                          end;
                        end;
                      end;
     for z:=0 to 18 do begin
          for y:=0 to 6 do begin
                for x:=0 to 2 do begin
if random (1000)+1 <=p
  then site [(x*10)+5,(y*6),(z*2)]:=1;
if random (1000)+1 <=p
  then site [(x*10)+6,(y*6)+1,(z*2)+1]:=2;
if random (1000)+1 <=p
  then site [(x*10)+7,(y*6)+1,(z*2)]:=3;
if random (1000)+1 <=p then
  site [(x*10)+8,(y*6)+2,(z*2)+1]:=4;
if random (1000)+1 <=p
  then site [(x*10)+8,(y*6)+0,(z*2)+1]:=5;
if random (1000)+1 <=p
  then site [(x*10)+9,(y*6)+2,(z*2)]:=6;
                          end;
                        end;
                      end;
writeln ('Lattice generation complete....');
  end;
  procedure first_plane;
          begin
   for x:=0 to 38 do begin
       for y:=0 to 38 do begin
      if site [x,y,1]<>0
then site[x,y,1]:=site[x,y,1]+6;
        end;
      end;
end;
  procedure upward_sweep;
          begin
    for z:=1 to 37 do begin
          for x:=2 to 36 do begin
           for y:=2 to 36 do begin
     if site [x,y,z]>6 then connector;
      if (site [x,y,z]<7) and (site [x,y,z]<>0)
       then major_down;
  end;
end;
```

```
end;
    end;
  procedure downward_sweep;
    begin
      for z:=37 downto 1 do begin
         for x:=2 to 36 do begin
                for y:=2 to 36 do begin
       if site [x,y,z]>6 then connector;
      if (site [x,y,z]<7) and (site [x,y,z]<>0)
    then major_down;
           end;
  end;
       end;
         end;
  procedure left_sweep;
      begin
        for x:=36 downto 2 do begin
            for y:=2 to 36 do begin
                  for z:=1 to 37 do begin
        if site [x,y,z]>6 then connector;
           end;
    end;
       end;
              end;
  procedure right_sweep;
      begin
      for x:=2 to 36 do begin
           for y:=2 to 36 do begin
                for z:=1 to 37 do begin
       if site [x,y,z]>6 then connector;
           end;
  end;
     end;
           end;
    procedure front;
    begin
     for y:=2 to 36 do begin
            for x:=2 to 36 do begin
               for z:=1 to 37 do begin
            if site [x,y,z]>6 then connector;
          end;
        end;
               end;
        end;
  procedure back;
    begin
   for y:=36 downto 2 do begin
            for x:=2 to 36 do begin
             for z:=1 to 37 do begin
               if site [x,y,z]>6 then connector;
           end;
        end;
```

```
        end;
          end;
    procedure zeroer;
      begin
      for x:=0 to 38 do begin
     for y:=0 to 38 do begin
      for z:=0 to 38 do begin
       site[x,y,z]:=0;
       end;
           end;
                end;
    writeln ('Initializing is complete....');
      end;
      procedure plotter;
    begin
        for x:=0 to 38 do begin
          for y:=0 to 38 do begin
            for z:=0 to 5 do begin
             if site [x,y,z+6]>6
      then putpixel (x+(z*50),y,1);
     if site [x,y,z+12]>6 then
      putpixel (x+(z*50),y+40,1);
     if site [x,y,z+18]>6
      then putpixel (x+(z*50),y+80,1);
     if site [x,y,z+24]>6
      then putpixel (x+(z*50),y+120,1);
     if site [x,y,z+30]>6
      then putpixel (x+(z*50),y+160,1);
            end;
             end;
                  end;
                        end;
    procedure checkif;
      begin
    for x:=0 to 38 do begin
       for y:=0 to 38 do begin
      if site [x,y,37]>6 then yes:=1;
        end;
        end;
            end;
{Main Program}
    begin
      yes:=0;
      randomize;
      p:=200  ;
           clrscr;
                zeroer;
    generator;
      first_plane;
           graphics;
                repeat
     upward_sweep;
```

```
downward_sweep;
     front;
        back;   }
      plotter;
  until keypressed;
 end.
```

Program IV

Purpose: To simulate a PLD process in 2D and calculate parameters of interest.

Algorithm IV

occupy the sites randomly with p_1
set spin of occupied sites down randomly

start from center to walk randomly
to sites occupied and have spin down

keep track of time

vary site occupation (only for case iii)

vary spin orientation (for cases ii and iii)

continue until stuck or limits reached

calculate parameters of interest

end.

Listing IVa

```
program PLD_full_memory;   (Case i)
 uses graph,crt,printer;
  type lat1=array[0..173,0..347] of byte;
    large=^lat1;
var
  p,rms_sum,rms_r,n,d,time:real;
   ymax,ymin,
      centerx,centery,
        rndy2,rndy,rndx2,rndx,rms_count,rms_check,
      super,rt,k1,l1,xmax,xmin,i,j,k,l,m,wh,check,mode,
       drive:integer;
pth:string;
   lat,lat2:large;
procedure graphics;
begin
 drive:=7;
  mode:=0;
        pth:='herc.bgi';
  initgraph(drive,mode,pth);
end;
procedure occupy_and_spin;
```

```
begin
for j:=0 to 347 do begin
 for i:=0 to 173 do begin
  if random(10000)+1 >p then lat^[i,j]:=0
                        else lat^[i,j]:=1;
            end;
            end;
            for j:=0 to 347 do begin
 for i:=0 to 173 do begin
  if random(10000)+1 >p then lat2^[i,j]:=0
                        else lat2^[i,j]:=1;
            end;
            end;
end;
procedure pathfinder;
begin
 wh:=random(4)+1;
   time:=time+1;
         case wh of
           1: begin
     if k<=172 then begin
     if (lat^[k+1,1]=1) or (lat^[k+1,1]=3) then begin
                          k:=k+1;
                    check:=1;
                             lat^[k,1]:=3;
                          if k>xmax then xmax:=k;
                                         end;
                   end;
if k>172 then begin
     if (lat2^[k-173,1]=1) or (lat2^[k-173,1]=3) then
                    begin
                           k:=k+1;
                    check:=1;
                             lat2^[k-174,1]:=3;
                          if k>xmax then xmax:=k;
                             end;
end;
  end;
    2: begin
    if k<=174 then begin
          if (lat^[k-1,1]=1) or (lat^[k-1,1]=3) then
               begin
                          k:=k-1;
               check:=1;
        lat^[k,1]:=3;
   if k<xmin then xmin:=k;
end;
end;
  if k>174 then begin
     if (lat2^[k-175,1]=1) or (lat2^[k-175,1]=3) then
               begin
                        k:=k-1;
```

```
                                    check:=1;
                                     lat2^[k-174,l]:=3;
                                  if k<xmin then xmin:=k;
                                     end;
  end;
end;
    3: begin
    if k<=173 then begin
           if (lat^[k,l+1]=1) or (lat^[k,l+1]=3) then
              begin
                                      l:=l+1;
                    check:=1;
                                     lat^[k,l]:=3;
                                  if l>ymax then ymax:=l;
                                  end;
                                    end;
if k>173 then begin
     if (lat2^[k-174,l+1]=1) or (lat2^[k-174,l+1]=3) then
                    begin
                        l:=l+1;
               check:=1;
                                     lat2^[k-174,l]:=3;
                                  if l>ymax then ymax:=l;
                                     end;
end;
      end;
    4: begin
    if k<=173 then begin
           if (lat^[k,l-1]=1) or (lat^[k,l-1]=3) then
              begin
                                     l:=l-1;
                    check:=1 ;
                                     lat^[k,l]:=3;
                                   if l<ymin then ymin:=1;
end;
end;
if k>173 then begin
     if (lat2^[k-174,l-1]=1) or (lat2^[k-174,l-1]=3) then
                    begin
                        l:=l-1;
                                    check:=1;
                                     lat2^[k-174,l]:=3;
                                  if l<ymin then ymin:=1;
                                     end;
end;
  end;
      end;
end;

procedure fractal;
        begin
            n:=0;
for i:=xmin to xmax do begin
```

```
  for j:=ymin to ymax do begin
    if getpixel (i,j)=1 then n:=n+1;
    end;
        end;
d:=2*ln(n)/(ln(xmax-xmin)+ln(ymax-ymin));
restorecrtmode;
writeln ('d= ',d,' time= ',time);
end;
procedure rms;
 begin
  repeat
   rndx:=xmin+(random(xmax-xmin));
    rndy:=ymin+(random(ymax-ymin));
     if getpixel(rndx,rndy)=1 then rms_check:=1
                                  else rms_check:=0;
   until rms_check=1;
 repeat
   rndx2:=xmin+(random(xmax-xmin));
    rndy2:=ymin+(random(ymax-ymin));
     if getpixel(rndx2,rndy2)=1 then rms_check:=1
                                  else rms_check:=0;
                                    until rms_check=1;
        end;
   procedure rms_calc;
        begin
        rms_r:=sqrt(sqr(rndy2-rndy)+sqr(rndx2-rndx));
        rms_sum:=rms_sum+rms_r;
        end;

begin
 graphics;
    randomize;
     p:=5700;
         time:=0;
    new(lat);
       new (lat2);
     occupy_and_spin;
        check:=0;
            k:=173;
                 l:=173;
               m:=1;
      xmax:=k;
            xmin:=k;
                 k1:=k;
                      l1:=1;
                        ymax:=1;
            ymin:=1;
                 lat^[k,l]:=3;
                           putpixel (k,l,1);
repeat
 pathfinder;
putpixel (k,l,1);
until keypressed;
```

```
 fractal;
rms_sum:=0;
for rms_count:=1 to 1000 do begin
   rms;
    rms_r:=0;
    rms_calc;
     end;
    dispose (lat);
         dispose (lat2);
rms_sum:=rms_sum/1000;
restorecrtmode;
writeln (lst,' mld:',rms_sum,'   p:',p);
     end.
```

Listing IVb

```
 program PLD_Sitememory;   {Case ii}
uses graph,crt,printer;
type
lat1 = array[0..173,0..347] of byte;
 large=^lat1;

   var
prob1, prob2, ymax,ymin,
spir,spin,centerx,centery,count,
xmax,xmin,i,j,k,l,m,wh,check,mode,drive,span,spana:integer;
pth:string;
    lat,lat2:large;     d,n,na,timea,da,time:real;

procedure graphics;
   begin
drive:=7;
   mode:=0;
        pth:='herc.bgi';
   initgraph(drive,mode,pth);
    setgraphmode(0);
end;

procedure occupy_and_spin;
       begin
              for i:=0 to 173 do begin
 for j:=0 to 347 do begin
  if random(1000)+1 >prob then lat^[i,j]:=0
                     else lat^[i,j]:=1;
                   end;
             end;
             for i:=0 to 173 do begin
    for j:=0 to 347 do begin
  if random(1000)+1 >prob then lat2^[i,j]:=0
                   else lat2^[i,j]:=1;
             end;
             end;
                        end;

procedure pathfinder;
       begin
   time:=time+1;
   wh:=random(4)+1;
     spir:=random(1000)+1;
  case wh of
    1: begin
if k<=172 then begin
if (lat^[k+1,l]=1) and (spir<=spin) then begin
                    putpixel(k+1,l,1);
                             k:=k+1;
check:=1;
                      if k>xmax then xmax:=k;
                         end;
```

```
end;
if k>172 then begin
     if (lat2^[k-173,l]=1) and (spir<=spin) then begin
                              putpixel(k+1,l,1);
                          k:=k+1;
check:=1;
                                if k>xmax then xmax:=k;
                              end;
end;
  end;
    2: begin
         if k<=174 then begin
    if (lat^[k-1,l]=1) and (spir<=spin) then begin
                         putpixel(k-1,l,1);
        k:=k-1;
check:=1;
   if k<xmin then xmin:=k;
        end;
end;
  if k>174 then begin
     if (lat2^[k-175,l]=1)  and (spir<=spin) then begin
                          putpixel(k-1,l,1);
k:=k-1;
   check:=1;
          if k<xmin then xmin:=k;
                                      end;
  end;
end;
 3: begin
    if k<=173 then begin
    if (lat^[k,l+1]=1) and (spir<=spin) then begin
                              putpixel(k,l+1,1);
l:=l+1;
   check:=1;
                        if l>ymax then ymax:=l;
                        end;
                          end;
if k>173 then begin
     if (lat2^[k-174,l+1]=1) and (spir<=spin) then begin
                              putpixel(k,l+1,1);
   l:=l+1;
        check:=1;
                        if l>lmax then ymax:=l;
                                      end;
end;
      end;
    4: begin
    if k<=173 then begin
           if (lat^[k,l-1]=1)  and (spir<=spin) then begin
                       putpixel(k,l-1,1);
   l:=l-1;
        check:=1;
```

```
                    if l<ymin then ymin:=l;
   end;
        end;
if k>173 then begin
if (lat2^[k-174,l-1]=1)  and (spir<=spin) then begin
                     putpixel(k,l-1,1);
   l:=l-1;
        check:=1;
                  if l<ymin then ymin:=l;
                                   end;
end;
  end;
      end;
end;

procedure fractal;
       begin
              n:=0   ;
for i:=xmin to xmax do begin
for j:=ymin to ymax do begin
             if getpixel (i,j)=1 then n:=n+1;
             end;
                  end;
if (xmax-xmin) > (ymax-ymin) then
     span:=xmax-xmin else
        span:=ymax-ymin;
d:=2*ln(n)/(ln(xmax-xmin)+ln(ymax-ymin));
end;

begin
 graphics;
   randomize;
    spin:=1000;
     prob:=600;
new(lat);
   new (lat2);
     occupy_and_spin;
                k:=173;l:=173;
                        m:=1;
              xmax:=k;
                  xmin:=k;
                     ymax:=l;
                       ymin:=l;
                            putpixel (k,l,1);
        time:=0;
 repeat
  pathfinder;
   until keypressed or (k=0) or (l=0)
             or (l=347) or (k=347);
    fractal;
        dispose (lat);
dispose (lat2);
 writeln (lst,'Spin=',spin,' Site=',prob);
```

```
writeln (lst,'D=',d,' mass=',n,' time=',time,' span=',span);
  end.
```

Listing IVc

```
program PLD_no_memory;  (Case iii)
  uses graph,crt;
var
n1,n2,prob1,prob2,times,driver,mode,
  i,j,k,l,m,wh,check:integer;
wrd:string;
mass,atime,time,RT1,r1,r2,rt,centerx,
  centery,ymax,ymin,xmax,xmin:real;

procedure graphics;
  begin
driver :=7;
  mode:=0 ;
       wrd:='herc.bgi';
initgraph(driver,mode,wrd);
end;

procedure fractal;
begin
  centerx:=xmin+((xmax-xmin)/2);
       centery:=ymin+((ymax-ymin)/2);
       r2:=(sqrt(sqr(xmax-xmin)+sqr(ymax-ymin)))/2;
r1:=r2 /2; r2:=sqr(r2); r1:=sqr(r1);
for i:=round(centerx-sqrt(r2)) to
       round(centerx+sqrt(r2)) do begin
for j:=round(centery-sqrt(r2)) to r
       ound(centery+sqrt(r2)) do begin
   rt:=sqr(i-centerx)+sqr(j-centery);
 if (rt<=r1) and (getpixel(i,j)=1)
                  then n1:=n1+1;
  rt1:=sqr(i-centerx)+sqr(j-centery);
 if (rt1<=r2) and (getpixel(i,j)=1)
                  then n2:=n2+1;
    end;
     end;
restorecrtmode;
writeln ('y ',ymin,' ',ymax,' x ',xmin,' ',xmax);
writeln ('r1 ',r1,' r2 ',r2);
writeln ('n1 ',n1,' n2 ',n2);
writeln ('cx ',centerx,' cy ',centery);
writeln ('D ',ln(n2/n1)/ln(2));
end;
procedure pathfinder;
begin
repeat
  wh:=random(4)+1;
   n1:=random (1000)+1;
    n2:=random (1000)+1;
  case wh of
       1: begin   if (n1<=prob1) and (n2<=prob2)
       then begin
```

```
          putpixel (k+1,l,1);
            k:=k+1;
if k>xmax then xmax:=k;
end;
       end;
       2: begin   if (n1<=prob1) and (n2<=prob2)
            then begin
          putpixel (k-1,l,1);
                 k:=k-1;
if k<xmin then xmin:=k;
                 end;
       end;
       3: begin   if (n1<=prob1) and (n2<=prob2)
            then begin
          putpixel (k,l+1,1);
                 l:=l+1;
            if l>ymax then ymax:=l;
            end;
      end;
       4: begin   if (n1<=prob1) and (n2<=prob2)
                 then begin
          putpixel (k,l-1,1);
                 l:=l-1;
if l<ymin then ymin:=l;
       end;
end;
until (keypressed) or (k=0) or (l=0)
            or (l=347) or (k=347);
end;

begin
  graphics;
        mass:=0;
  randomize;
   k:=174;
       l:=174;
             xmin:=174;
            xmax:=174;
       ymin:=174;
  ymax:=174;
    putpixel (k,l,1);
     prob1:=800;
            prob2:=1000;
       pathfinder;
fractal;
end.
```

Appendix II

Derivation of the equation to calculate D_H

For a cluster of a finite size, made up of particles, represented by discs of radius R_o (Fig. AII.1), the fractal dimension is given by[36]

$$D_H = \log M/\log [\rho(R/R_0)], \qquad \text{(AII.1)}$$

where ρ, R, and M are the density, the radius of the smallest circle containing the cluster, and the number of unit discs inside this circle, respectively. Eq. (AII.1) can, alternatively, be written as

$$D_H = 2 \log M/\log[\rho\ (A/A_o)], \qquad \text{(AII.2)}$$

where A and A_o are the areas of the circles of radii R and R_o respectively.

For the present calculations, a cluster is considered to consist of particles, being represented as rectangles (Fig. AII.2). Eq. (AII.2) can then be expressed as:

$$D_H = 2 \log M/ \log [\rho\ (ab/a_o b_o)], \qquad \text{(AII.3)}$$

where a_o and b_o are the sides of the rectangle, representing a particle.

For perfect tiling, the area of each particle is matched exactly by the unit rectangle: $a_o b_o = 1$, with $\rho = 1$. Eq. (AII.3), then, leads to

$$D_H = 2 \log M / \log (ab). \qquad (V.1)$$

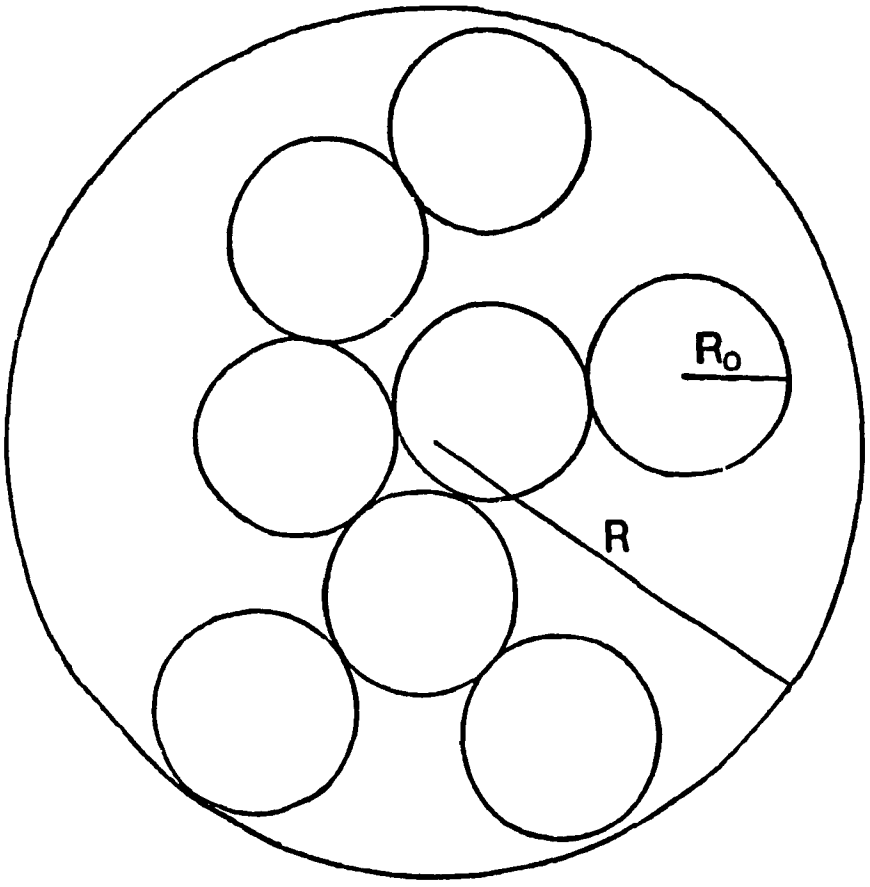

Figure AII.1. A cluster of a finite size of a circle of radius R, constituted by unit discs of radius R_o.

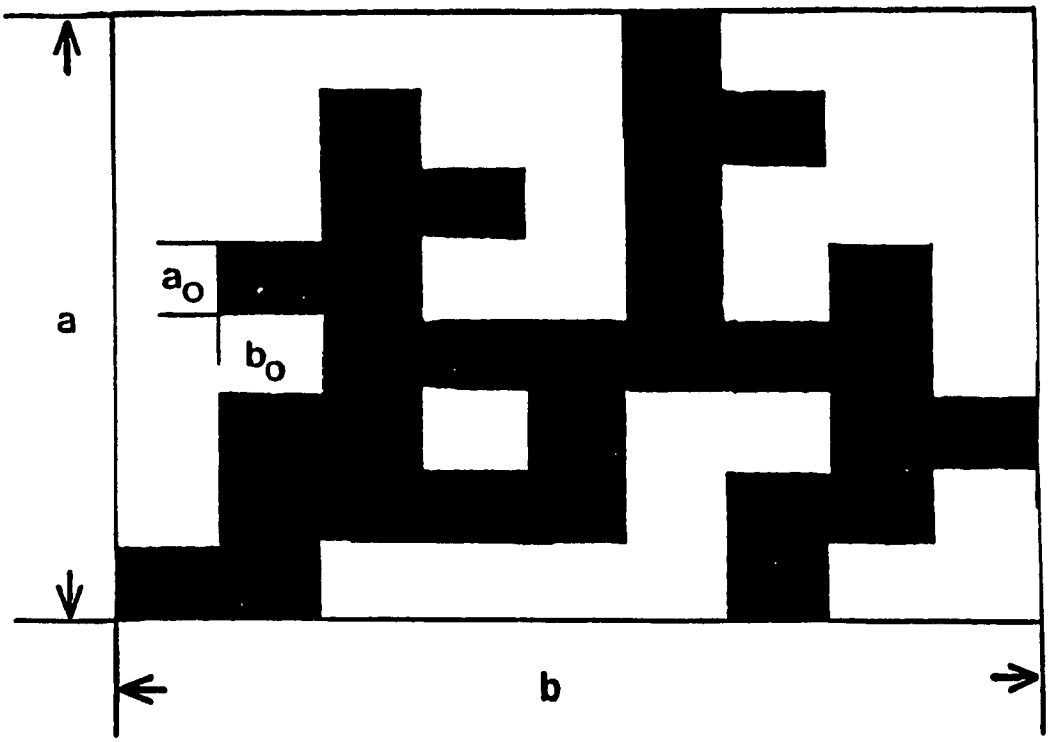

Figure AII.2 A rectangular cluster of size a x b, constituted by unit rectangles of dimension a_o x b_o each, as used in the simulation considered in this paper.

Appendix III

Publications

RAPID COMMUNICATIONS

PHYSICAL REVIEW B VOLUME 39, NUMBER 4 1 FEBRUARY 1989

Calculation of the paramagnetic host spin-lattice relaxation time from impurity-ion EPR linewidth

Sushil K. Misra and Ufuk Orhun
Department of Physics, Concordia University, 1455 De Maisonneuve Boulevard West, Montreal, Quebec, Canada H3G 1M8
(Received 21 June 1988)

An expression, appropriate to calculate the spin-lattice relaxation time (SLRT) of the host paramagnetic ions, using the EPR linewidths of the impurity ion, is derived by use of the second moment for crystals consisting of two different kinds of spins. Estimations have been made of the SLRT of the Yb^{3+} ion in Gd^{3+}-doped $YbCl_3 \cdot 6H_2O$ and $LiYbF_4$ single crystals, as well as that of the Co^{2+} ion in a Mn^{2+}-doped $Cs_2Co(SeO_4)_2 \cdot 6H_2O$ single crystal. Significant differences are found in the values of SLRT as calculated using the presently derived expression from those calculated using the commonly used expression.

I. INTRODUCTION

The effect of dipolar interactions on resonance line shape was first treated by Waller,[1] and later by Broer[2] and Van Vleck.[3] Subsequently, Anderson and Weiss[4] presented a theory, which treats the motion of spins induced by the exchange interactions as a stochastic process, and makes it possible to describe the line shape in a fairly reasonable way. This stochastic theory was developed further by Anderson.[5] His method goes a step further than the moment method of Van Vleck.[3] More quantitative calculations of relaxation times were later reported by Mitsuma.[6]

It has been shown by Anderson and Weiss,[4] that rapid motions of the host spins narrow the impurity EPR lines in crystals, consisting of only one paramagnetic specie. Anderson and Weiss[4] considered the exchange interactions between the ions as the source of random spin motions, with the rate of motion being ω_e. They derived the linewidth as

$$\Delta H = \tfrac{1}{2}\pi H_{\rm dip}^2/H_e . \tag{1}$$

In Eq. (1), H_e is not really a magnetic field but rather ω_e, expressed in magnetic-field units, and $H_{\rm dip}$ is the linewidth due to dipole-dipole interactions. Anderson and Weiss[4] also showed that, subject to the condition $H_e \gg H_{\rm dip}$, $H_{\rm dip}^2 = h^2(\Delta\nu^2)_{\rm av}/g^2\beta^2$, where h is Planck's constant, g is the Lande's factor of the paramagnetic ions, β is the Bohr magneton, and $(\Delta\nu^2)_{\rm av}$ is the second moment (mean-square deviation from Larmor frequency). As a sample calculation, Anderson and Weiss[4] used the second moment for a simple cubic lattice with one kind of magnetic ion, given by Van Vleck,[3] as

$$(\Delta\nu^2)_{\rm av} = 36.8 g^4\beta^4 h^{-2} d^{-6}[\tfrac{1}{2}S(S+1)] \times (\lambda_1^4+\lambda_2^4+\lambda_3^4-0.187) , \tag{2}$$

where d, S, and λ_1, λ_2, λ_3 are the spacing of a simple cubic lattice, the effective spin, and the direction cosines of the applied field, relative to the principal cubic axes, respectively. Using Eq. (2), Anderson and Weiss[4] showed that

$$H_{\rm dip}^2 = 5.1(g\beta n)^2 S(S+1) , \tag{3}$$

where n is the number of host paramagnetic spins per unit volume.

In order to explain the highly temperature-dependent EPR linewidths, Mitsuma[6] suggested that the spin-lattice relaxation process might be responsible for the narrowing of EPR lines in a way, which is similar to that caused by the exchange interactions, described above. In parallelism to the theory of Anderson and Weiss,[4] Mitsuma[6] derived the EPR linewidth as

$$\Delta H = \tfrac{1}{2}\pi 2H_{\rm dip}^2/H_{\rm mod} . \tag{4}$$

The $\frac{1}{2}\pi$ factor, both in Eqs. (1) and (4), is due to the extreme narrowing, as pointed out by Anderson and Weiss.[4] The factor of 2 appearing in Eq. (4) is due to Lorentzian line shape of the narrowed resonance lines. As seen from Eq. (4), the quantity $H_{\rm mod}$ replaces H_e in Eq. (1). Again, it is noted that $H_{\rm mod}$ is not a magnetic field, but rather the host-ion spin-lattice relaxation time, $\tau_{\rm host}$, expressed in magnetic-field units, i.e.,[6]

$$H_{\rm mod} = h/\tau_{\rm host} g\beta \tag{5}$$

($\tau_{\rm host}$ will be referred to as SLRT, hereafter).

Combining Eqs. (3), (4), and (5), $\tau_{\rm host}$ can be expressed as

$$\tau_{\rm host} = \frac{3h\Delta H}{102(g\beta)^3 n^2 S(S+1)} . \tag{6}$$

Thus, $\tau_{\rm host}$ can be calculated from Eq. (6), using the experimentally observed EPR linewidth (ΔH).

As stated earlier, Eq. (3) is derived for a simple cubic lattice, consisting of only one kind of paramagnetic ion. Thus, Eq. (6) is invalid for crystals, which consist of two different kinds of paramagnetic ions.

Recently, numerous EPR experimental studies have been reported on doped crystals, wherein the paramagnetic host ions are different from impurity paramagnetic ions.

Papers continue to be published in the literature dealing with such crystals, where Eq. (6) has been employed to calculate the SLRT of the host ions (for example, see Refs. 7–12). However, as discussed above, use of Eq. (6) is not, indeed, valid in such cases.

It is the purpose of this paper to derive an equation, appropriate to calculate the SLRT of paramagnetic host ions in crystals from the impurity ion EPR linewidths, taking into account the presence of two different kinds of spins in the crystal. The derivation of this equation is given in Sec. II. Sample calculations and discussion are given in Sec. III, followed by the concluding remarks in Sec. IV.

II. THEORY

The second moment, for crystals, containing two kinds of paramagnetic spins, is given by Van Vleck,[3] as follows:

$$(\Delta\nu^2)_{\text{IIav}} = \tfrac{1}{3}S(S+1)\hbar^{-2}\sum_k[-3g^2\beta^2r_{jk}^{-3}(\tfrac{1}{3}\gamma_{jk}^2-\tfrac{1}{2})]^2+\tfrac{1}{3}S'(S'+1)\hbar^{-2}\sum_{k'}[(-2z^2J_{jk'})+(1-3\gamma_{jk'}^2)gg'\beta^2r_{jk'}^{-3}]^2. \tag{7}$$

In Eq. (7), S, r_{jk}, γ_{jk}, z, and $J_{jk'}$ represent the effective spin, the distance between the j and k ions, the direction cosine of r_{jk} with the external field, the number of electrons not in complete shells of the host ions, and the exchange integral between the host (k') and the impurity ions (j), respectively; the primed quantities describe the host ions, while the unprimed ones the impurity ion. The external field is assumed to be along the z axis.[3] The impurity and host Lande factors (g,g') are assumed to be sufficiently different from each other, so that the resonances of these two different ions do not overlap each other.[3] [It should be pointed out, here, that it is the impurity ion (unprimed) whose resonance is of interest.] Assuming that the distances between the impurity ions are sufficiently large, the first term in Eq. (7) can be neglected, compared to the other terms. If the number of the neighbors, to be considered, is limited to N, Eq. (7) reduces to

$$(\Delta\nu^2)_{\text{IIav}} = \tfrac{1}{3}S'(S'+1)\hbar^{-2}\left[NJ_p^2+(gg')^2\beta^4\mu_0^2\sum_{k'}^{N}(1-3\gamma_{jk'}^2)^2r_{jk'}^{-6}+2J_pgg'\beta^2\mu_0\sum_{k'}^{N}(1-3\gamma_{jk'}^2)r_{jk'}^{-3}\right]. \tag{8}$$

In Eq. (8), J_p is the average host-impurity pair-exchange constant. (μ_0 is the permeability constant, required for the purpose of calculations in SI units.) In reducing Eq. (7) to Eq. (8), it should be noted that J_p, the average host-impurity exchange constant,[13] stands for the quantity $\bar{A}_{jk'}=-2z^2J_{jk'}$, as defined by Van Vleck;[3] the same value (J_p) for $A_{jk'}$ has been assumed for all the neighbors taken into consideration. In magnetic field units, the full width at half peak (FWHP) of a Gaussian distribution, taking into account both the dipole-dipole and exchange interactions, can be written as

$$H_{\text{dip ex}}^2 = (2.35)^2\hbar^2(\Delta\nu^2)_{\text{IIav}}/g^2\beta^2, \tag{9}$$

where $(\Delta\nu^2)_{\text{IIav}}$ is as given by Eq. (8). Equation (9) is a generalization of Eq. (3), which is valid for crystals consisting of only one kind of paramagnetic ion, to the presence of two dissimilar kinds of paramagnetic ion in the crystal. It should be noted here, that the second moment [and, therefore, Eq. (3) which depends on it] for crystals consisting of only one kind of paramagnetic ions does not include exchange terms, whereas the second moment [and, therefore, Eq. (9) which depends on it] for crystals consisting of two different kinds of paramagnetic ions, does include exchange between dissimilar ions as well. Further, the exchange between similar ions does not appear in the expression for the second moment.[3] Replacing H_{dip}^2 in Eq. (4) by $H_{\text{dip ex}}^2$, one obtains

$$\Delta H = \tfrac{1}{2}\sqrt{2}H_{\text{dip ex}}^2/H_{\text{mod}}. \tag{10}$$

Using Eqs. (5), (8), (9), and (10) τ_{host}, the SLRT of the host ions in crystals with two different kinds of paramagnetic ingredients, can be expressed as

$$\tau_{\text{host}} = (3\Delta Hg^2\beta)/(110\hbar g'^2(\Delta\nu^2)_{\text{IIav}}), \tag{11}$$

where ΔH is the impurity-ion EPR linewidth FWHP, observed experimentally; the primed Landé factor is that for the host, while the unprimed one refers to the impurity.

Equation (11), derived using the second moment for crystals with two kinds of magnetic ions, is, really, the appropriate equation for the usual EPR situation, i.e., for crystals consisting of paramagnetic host ions, doped with impurity paramagnetic ions, which are different from the host ions. One should, therefore, use Eq. (11) in order to calculate the SLRT of the host ions, rather than Eq. (6), which is valid for crystals consisting of only one kind of paramagnetic ions.

III. ILLUSTRATIVE EXAMPLES AND DISCUSSION

Using Eq. (11), the SLRT of the host paramagnetic Yb^{3+} ions in Gd^{3+}-doped $YbCl_3\cdot 6H_2O$ and $LiYbF_4$ and that of the host paramagnetic Co^{2+} ions in Mn^{2+}-doped

TABLE I. The spin-lattice relaxation times (SLRT, in sec) of the host Yb^{3+} ions in $YbCl_3 \cdot 6H_2O$ and in $LiYbF_4$, and that of the host Co^{2+} ions in $Cs_2Co(SeO_4)_2 \cdot 6H_2O$ at room temperature, as calculated using the correct Eq. (11), and those calculated using the incorrect Eq. (6). The required g,g' values have also been included.

Lattice	Impurity ion (g value)	Host ion (g' value)	SLRT [Eq. (11)]	SLRT [Eq. (6)]
$YbCl_3 \cdot 6H_2O$	Gd^{3+} (1.992)	Yb^{3+} (1.339)	1.0×10^{-13}	4.0×10^{-14}
$LiYbF_4$	Gd^{3+} (1.992)	Yb^{3+} (1.339)	4.3×10^{-14}	2.5×10^{-11}
$Cs_2Co(SeO_4)_2 \cdot 6H_2O$	Mn^{2+} (1.998)	Co^{2+} (7.1)	3.7×10^{-13}	1.8×10^{-12}

$Cs_2Co(SeO_4)_2 \cdot 6H_2O$ single crystals at room temperature are estimated in this section for illustration. Equation (11) requires rather detailed crystal structure information, such as the location of the host ions with respect to the impurity ion and the external magnetic field for the evaluation of lattice sums required in $(\Delta\nu^2)_{\text{IIa}}$ [Eq. (8)]. The following crystal structures and EPR linewidth data were used for the estimation of SLRT.

(a) *Gd^{3+}-doped $YbCl_3 \cdot 6H_2O$.* The structure of this crystal is monoclinic, with the unit cell parameters, $a = 0.953$ nm, $b = 0.643$ nm, $c = 0.780$ nm, and $\beta = 93°40'$.[14] The average Gd^{3+} EPR linewidth, with the external magnetic field being along the z axis, at room temperature, was reported to be 14×10^{-4} T.[14]

(b) *Gd^{3+}-doped $LiYbF_4$.* The structure of this crystal is tetragonal, with the space group $I4_1/a$, and the lattice constants $a = 0.51335$ nm, and $c = 1.0588$ nm.[15] The average Gd^{3+} EPR linewidth, with the external magnetic field being along the z axis, was measured to be 10×10^{-4} T.[16]

(c) *Mn^{2+}-doped $Cs_2Co(SeO_4)_2 \cdot 6H_2O$.* The structure of this crystal is monoclinic,[11] the unit-cell parameters are not known. Therefore, the unit-cell parameters of the isostructural crystal $(NH_4)_2Mg(SeO_4)_2 \cdot 6H_2O$ were used: $a = 0.94$ nm, $b = 1.27$ nm, $c = 0.63$ nm, and $\beta = 106°$.[17] The average Mn^{2+} EPR linewidth, with the external magnetic field being along the z axis, has been reported to be 14×10^{-4} T.[11]

In the present calculations, up to third-nearest neighbors, for the three cases, were taken into account.

SLRT of Yb^{3+} in Gd^{3+}-doped $YbCl_3 \cdot 6H_2O$ and Gd^{3+}-doped $LiYbF_4$, as well as that of Co^{2+} in Mn^{2+}-doped $Cs_2Co(SeO_4)_2 \cdot 6H_2O$, calculated using Eq. (11), are given in Table I, which also lists the g and g' values used. For comparison purposes, SLRT values, as calculated using the incorrect Eq. (6), are also included in Table I. The exchange constant J_p, for a Mn^{2+}-Co^{2+} pair is not known; various typical J_p values (0.2–4 GHz), were, therefore, used to calculate the SLRT of Co^{2+}. Since the resulting SLRT values did not vary in order of magnitude for these J_p values, only the average SLRT value is listed in Table I. The exchange constant for a Gd^{3+}-Yb^{3+} pair has been calculated to be 2.8 GHz in $LiYbF_4$.[18] As for the exchange interaction in $YbCl_3 \cdot 6H_2O$, between Gd^{3+} and Yb^{3+} ions, it was assumed to be negligible, since the Gd^{3+}-Yb^{3+} distance in this crystal is considerably greater than that in $LiYbF_4$. As seen from Table I, the SLRT calculated using the correct Eq. (11), and those calculated using the incorrect Eq. (6), are quite different from each other. It should also be noted that the Yb^{3+} SLRT, as estimated from Eq. (11), is shorter in $LiYbF_4$ than that in $YbCl_3 \cdot 6H_2O$ at room temperature. On the other hand, the SLRT as estimated from Eq. (6) indicates that the opposite is true.[7,16] Physically, Yb^{3+} ions are expected to have shorter SLRT in $LiYbF_4$ than that in $YbCl_3 \cdot 6H_2O$, in accordance with that estimated from Eq. (11), since in this crystal the paramagnetic Yb^{3+} ions are packed more closely than they are in $YbCl_3 \cdot 6H_2O$. As well, one notes that the SLRT of Co^{2+} in $Cs_2Co(SeO_4)_2 \cdot 6H_2O$, calculated from Eq. (11), is three orders of magnitude smaller than that calculated using Eq. (6).[11]

IV. CONCLUDING REMARKS

As pointed out earlier (Sec. I), the use of Eq. (6) to calculate the host-ion SLRT in crystals with two different kinds of paramagnetic ions is not, indeed, valid, since in deriving Eq. (6), the second moment due to only one kind of paramagnetic ions is considered; the important dipolar and exchange interactions between the host and the impurity ions are not taken into account. Equation (11) is, instead, the correct expression to calculate the host ion SLRT, since it takes into account appropriately the interactions between the host and the impurity ions, in the calculation of the second moment, as well as the interactions amongst the host ions.

As seen in Sec. III, the correct Eq. (11) yields SLRT values, which are significantly different from those predicted by the incorrect Eq. (6).

ACKNOWLEDGMENT

The authors are grateful to the Natural Sciences and Engineering Research Council of Canada for partial financial support (Grant No. A4485).

[1]I. Waller, Z. Phys. 79, 370 (1932).
[2]L. J. Broer, Physica 10, 801 (1943).
[3]J. H. Van Vleck, Phys. Rev. 74, 1168 (1948).
[4]P. W. Anderson and P. R. Weiss, Rev. Mod. Phys. 25, 269 (1953).
[5]P. W. Anderson, J. Phys. Soc. Jpn. 9, 316 (1954).
[6]T. Mitsuma, J. Phys. Soc. Jpn. 17, 128 (1962).
[7]V. M. Malhotra, H. A. Buckmaster, and J. M. Dixon, J. Phys. C 13, 3921 (1980).
[8]V. M. Malhotra, J. M. Dixon, and H. A. Buckmaster, Physica B 101, 147 (1980).
[9]M. R. St. John, Ph. D. thesis, University of California, Berkeley, 1975 (unpublished).
[10]R. S. Saraswat and G. C. Upreti, J. Chem. Phys. 67, 5428 (1977).
[11]V. K. Jain and S. K. Yadav, Phys. Rev. B 33, 5034 (1986).
[12]V. K. Jain, N. V. Vugman, and V. S. Yadav, Phys. Rev. B 37, 9716 (1988).
[13]S. A. Al'tshuler and B. M. Kozyrev, *Electron Paramagnetic Resonance in Compounds of Transition Elements* (Keter, Jerusalem, 1974).
[14]S. K. Misra and G. R. Sharp, J. Phys. C 10, 897 (1977).
[15]R. E. Thoma, G. D. Brunton, R. A. Penneman, and T. K. Keenan, Inorg. Chem. 9, 1096 (1970).
[16]S. K. Misra, L. E. Miniak, and U. Orhun (unpublished).
[17]W. Hofman, Z. Kristallogr. 78, 279 (1931)
[18]S. K. Misra and L. E. Miniak (unpublished).

RAPID COMMUNICATIONS

PHYSICAL REVIEW B VOLUME 41, NUMBER 4 1 FEBRUARY 1990

Effect of paramagnetic percolation on Gd^{3+} EPR linewidths in $LiYb_xY_{1-x}F_4$ single crystals

Sushil K. Misra and Ufuk Orhun
Physics Department, Concordia University, 1455 de Maisonneuve Boulevard West, Montreal, Quebec, Canada H3G 1M8
(Received 13 June 1989)

Three-dimensional paramagnetic-site percolation calculations of Gd^{3+}-doped $LiYb_xY_{1-x}F_4$ mixed crystals have been made in order to explain the experimentally observed Gd^{3+} EPR linewidths in these hosts as functions of temperature. The calculated percolation threshold, $x_c=0.27$, is in agreement with the disappearance of the observed EPR linewidths at low temperatures for $LiY_{1-x}Yb_xF_4$ crystals with $x \geq 0.3$. It is concluded that the contribution to the spin-lattice relaxation by the paramagnetic host ions is insignificant below $x=x_c$.

I. INTRODUCTION

X-band EPR measurements on single crystals of Gd^{3+}-doped $LiYF_4$ and $LiYbF_4$ have been previously reported by Vaills, Buzaré, and Gesland[1] at room temperature, and by Misra *et al.*[2] from room temperature down to liquid-helium temperature. X-band EPR measurements on mixed single crystals of Gd^{3+}-doped $LiYb_xY_{1-x}F_4$ with values of $x=0.0$, 0.01, 0.05, 0.1, 0.2, 0.3, 0.4, 0.5, 0.6, 0.7, 0.8, 0.9, 0.95, 1.0, from room temperature to liquid-helium temperature (LHT), have recently been reported by Misiak and co-workers,[3,4] who observed that the Gd^{3+} EPR lines could be observed down to LHT only for samples with $x \leq 0.2$, while the lines disappeared much above LHT as the temperature was lowered for samples with $x \geq 0.3$. Specifically, although Gd^{3+} EPR lines for samples with $x \leq 0.2$ could be observed down to 4.2 K, they could not be observed below 88 K for samples with $x=0.3$. Such an abrupt behavior of EPR linewidth as a function of x cannot be explained by the increase of dipolar contribution by the paramagnetic Yb^{3+} host ions to the second moment, which is proportional to the EPR linewidth, as the temperature is lowered, since the second moment is a continuous function of both the fraction x of the paramagnetic host ions and the temperature.

Site percolation has been used, mostly in the last several years, as a model for describing the behavior of many dilute physical systems. Percolation processes have been employed to study diverse physical phenomena, such as conduction and phase transitions. Various fractal-related properties of percolation clusters have also been studied extensively; see, e.g., the reviews by Stauffer[5] and Essam.[6] Basically, in site percolation, a random fraction p of the sites on a lattice is assumed to be occupied, while the rest of the lattice remains vacant. The most remarkable feature of a percolation process is the existence of a percolation threshold, below which the spreading of quantity of interest in the medium is limited to a finite region only, and does not propagate throughout the sample. In the present study, the sites occupied by the paramagnetic ions will represent the occupied sites, while those occupied by the diamagnetic ions represent the vacant sites. The process whose spread will be studied through the occupied sites is the relaxation process, in which the relaxation of a host spin (Yb^{3+}) is carried through the lattice by the mutual spin flips of other host ions. (Hereafter, spin-lattice relaxation will refer to the relaxation of host spins by their mutual spin flips through the lattice.) This is the first-ever application of the percolation process to study the influence of the host ion (Yb^{3+}) spin-lattice relaxation on the impurity (Gd^{3+}) linewidth. It should be pointed out, here, that the presence of paramagnetic host ions can have a drastic influence on the spin-lattice relaxation, see, e.g., the review article by Misra[7] (for more details see Sec. IV).

The purpose of the present paper is to investigate the relationship between the paramagnetic-site percolation properties of the mixed $LiYb_xY_{1-x}F_4$ single crystals, and the experimentally observed Gd^{3+} EPR linewidths, as functions of the fraction x, representing the Yb^{3+} ions in these samples. In Sec. III, the second moment is calculated for samples with $x=0.1-1$, in steps of 0.1, to show that the second moment does not explain the observed linewidths as functions of x. It is followed in Sec. IV by computer simulations of the percolation effect to see if the relaxation of paramagnetic host ions percolates all the way through the sample for various values of x, in order to relate it to the disappearance of EPR lines at low temperatures for $x \geq 0.3$. The discussion of the present calculations is provided in Sec. V.

II. CRYSTAL STRUCTURE

In order to calculate the second moment, the details of the crystal structure are required. $LiYF_4$ and $LiYbF_4$ crystals are characterized by the scheelite (tetragonal) structure.[8,9] The unit-cell parameters of $LiYF_4$ are $a=5.167$ Å, $c=10.735$ Å,[10] while those for $LiYbF_4$ are $a=5.134$ Å and $c=10.588$ Å.[9] There are five rare-earth ions in the unit cell, which are at the following locations:[11] (0.5,0.0), (0.5,1.0), (0.5,0.5,0.5), (0.0,0.5), and (1.0,0.5,1). The unit-cell parameters of the mixed $LiYb_xY_{1-x}F_4$ crystals can be estimated using Vegard's law.[3] In $LiYbF_4$ there are four nearest ($r_N=5.13$ Å), four next-nearest ($r_{NN}=5.88$ Å), and four next-next-nearest ($r_{NNN}=7.26$ Å) rare-earth neighbors to a rare-earth ion. Thus r_N and r_{NN} are very close to each other. Similar situations apply to the mixed crystals $LiYb_xY_{1-x}F_4$. The Gd/(Yb+Y) ratio in the $LiYb_xY_{1-x}F_4$ samples, experimentally investigated, was 1/200, which is rather small; the present cal-

culations take this value into account by not considering any Gd^{3+} ion sufficiently close to another Gd^{3+} ion to have any effect.

III. CALCULATION OF THE SECOND MOMENT

The EPR linewidth of the impurity ion (Gd^{3+}) due to the paramagnetic host ions (Yb^{3+}) is determined by the second moment. The second moment of the impurity ion for crystals consisting of two kinds of paramagnetic ions, e.g., the impurity (Gd^{3+}) and the host (Yb^{3+}) ions in the present case, has been considered by Van Vleck.[12] If the distance between the impurity ions is sufficiently large, the second moment as given by Van Vleck[12] can be simplified[13] as follows

$$\langle \Delta\nu^2 \rangle = \tfrac{1}{4} S'(S'+1) h^{-2} \left[N J_{jk'}^2 + (gg')^2 \beta^2 \mu_0^2 \sum_k^N (1 - 3\gamma_{jk'}^2)^2 r_{jk'}^{-6} + 2 J_{jk} g g' \beta^2 \mu_0 \sum_k^N (1 - 3\gamma_{jk'}^2) r_{jk'}^{-3} \right], \quad (1)$$

where the subscripts j and k' refer to the impurity and host ions, respectively, while S', h, N, $J_{jk'}$, β, μ_0, $\gamma_{jk'}$, $r_{jk'}$, g, and g' are, respectively, effective spin of the host ion, Planck's constant, the number of neighboring ions considered, average pair-exchange constant, the Bohr magneton, the permeability constant, the cosine of the angle between $r_{jk'}$ and the external magnetic field, and the distance between the impurity (j) and the host (k') ions, the g factor for the impurity ion, and the g factor of the host ion. The second moment, as given by Eq. (1), does not itself depend significantly on temperature; its dependence on temperature is indirectly due to change in lattice spacings due to thermal expansion (contraction) affecting $r_{jk'}$ and $\gamma_{jk'}$. The sums in Eq. (1) are expected to be continuous and convergent functions of x, determined by the number and locations of the Yb^{3+} ions. Thus, the second moment cannot account for the entire disappearance of Gd^{3+} EPR lines, namely, the EPR linewidth approaching infinity below certain temperatures for $x \geq 0.3$.

The calculation of the second moment for $x = 1$ is trivial, since for this case all lattice sites are occupied. In order to calculate the second moment for $x < 1$ a computer program was used to generate the $LiYb_xY_{1-x}F_4$ lattices as three-dimensional arrays of rare-earth ion sites. An array size of $50 \times 50 \times 50$ was employed for the present calculations. The initial unit cell was represented by the elements of a $3 \times 3 \times 3$ array segment, with the following five possible rare-earth sites in the unit cell: (0,1,0), (2,1,0), (1,1,1), (1,0,2), and (1,2,2), as depicted in Fig. 3. The unit-cell parameters were inputs to the program, in order to calculate the distance between any two ions ($r_{jk'}$) and the direction cosines ($\gamma_{jk'}$). After choosing proper steps along each direction an array was created, using a three-dimensional loop, whose occupied elements represent the Yb^{3+} ions on the lattice. In order to determine the sites occupied by the paramagnetic Yb^{3+} ions random integers between one and ten were used to fill the lattice sites one by one, corresponding to the value of x between 0.1 and 1 in steps of 0.1. For example, if $x = 0.3$, then for any random integer ≤ 3 a lattice site will be considered occupied by a paramagnetic Yb^{3+} ion, otherwise it will be considered occupied by a diamagnetic Y^{3+} ion. Ideally, in order to calculate the second moment for a given value of x, for samples with $x < 1$, all possible configurations of the host ions (Yb^{3+} and Y^{3+}) around an impurity ion (Gd^{3+}) should be considered. Since this would have taken prohibitively long computer time, the second moment was calculated around 1000 randomly chosen sites; finally, the average of these second moments was computed. Up to next-next-nearest neighbors around each of these 1000 sites were taken into account in the sums in Eq. (1) to calculate the second moment for the various values of x. Figure 1 exhibits the plot of the second moment $\langle \Delta\nu^2 \rangle$ vs x. It shows a linear relation of $\langle \Delta\nu^2 \rangle$ to x, without exhibiting any divergence, implying that the second moment does not explain the observed disappearance of EPR lines at low temperatures for samples with certain values of x

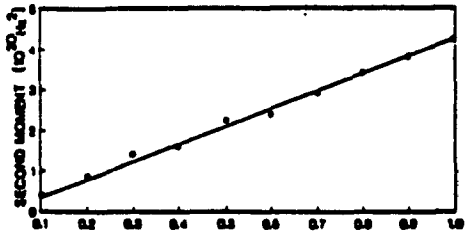

FIG. 1. The calculated second moment as a function of x in Gd^{3+}-doped $LiYb_xY_{1-x}F_4$ single crystals.

IV. CALCULATION OF THE PERCOLATION EFFECT

In order to explain the temperature variation of the impurity EPR linewidth, the spin-lattice relaxation (SLR) process, a highly temperature-dependent phenomenon, of the host paramagnetic ions should be taken into account. The SLR influences the impurity linewidth through the process of random-frequency modulation.[13–15] Misra and Orhun[13] showed that the impurity linewidth, influenced by SLR, can be expressed as

$$\Delta H = 1.10 h g' \langle \Delta\nu^2 \rangle \tau / (3 g^2 \beta), \quad (2)$$

where τ is the spin-lattice relaxation time (SLRT) of the host ion, which is highly temperature dependent. It is this variation of τ, as a function of x, the fraction of the paramagnetic host ions, that determines the divergent behavior of the linewidth ΔH for certain values of x. It is seen from Fig. 2, exhibiting experimental data, that the EPR lines broaden considerably for samples with $x \geq 0.3$, as the temperature is lowered from room temperature. However, the linewidths do not change significantly with temperature for samples with $x < 0.3$; the EPR lines for them can be observed down to LHT. The SLR mecha-

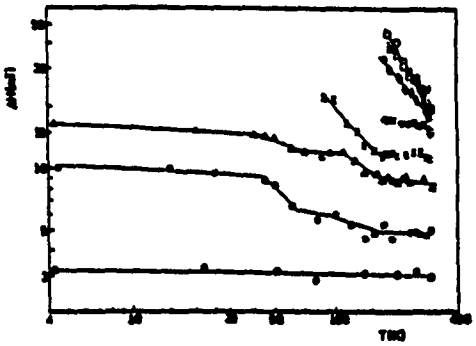

FIG. 2. The experimentally observed Gd^{3+} EPR linewidths (ΔH) as function of temperature in $LiYb_xY_{1-x}F_4$ for various values of x (Refs. 3 and 4). ●: 0.0; ■: 0.1; △: 0.2; ×: 0.3; ▽: 0.4; ◇: 0.6; □: 0.8; ○: 0.9; +: 1.0.

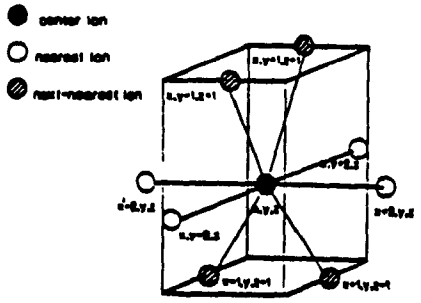

FIG. 3. The array segment showing the center ion and the surrounding nearest and the next-nearest ions, through which the percolation is allowed. The corresponding array indices (lattice positions) of each ion are also indicated.

nism, due to percolation of host ions, determines predominantly the temperature dependence of EPR linewidths; as seen below, it has a cutoff for $x < 0.3$.

It is suggested presently that the cutoff of the SLR mechanism is due to the site percolation of the paramagnetic host ions (Yb^{3+}) in the $LiYb_xY_{1-x}F_4$ lattices. A $LiY_{1-x}Yb_xF_4$ lattice will be considered "percolating" if there exists a path from a Yb^{3+} site at one end of the lattice all the way to the other end of the lattice, through the Yb^{3+} ions, each of which lies within a distance of r_{NN} from a Yb^{3+} ion. That is, a percolation cluster exists. A paramagnetic site was allowed to percolate to both the nearest (N) and the next-nearest (NN) neighbors, since, as mentioned in Sec. II, the difference between r_N and r_{NN} for the $LiYb_xY_{1-x}F_4$ hosts is very small. Figure 3 shows a Yb^{3+} ion and its neighbors (N and NN) to which percolation is allowed, along with their coordinates in the lattice. The possible lattice sites in the array were first filled randomly with concentration x, using random numbers as described in Sec. III. Next, the lattice was divided into z planes: $z=0,1,2,\ldots$, in units of $c/2$, where c is the unit-cell dimension along the z axis. To begin with, all sites occupied by Yb^{3+} ions of the $z=0$ plane were assumed to belong to the percolation cluster. Next, all the occupied sites of the $z=1$ plane, which are within r_{NN} of the percolating ions of the $z=0$ plane, i.e., the nearest and next-nearest neighbors, were included in the percolation cluster. In the same way, all the planes along the z axis were taken into account one by one, by considering $z=1,2,3,\ldots$ planes in turn, attaching to the percolation cluster the occupied sites of the $z=n$ plane under consideration, which lie within r_{NN} of an ion, located on the $z=n-1$ plane, belonging to the percolation cluster already constructed. In addition, a downwards sweep, from the current z plane to the $z=0$ plane, was performed in order to ascertain that no possible ions which should have been included, i.e., those within a distance of r_{NN} from a Yb^{3+} ion of the percolation cluster, were missed out in the percolation cluster already formed. Finally, the algorithm used checked if there was a percolation path from the $z=0$ all the way to the $z=49$ plane, through the paramagnetic Yb^{3+} ions, within r_{NN} of each other, i.e., if the percolation cluster extended all the way from one end of the lattice to the other end of the lattice considered, for the various values of x considered.

The calculation of the percolation cluster was performed for $x=0.1$ to 1 in steps of 0.1. This initial consideration of values of x revealed that x_c, the critical value of x above which percolation exists, but not below, lies between $x=0.2$ and $x=0.3$. Thereafter, the values of x between 0.2 and 0.3 were considered in steps of 0.01, using random integers in the range 1 to 100 to determine the occupied sites of the lattice in the similar way to that described in Sec. III for x between 0.0 and 1.0. This yielded the critical value of x to be $x_c=0.27$. Better accuracy than this could not be achieved due to the limited size of the array used; however, this value is reasonably satisfactory to explain the present experimental data.

V. DISCUSSION

The present results indicate that the SLR threshold is directly linked to x_c. This is in accordance with the temperature behavior of the observed EPR linewidth. The existence of a path for mutual spin flips for the transmission of energy of spins in the Zeeman field, via the paramagnetic ions through the entire lattice, is necessary for the SLR process to be effective. If a Yb^{3+} ion is completely surrounded by diamagnetic Y^{3+} ions, a spin flip of that Yb^{3+} ion will not be transmitted to the rest of the lattice because of diamagnetic shielding by the Y^{3+} ions. For the diamagnetic ions (i.e., Y^{3+}) develop net magnetic moments that tend to oppose any changes in the magnetic field. In fact, paramagnetic (Yb^{3+}) ions, situated sufficiently closely, are needed to transmit the magnetic energy to the rest of the lattice by mutual spin flips.

The experimental EPR linewidth data can be divided into the following three regions for a proper understanding (see Fig. 2):

(i) *High T*, $x \geq 0.3$. In this region, the SLR mechanism is fully effective because of the existence of a percolation cluster. The linewidths become larger, as the temperature is lowered, because the spin-lattice relaxation time of the host ions becomes longer. Since $x > x_c$, the spin flip of a Yb^{3+} ion can be transmitted through the lattice by mutual spin flips of Yb^{3+} ions. The present percolation results suggest that, as long as $x > x_c$, there will be a path via the Yb^{3+} ions that spans the entire lattice even if there are more Y^{3+} ions present than Yb^{3+} ions in the lattice.

(ii) *Low T*, $x \geq 0.3$. Here, the experimental data indicate that EPR lines could not be observed at temperatures below 85 K. Since $x \geq x_c$, broadening due to SLR is expected to be fully operative, and the EPR lines will be broadened since at low temperatures the SLRT is much longer than that at high temperatures.

(iii) *Any T*, $x \leq 0.2$. For this case, the experimental EPR linewidths do not exhibit significant temperature dependence. Since $x < x_c$, the paramagnetic ions (Yb^{3+}) are not able to span a path all the way through the entire lattice for percolation; the flips of the Yb^{3+} ions will be shielded by the Y^{3+} ions, causing the effect of the flips of the Yb^{3+} ions to remain localized. Thus, the broadening due to SLR will not be effective for this case; and the Gd^{3+} EPR lines can be observed at all temperatures.

VI. CONCLUDING REMARKS

From the present calculations it can be concluded that the SLR mechanism is closely tied to the percolation properties of the paramagnetic Yb^{3+} ions in $LiYb_xY_{1-x}F_4$ single crystals. The calculated paramagnetic percolation threshold for the concentration $x_c = 0.27$ agrees quite well with the observed EPR-linewidth behavior. In other words, the SLR due to paramagnetic host ions is not at all effective for concentrations of Yb^{3+} ions below x_c; whereas it is fully effective above x_c, for which concentrations there is a percolation path for mutual spin flips of Yb^{3+} ions throughout the entire lattice, i.e., a percolation cluster exists.

The paramagnetic ions interact with each other via the exchange interaction, which is a short-range interaction, and via dipole-dipole interaction, which is a long-range interaction. The definition of a percolating cluster depends crucially on the assumed range of connectivity. In the present calculation only the nearest (N) and next-nearest (NN) neighbors have been considered, which is obviously justified for the short-range exchange interaction. As for the long-range dipolar interaction, one has to make a choice of the ions which should be considered "connected." Since the dipolar interaction falls off as one cube of the distance, it becomes weaker, in the present case, by a factor of 10 for two ions separated by the next-next-nearest-neighbor (NNN) distance. As for the other ions, this factor increases even further in proportion to the cube of the distance. In this way, the neglect of dipolar interactions from ions separated by a distance equal to, or greater than, the NNN distance can be justified. The present results, which eminently explain the experimental data, thus justify *a posteriori* the assumed connectivity limited to N and NN neighbors. On the other hand, if one extends the connectivity arbitrarily without giving consideration to relative strengths of dipolar interactions there would always be a cluster formed and no cluster calculation will be required.

The present calculation only estimate x_c, the value of x, above which a cluster is formed. They are incapable of calculating the EPR linewidths or spin-lattice relaxation times. The experimentally observed (Fig. 2) sharp increase of linewidths for $x \geq 0.3$ at a temperature that seems to depend on x can only be explained by taking into account the spin-lattice relaxation mechanisms, as specifically considered in detail by Misiak, Misra, and Orhun,[4] applying the theories of Anderson and Weiss[14] and Mitsuma.[15] For more details see Ref. 4.

ACKNOWLEDGMENTS

The authors are grateful to the Natural Sciences and Engineering Research Council of Canada for partial financial support (Grant No. A4485).

[1] Y. Vaills, J. Y. Buzaré, and J. Y. Gesland, Solid State Commun. 45, 1093 (1983).
[2] S. K. Misra, M. Kahrizi, P. Mikolajczak, and L. Misiak, Phys. Rev. B 32, 4738 (1985).
[3] L. E. Misiak, S. K. Misra, and P. Mikolajczak, Phys. Rev. B 38, 8673 (1988).
[4] L. E. Misiak, S. K. Misra, and U. Orhun, Phys. Status Solidi (B) 154, 249 (1989).
[5] D. Stauffer, Phys. Rep. 54, 1 (1979).
[6] J. W. Essam, Rep. Prog. Phys. 43, 833 (1980).
[7] S. K. Misra, Magn. Reson. Rev. 12, 191 (1987).
[8] R. E. Thoma, C. F. Weaver, H. A. Friedman, H. Insley, L. A. Harris, and H. A. Yakel, Jr., J. Phys. Chem. 65, 1096 (1961).
[9] R. E. Thoma, G. D. Brunton, R. A. Penneman, and T. K. Keenan, Inorg. Chem. 9, 1096 (1970).
[10] L. Misiak, P. Mikolajczak, and M. Sabotowicz, Phys. Status Solidi (A) 97, 353 (1986).
[11] L. M. Holmes, T. Johansson, and H. J. Guggenheim, Solid State Commun. 12, 993 (1973).
[12] J. H. Van Vleck, Phys. Rev. 74, 1168 (1948).
[13] S. K. Misra and U. Orhun, Phys. Rev. B 39, 2856 (1989).
[14] P. W. Anderson and P. R. Weiss, Rev. Mod. Phys. 25, 269 (1953).
[15] T. Mitsuma, J. Phys. Soc. Jpn. 9, 316 (1962).

phys. stat. sol. (b) 154, 249 (1989)

Subject classification: 76.30; S9.16

Department of Physics, Concordia University, Montreal[1])

Study of Temperature Variation of EPR Linewidth of Gd^{3+}-Doped $LiYb_xY_{1-x}F_4$ Single Crystals

Estimation of Yb^{3+} Spin–Lattice Relaxation Times

By

L. E. MISIAK[2]), S. K. MISRA, and U. ORHUN

X-band EPR linewidths of Gd^{3+}-doped $LiYb_xY_{1-x}F_4$ crystals ($0.0 \leqq x \leqq 1.0$) are measured in the temperature range 4.2 to 290 K. It is found that the peak-to-peak linewidth of the first derivative lineshape (ΔH_{pp}) can be fitted to T^{-n} (T = temperature), where generally $n < 2$, in the various temperature regions, for all the crystals. ΔH_{pp} is, in general, found to be quite sensitive to the mole fraction (x) of Yb^{3+} ions. The Yb^{3+} spin–lattice relaxation times (τ_1') are estimated in these crystals, using the theories of Anderson-Weiss and Mitsuma, taking into account the fact that there are present two different kinds of paramagnetic ions, Gd^{3+} and Yb^{3+}. It is concluded that the dipole–dipole interactions play an important role in the spin–lattice relaxation of Yb^{3+} ions.

On a mesuré les largeurs des raies RPE à bande X pour l'ion Gd^{3+} dopant les cristaux de $LiYb_xY_{1-x}F_4$ ($0.0 \leqq x \leqq 1.0$) dans l'intervalle entre les températures de 4.2 et 300 K. La largeur d'un pic à l'autre selon la forme de la première dérivée de raie (ΔH_{pp}) peut être adaptée à T^{-n} (T = température), où $n < 2$ en général, dans les divers intervalles de température, pour tous les cristaux. On trouve, en général, que ΔH_{pp} est très sensible à la fraction mole (x) des ions Yb^{3+}. Les temps de relaxation (τ_1') réseau–spin de Yb^{3+} ont été estimés pour ces cristaux, en utilisant les théories d'Anderson-Weiss et de Mitsuma, en tenant compte du fait qu'il y a, en présence, deux sortes différentes d'ions paramagnétiques, Gd^{3+} et Yb^{3+}. On en conclut que les interactions dipolaires jouent un rôle important dans la relaxation du réseau–spin des ions Yb^{3+}.

1. Introduction

Detailed EPR study of Gd^{3+}-doped $LiYb_xY_{1-x}F_4$ single crystals, dealing with the evaluation of spin-Hamiltonian parameters at various temperatures, including angular variation of EPR spectra for the orientation of the Zeeman field in various planes, has been previously reported [1]. Although, some of these crystals have been previously investigated by EPR [1 to 3], the present study of temperature dependence of EPR linewidths ΔH_{pp} in Gd^{3+}-doped $LiYb_xY_{1-x}F_4$, over an extended temperature range, is the first-ever study on these crystals. Very few systematic studies have, so far, been reported on EPR linewidth [4 to 7], as compared with those on the determination of spin-Hamiltonian parameters. As for the Gd^{3+} EPR linewidth variation with temperature, they have been reported in the $YbCl_3 \cdot 6\,H_2O$, $Yb_xY_{1-x}Cl_3 \cdot 6\,H_2O$, and $La_xCe_{1-x}F_3$ single crystals by Misra and Sharp [4] and Malhotra et al. [5], by Misra and Mikołajczak [6], and by Korczak et al. [7], respectively.

[1]) 1455 de Maisonneuve Boulevard West, Montreal, Quebec H3G 1M8, Canada.

[2]) Permanent address: Department of Experimental Physics, Maria Curie-Skłodowska University, Pl. M. Curie-Skłodowskiej 1, PL-20-031 Lublin, Poland.

The measurements of linewidths in Gd^{3+}-doped $LiYb_xY_{1-x}F_4$ single crystals have been made in the present study for crystals with $x = 0.\ 0.01.\ 0.05.\ 0.1.\ 0.2.\ 0.3.\ 0.4.\ 0.5.\ 0.6.\ 0.7.\ 0.8.\ 0.9.\ 0.95.\ 1.0$. With increasing mole fraction x of Yb^{3+} ions, the EPR lines become broader due to Gd^{3+}–Yb^{3+} dipole–dipole interaction, similar to that in Gd^{3+}-doped $Yb_xY_{1-x}Cl_3 \cdot 6\ H_2O$ host lattices ($x \neq 0$). The $LiYb_xY_{1-x}F_4$ crystals have been chosen for the present study, because in the pure $LiYbF_4$ crystal the Gd^{3+} EPR lines broaden and disappear completely at liquid-nitrogen temperature, with lowering temperature. In the $LiYb_xY_{1-x}F_4$ crystals, with a sufficiently large fraction of diamagnetic Y^{3+} ions, it is possible to observe well-resolved EPR spectra even below liquid-nitrogen temperature. The temperature dependence of EPR linewidths in these crystals is a measure of the interaction of the Gd^{3+} ion with the host Yb^{3+} ions. It is the purpose of the present paper to analyse the Gd^{3+} EPR linewidths, as observed in the $LiYb_xY_{1-x}F_4$ crystals, in the temperature range 4.2 to 290 K.

2. Sample Preparation, Crystal Structure, and Experimental Details

$LiYb_xY_{1-x}F_4$ crystals, to which 0.2 mol% Gd^{3+} were added as dopant, were grown by modified Bridgman-Stockbarger method, using induction furnace (460 kHz r.f. and 10 kW maximum power); the method is described in [8]. Since both the $LiYF_4$ and $LiYbF_4$ crystals have the same structure (tetragonal, Scheelite type, space group $I4_1/a$ [9, 10]), it is assumed that the $LiYb_xY_{1-x}F_4$ crystals also have the same structure. The lattice constants for $LiYF_4$ are: $a = 0.5167 \pm 0.0003$ nm and $c = 1.0734 \pm 0.0003$ nm [8], for $LiYbF_4$: $a = 0.51335 \pm 0.00002$ nm and $c = 1.0588 \pm 0.0002$ nm [10]. The lattice constants for the various $LiYb_xY_{1-x}F_4$ crystals can be calculated by the use of Vegard's law [6, 11] from the lattice constants of $LiYF_4$ and $LiYbF_4$ crystals. In $LiYb_xY_{1-x}F_4$ host crystals Gd^{3+} ion substitutes either for Yb^{3+} or Y^{3+} ion (S_4 local symmetry).

The EPR experimental arrangement has been described elsewhere [1]. The magnetic z-axis was found to be parallel to the crystal c-axis, while the x-axis was found to be at $34° 30' \pm 30'$ from the crystal a-axis in the ab plane. The magnetic x, y, z axes are those directions of the external magnetic field ($\boldsymbol{H}$) for which the overall splitting of the allowed lines exhibit extrema [1]. The measurements of EPR linewidths were performed for $\boldsymbol{H}$ parallel to both the x- and z-axes. For $\boldsymbol{H} \parallel x$, there were observed seven clearly-resolved allowed resonance lines for $LiYF_4$ single crystal at all temperatures, while for $LiYb_xY_{1-x}F_4$ with $x \neq 0$, two of the allowed lines were not clearly resolved due to overlap by other lines at those temperatures at which corresponding well-resolved EPR spectra could be observed, except for $LiYb_{0.1}Y_{0.9}F_4$ at room temperature, for which only one line was not clearly resolved. Fig. 1 displays typical spectra for $\boldsymbol{H} \parallel z$ and $\boldsymbol{H} \parallel x$ at room temperature for $LiYb_{0.5}Y_{0.5}F_4$; it also serves to identify the resonance transitions. The lines were found to be predominantly of Lorentzian shape.

3. Linewidths

3.1 *Dependence of ΔH_{pp} on T*

The log–log plots of the Gd^{3+} peak-to-peak EPR linewidths, ΔH_{pp}, versus temperature (T) for the various $LiYb_xY_{1-x}F_4$ hosts are displayed in Fig. 2 a and b for the transitions $5/2 \leftrightarrow 3/2$ ($\boldsymbol{H} \parallel z$) and $-1\ 2 \leftrightarrow -3/2$ ($\boldsymbol{H} \parallel x$), respectively. These are two of the four clearly-resolved transitions, not overlapped by other transitions at any temperature, the other being $3/2 \leftrightarrow 1/2$ ($\boldsymbol{H} \parallel z$) and $-5/2 \leftrightarrow -7\ 2$ ($\boldsymbol{H} \parallel x$). It is, further, seen from Fig. 2 a and b that the linewidths increase rapidly with lowering tempera-

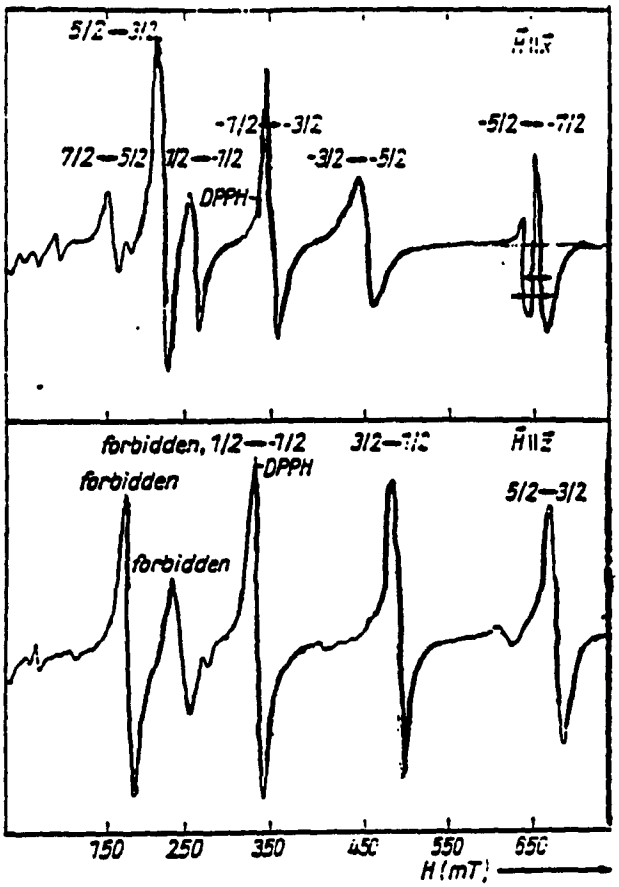

Fig. 1. EPR spectra for Gd^{3+}-doped $LiYb_{0.5}Y_{0.5}F_4$ crystal, for $H \| x$ and $H \| z$ at room temperature. The lineshapes are Lorentzian, since here $3 \leqq h_1/h_2 \leqq 6$, where h_1 is the height of the peak of the first derivative lineshape from the base line and h_2 is the height of the first derivative lineshape at $3\Delta H_{pp}/2$ from the centre of the line. The forbidden transitions are those found by diagonalization of the spin-Hamiltonian matrix, for which $\Delta M = \pm 1$

ture, especially for samples with larger values of x. (Similar results are found for all the observed transitions.) It is seen from Fig. 2 a and b that there are regions, where ΔH_{pp} is linear with respect to T on the log-log plot. The successive linear regions are connected by jumps. Over these linear regions one can express $\Delta H_{pp} \sim T^{-n}$. The values of n, as found from numerical fitting of T^{-n} to the observed linewidths, in the various temperature regions in the $LiYb_xY_{1-x}F_4$ hosts, for the various observed transitions, are listed in Table 1.

It is, now, noted that spin-lattice relaxation time (τ_1^{-1}) is proportional to ΔH_{pp}, as given by (4.4) below. The jumps in the ΔH_{pp} versus T log-log plots as seen from Fig. 2 a and b and Table 1, i.e., the change in the n values with change in temperature in the ranges 290 to 180 K, 180 to 30 K, and 30 to 4.2 K, can be explained to be due to simple relaxation processes or by processes, which are combined with those responsible for the jumps, being effective in these ranges.

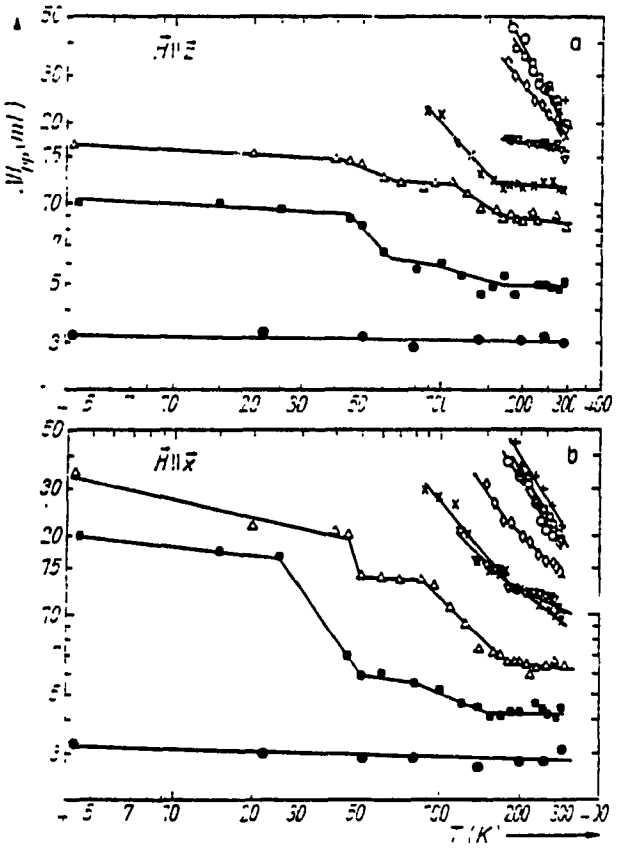

Fig. 2. Log–log plot of the peak-to-peak first derivative EPR linewidth (ΔH_{pp}) vs. temperature for Gd^{3+}-doped $LiYb_xY_{1-x}F_4$ crystals for the transitions: a) $5/2 \rightarrow 3/2$ ($H \parallel z$) and b) $-1/2 \rightarrow -3/2$ ($H \parallel x$). The points represent the values which are least-squares fitted. The various symbols correspond to different x values. ● $x = 0$, ■ 0.1, △ 0.2, ◺ 0.3, ▽ 0.4, ◇ 0.6, ○ 0.8, □ 0.9, + 1.0

The jumps in the log–log ΔH_{pp} versus T plots are not due to the changes in the effective spin of Yb^{3+} ions, contrary to that pointed out in [5] and [6]. For, the occupation of the excited crystal-field levels changes smoothly with temperature, as can be seen by calculating the relative populations using Boltzmann factors and the energies of the excited levels. (Miller and Sharp [12] determined the energies of the three higher-lying doublets, relative to the ground-state doublet, to be 212, 364, and 455 cm^{-1}.)

3.2 Mechanisms responsible for the observed n values

The spin-lattice relaxation time (τ_1') of Yb^{3+} ion is proportional to ΔH_{pp} (see (4.4) below). Thus the same n values, as those given in Table 1 for ΔH_{pp}, govern the $\tau_1' \sim T^{-n}$ relationship. It is seen from Table 1, in all temperature ranges over which resolved lines can be observed, that $n \leqq 2$, except for the $-5/2 \rightarrow -7/2$ ($H \parallel x$) transition in $LiYbF_4$, for which $n = 2.25$ in the temperature range 180 to 290 K. It is, therefore, concluded that the processes, such as Orbach resonance and two-phonon Raman scattering [13], and their combinations ($\tau_1' \sim \sum T^{-n}$; $n = 5, 6, 7, 8, 9$ [5]), for which

Table 1

The values of the slopes (n) in the relation $\Delta H_{pp} \sim T^{-n}$, as obtained from fits of the experimental data for the various Gd^{3+}-doped $LiYb_xY_{1-x}F_4$ crystals for the magnetic-field orientations $H \parallel x$ and $H \parallel z$, in the various temperature ranges. $\frac{n_1}{n_2}$ denotes the values of the slopes n_1 and n_2 for the $-1/2 \leftrightarrow -3/2$ and $-5/2 \leftrightarrow -7/2$ resonance transitions, respectively, for $H \parallel x$, while they are for $3/2 \leftrightarrow 1/2$ and $5/2 \leftrightarrow 3/2$ transitions, respectively, for $H \parallel z$

concentration (x)	290 to 180 K		180 to 100 K		100 to 50 K		50 to 4.2 K	
	$H \parallel x$	$H \parallel z$	$H \parallel x$	$H \parallel z$	$H \parallel x$	$H \parallel z$	$H \parallel x$	$H \parallel z$
0	0.03	0.02	0.03	0.02	0.03	0.02	0.03	0.02
	0.00	0.01	0.00	0.01	0.00	0.01	0.00	0.01
0.1	0.03	0.00	0.43	0.92	0.16	0.31	0.11	0.06
	0.07	0.04	0.11	0.29	0.11	0.20	0.08	0.06
0.2	0.07	0.11	0.65	1.13	0.06	1.13	0.23	—
	0.10	0.12	0.20	0.70	0.20	0.05	0.16	0.06
0.3	0.71	0.24	1.19	1.45				
	0.13	0.08	0.31	1.09				
0.4	0.43	0.42	1.05					
	0.31	0.22	0.56					
0.6	0.94	1.26	1.44					
	0.77	1.18	1.19					
0.8	1.68	1.95						
	1.47	1.82						
0.9	1.58	1.58						
	1.33	1.48						
1.0	1.55							
	2.25							

$n > 2$ are not effective in the $LiYb_xY_{1-x}F_4$ hosts, over the temperature ranges for which resolved EPR lines can be observed. The presently observed values of n ($\leqq 2$) are most likely due to the dipole–dipole interactions between gadolinium and the host paramagnetic ytterbium ions as discussed by Misra et al. in Gd^{3+}-doped $Yb_xY_{1-x}Cl_3 \cdot 6\,H_2O$ [14].

3.3 Dependence of ΔH_{pp} on the mole fraction x of Yb^{3+} ions

Fig. 3 a and b show the dependence of the Gd^{3+} linewidths on the mole fraction (x) of the $LiYb_xY_{1-x}F_4$ crystals, for the various well-resolved EPR lines at room temperature. In general, it is seen that ΔH_{pp} increases nearly linearly with the concentration (x) of the paramagnetic Yb^{3+} ions with increasing x up to $x = 0.8$. All transitions, except for $-1/2 \leftrightarrow -3/2$, for which ΔH_{pp} increases linearly with x in the entire range $0 \leqq x \leqq 1.0$, exhibit a small decreases of ΔH_{pp} with increasing x in the range $0.8 \leqq \leqq x \leqq 1.0$. (See Fig. 3 a and b.) These results are different from those obtained for Gd^{3+}-doped $La_xCe_{1-x}F_3$ crystals [7], in which the linewidths for $H \parallel z$ are approximate-

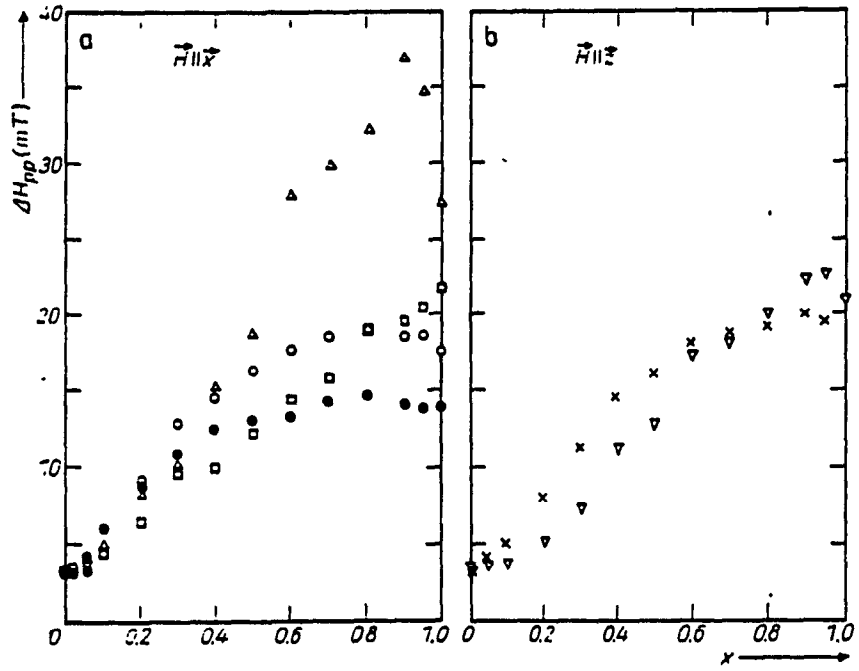

Fig. 3. The dependence of the first-derivative peak-to-peak EPR linewidth (ΔH_{pp}) upon the mole fraction (x) of Yb^{3+} ions at room temperature, in Gd^{3+}-doped $LiYb_xY_{1-x}F_4$ crystals for a) $H \| x$ and b) $H \| z$. The various symbols correspond to different allowed transitions. ○ $-5/2 \leftrightarrow -7/2$, △ $-3/2 \leftrightarrow -5/2$, □ $-1/2 \leftrightarrow -3/2$, ● $7/2 \leftrightarrow 5/2$, ▽ $3/2 \leftrightarrow 1/2$, × $5/2 \leftrightarrow 3/2$

ly constant in the range $0.2 \leqq x \leqq 0.8$. while they increase as x increases from 0 to 0.2. and decrease as x increases from 0.8 to 1.0.

The observed ΔH_{pp} versus x dependence can be explained as follows. One can express $\Delta H_{1/2}$, which is related to ΔH_{pp} (see Section 4), as follows [15, 16]:

$$\Delta H_{1/2} = \frac{20 \Delta H_{dip\text{-}ex}^2}{3 H_{mod}} . \tag{3.1}$$

In (3.1) $\Delta H_{dip\text{-}ex}$ is the dipolar–exchange field. which increases with x in the range $0 \leqq x \leqq 0.8$. and then remains constant in the region $0.8 \leqq x \leqq 1.0$; on the other hand. H_{mod} is the magnitude (in magnetic field units) of $\mathcal{H}_{mod}$, the Hamiltonian. consisting of spin operators of Yb^{3+} ion. representing the modulation of the dipolar fields at the Gd^{3+} ions by the spin–orbit and orbit–lattice coupling in Yb^{3+} ions [6, 15], which increases with increasing x for $0 \leqq x \leqq 1.0$. With these behaviours of $\Delta H_{dip\text{-}ex}$ and H_{mod} in (3.1), the observed ΔH_{pp} dependence on x can be well explained.

Kittel and Abrahams [17] estimate that. when more than 10% of the lattice sites are populated by paramagnetic ions. the EPR linewidth is proportional to the square root of the concentration of the paramagnetic ions. On the other hand, for lower concentrations ($< 10\%$) of paramagnetic ions the linewidth is directly proportional to the concentration. Although the estimates of [17] were made for cubic crystals, with randomly-populated identical paramagnetic ions, without taking into account the exchange and hyperfine interactions. they appear to be in agreement with the present experimental data on $LiYb_xY_{1-x}F_4$.

3.4 Dependence of ΔH_{pp} on magnetic field

It is found that the Gd^{3+} linewidth in the $LiYb_xY_{1-x}F_4$ hosts depends on the value of the magnetic field (H) at which a transition occurs. Plots of ΔH_{pp} versus H at room temperature reveal that, generally, ΔH_{pp} increases linearly with H for both $H \parallel z$ and $H \parallel x$ for all values of x. The only departure is found for the second highest-field transition for $H \parallel x$ in samples with $x \geqq 0.4$, for which the linewidth is the largest of all the transitions. No serious theoretical attempt has been made in the present paper to explain this. The overall increase of ΔH_{pp} with H may be ascribed to the dipole–dipole interaction of the Gd^{3+} ion with the surrounding Yb^{3+} ions.

3.5 Effect of hyperfine interactions on the linewidth

The Gd^{3+} linewidths are also modified by (i) the hyperfine splittings (HFS) of Yb^{3+} ions (^{171}Yb, $I = 1/2$; ^{173}Yb, $I = 5/2$ are the responsible isotopes with non-zero nuclear moments), (ii) the superhyperfine interaction (SHF1) of ^{19}F with Gd^{3+}, and (iii) the direct Gd^{3+}–^{89}Y superhyperfine interaction (SHF2) [18]. Their relative strengths are HFS $\gg$ SHF1 $\gg$ SHF2. The Gd^{3+} EPR linewidth in the purely diamagnetic host $LiYF_4$ is practically independent of temperature in the entire range 4.2 to 290 K, because of the absence of paramagnetic Yb^{3+} ions.

4. Host Spin–Lattice Relaxation Time (τ_1')

In the past, τ_1', the spin–lattice relaxation time of the host ions (Yb^{3+} ions in the present case), has been estimated from the impurity (Gd^{3+}) EPR linewidth (ΔH_{pp}), using the theories of Mitsuma [15] and Anderson and Weiss [19]. The required conditions are clearly satisfied for the present X-band experiment, as discussed in context with Gd^{3+}-doped $Yb_xY_{1-x}Cl_3 \cdot 6\,H_2O$ single crystals [6]. The final expression, to be used, is

$$\tau_1' = \frac{h\,\Delta H_{1/2}}{34(g'\beta)^3\, n'^2 S'(S'+1)}, \tag{4.1}$$

where h is Planck's constant, the primed quantities refer to the host ions (Yb^{3+}), while the unprimed quantities designate the impurity ions (Gd^{3+}); the effective spin of Yb^{3+} ion S' is 5/2 in the temperature range 180 to 290 K, and n' is the number of Yb^{3+} host ions per unit volume. $\Delta H_{1/2}$ in (4.1) is $1.73\Delta H_{pp}$ for Lorentzian lineshape and $1.18\Delta H_{pp}$ for Gaussian lineshape.

Many authors have used (4.1) to calculate spin–lattice relaxation times. However, (4.1) is not valid to estimate τ_1' in doped paramagnetic crystals, for the following reasons [16]:

(i) This expression is valid only for crystals with one kind of magnetic ion, i.e., when there is no doping.

(ii) Anderson-Weiss expression [19], used to derive (4.1), is applicable only to a simple cubic lattice, for which the total number of the nearest and the next-nearest paramagnetic neighbour ions is six. The correct expression for τ_1' in the presence of two different species of paramagnetic ions is now developed. The second moment has been calculated to be as follows [16]:

$$\langle \overline{\Delta\nu^2} \rangle = \tfrac{1}{3} S'(S'+1)\, h^{-2} \left[N J^2 + (gg')^2 \beta^4 \mu_0^2 \sum_{k'}^{N} (1 - 3\cos^2\theta_{jk'})^2\, r_{jk'}^{-6} + \right.$$

$$\left. + 2Jgg'\beta^2\mu_0 \sum_{k'}^{N} (1 - 3\cos^2\theta_{jk'})\, r_{jk'}^{-3} \right], \tag{4.2}$$

where J is the effective pair exchange-interaction constant (between one pair of host-impurity ions); N is the number of nearest and next-nearest neighbour ions; g, g' and S, S' are the g-factors and the effective ionic spins of the impurity and host ions, respectively; θ_{jk} is the angle between r_{jk} and the field direction. β is the Bohr magneton, and μ_0 ($= 1.26 \times 10^{-6}$ Hm^{-1}) is the magnetic permeability constant.

The spin–lattice relaxation modulation can now be introduced in the same way as that done by Anderson and Weiss [19]. Thus, assuming strong narrowing, the linewidth at half maximum can be expressed, in frequency units, as

$$\Delta\nu_{1/2} = 2\frac{10}{3}(2.35)^2\frac{\langle\overline{\Delta\nu^2}\rangle}{\nu_{\text{mod}}}, \tag{4.3}$$

where $\langle\overline{\Delta\nu^2}\rangle$ is given by (4.2) and $\nu_{\text{mod}} = 1/\tau_1'$. Thus,

$$\tau_1' = \frac{3\Delta\nu_{1/2}}{110.45\langle\overline{\Delta\nu^2}\rangle}. \tag{4.4}$$

The $\Delta\nu_{1/2}$ and $\langle\overline{\Delta\nu^2}\rangle$, required in (4.4) to estimate τ_1', are respectively the experimental value of EPR linewidth (in frequency units) and the second moment given by (4.2). The J values for $LiYb_xY_{1-x}F_4$, required to calculate $\langle\overline{\Delta\nu^2}\rangle$ in (4.2) have been estimated in [20]. The calculation of τ_1', using (4.4), requires very precise crystal-structure data [10, 21 to 23]. In order to take into account the change in the lattice constants with temperature, the contraction of the unit-cell parameter a by 0.3%, and that of c by 0.2%, as the temperature is lowered from 290 to 90 K, have been taken into account for both the $LiYF_4$ and $LiYbF_4$ crystals [8]. For $LiYb_xY_{1-x}F_4$ crystals ($x = 0$, 1), the use of Vegard's law to estimate the respective unit-cell parameters a and c, as described in Section 2, has been made. The spin–lattice relaxation times (τ_1') for the various hosts $LiYb_xY_{1-x}F_4$ ($x = 0$ to 1.0), as estimated from the correct expression (4.4), at room temperature, 250, and 200 K are plotted in Fig. 4 for $H \parallel z$. For illustration, Fig. 5 exhibits the temperature dependence of τ_1' in $LiYb_{0.6}Y_{0.4}F_4$ ($H \parallel z$), as estimated using the correct expression (4.4) and ΔH_{pp} values at different temperatures. It is clear, from Fig. 4, that τ_1' becomes shorter as the mole fraction (x) increases. On the other hand, it is seen from Fig. 5 that for a given x value τ_1' decreases as the temperature increases. This is in agreement with the predictions of Mitsuma [15] and Kittel and Abrahams [17]. The calculation of τ_1' from the incorrect equation (4.1) yields the value $\tau_1' =$

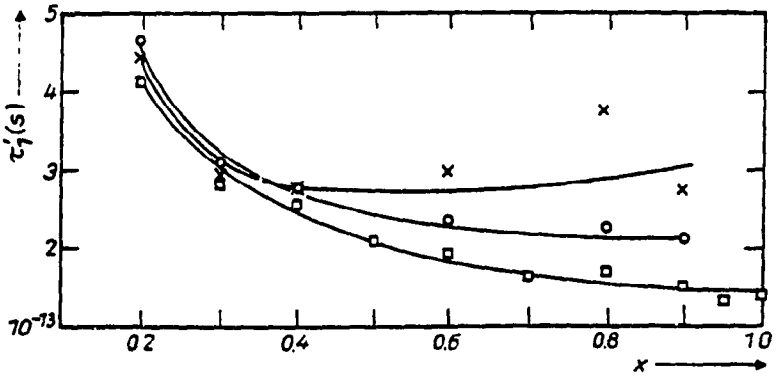

Fig. 4. Spin–lattice relaxation time (τ_1'), as calculated using (4.4), of Yb^{3+} ions as function of Yb^{3+} mole fraction (x) for Gd^{3+}-doped $LiYb_xY_{1-x}F_4$ crystals at room temperature (□), 250 (○), and 200 K (×), for $H \parallel z$. Continuous lines join data points obtained at the same temperature

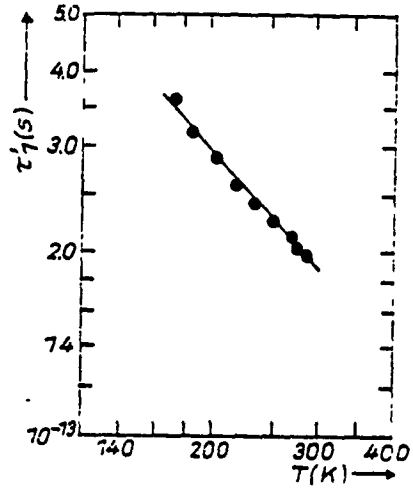

Fig. 5. Spin-lattice relaxation time (τ_1'), as calculated using (4.4), of Yb^{3+} ions as a function of temperature for Gd^{3+}-doped $LiYb_{0.6}Y_{0.4}F_4$ host for $H \parallel z$

$= 2.5 \times 10^{-11}$ s at room temperature for $LiYbF_4$ ($H \parallel z$), whereas the use of the correct expression (4.4) yields $\tau_1' = 1.45 \times 10^{-13}$ s: these two τ_1' are different from each other by two orders of magnitude.

The following conclusions can be drawn regarding the various mechanisms that may be effective. From the slope of the log–log plot of τ_1' versus T in Fig. 5 one finds $\tau_1' \sim T^{-1.2}$ for Gd^{3+}-doped $LiYb_{0.6}Y_{0.4}F_4$ ($H \parallel z$). This power dependence suggests that the dipole–dipole interactions might be effective in the $LiYb_{0.6}Y_{0.4}F_4$ crystal, in the temperature range 180 to 290 K [14].

5. Concluding Remarks

The present X-band EPR investigation of linewidths in Gd^{3+}-doped $LiYb_xY_{1-x}F_4$ single crystals has led to the following conclusions:

(i) The processes which dictate $\Delta H_{pp} \sim T^{-n}$, with $n > 2$ for Gd^{3+}, are not at all effective at any temperature for Gd^{3+}-doped $LiYb_xY_{1-x}F_4$ crystals: it is found that $n \leqq 2$ at all temperatures of investigation.

(ii) The observed decrease in ΔH_{pp} with decrease of the mole fraction (x) of Yb^{3+} ions can be understood to be due to the magnetic dilution of the crystals, which weakens the dipolar and exchange interactions.

(iii) The spin–lattice relaxation times, as calculated from the correct equation (4.4), are different by two orders of magnitude from those calculated using the incorrect equation (4.1), being used previously.

(iv) The observed dependence $\tau_1' \sim T^{-1.2}$, in the temperature range 180 to 290 K, in Gd^{3+}-doped $LiYb_{0.6}Y_{0.4}F_4$ crystal for $H \parallel z$ indicates that the dipole–dipole interactions in this crystal might be effective, when the dilution of paramagnetic lattice by Y^{3+} ions is taken into account.

Acknowledgements

The authors are grateful to the Natural Sciences and Engineering Research Council of Canada (grant No. A4485) for partial financial support. One of us (L.E.M.) also acknowledges sponsorship by the Institute of Low Temperatures and Structural Research of Polish Academy of Sciences (programme CPBP-01.12.2.11-"Structure, phase transitions and properties of molecular systems and condensed phases").

References

[1] L. E. Misiak, S. K. Misra, and P. Mikołajczak, Phys. Rev. B 38, 8673 (1988).
[2] Y. Vaills, J. Y. Buzaré, and J. Y. Gesland, Solid State Commun. 45, 1003 (1983).
[3] S. K. Misra, M. Kahrizi, P. Mikołajczak, and L. E. Misiak, Phys. Rev. B 32, 4738 (1985).
[4] S. K. Misra and G. R. Sharp, J. Phys. C 10, 897 (1977).
[5] V. M. Malhotra, H. A. Buckmaster, and J. M. Dixon, J. Phys. C 13, 3921 (1980).
[6] S. K. Misra and P. Mikołajczak, phys. stat. sol. (b) 109, 39 (1982).
[7] W. Korczak, M. Paradowski, and M. Subotowicz, phys. stat. sol. (b) 115, 89 (1983).
[8] L. Misiak, P. Mikołajczak, and M. Subotowicz, phys. stat. sol. (a) 97, 353 (1986).
[9] R. E. Thoma, C. F. Weaver, H. A. Friedman, H. Insley, L. A. Harris, and H. A. Yakel, Jr., J. phys. Chem. 65, 1096 (1961).
[10] R. E. Thoma, G. D. Brunton, R. A. Penneman, and T. K. Keenan, Inorg. Chem. 9, 1096 (1970).
[11] L. Vegard, Z. Krist. 67, 239 (1928).
[12] J. E. Miller and E. J. Sharp, J. appl. Phys. 41, 4718 (1970).
[13] A. Abragam and B. Bleaney, Electron Paramagnetic Resonance of Transition Ions, Clarendon Press, Oxford 1970.
[14] S. K. Misra and U. Orhun, Solid State Commun. 63, 867 (1987).
S. K. Misra, U. Orhun, and J. M. Daniels, Phys. Rev. B 38, 8683 (1988).
[15] T. Mitsuma, J. Phys. Soc. Japan 17, 128 (1962).
[16] S. K. Misra and U. Orhun, Phys. Rev. B 39, 2856 (1989)
[17] C. Kittel and E. Abrahams, Phys. Rev. 90, 238 (1953).
[18] F. Mehran, K. W. H. Stevens, T. S. Plaskett, and W. J. Fitzpatrick, Phys. Rev. B 22, 2206 (1980).
[19] P. W. Anderson and P. R. Weiss, Rev. mod. Phys. 25, 269 (1953).
[20] S. K. Misra and L. E. Misiak, unpublished.
[21] Vishwamittar and S. P. Puri, J. Phys. C 7, 1337 (1974).
[22] S. K. Misra and J. Felsteiner, Phys. Rev. B 15, 4309 (1977).
[23] L. M. Holmes, T. Johansson, and H. J. Guggenheim, Solid State Commun. 12, 993 (1973).

(Received July 25, 1988; in revised form March 13, 1989)

Solid State Communications, Vol. 76, No. 7, pp. 949–954, 1990.
Printed in Great Britain.

0038-1098/90 $3.00 + .00
Pergamon Press plc

DETERMINATION OF HOST-ION SPIN-LATTICE RELAXATION TIMES FROM Gd^{3+} EPR LINEWIDTHS IN $NH_4R(SO_4)_2 \cdot 4H_2O$ (R = Pr, Sm, Ce, Nd) SINGLE CRYSTALS

Sushil K. Misra, Ufuk Orhun and Jiansheng Sun*

Physics Department, Concordia University, 1455 de Maisonneuve Blvd. West, Montreal, Quebec, Canada H3G 1M8

(*Received* 15 *June* 1990 *by P. Burlet*)

Spin-lattice relaxation times (τ) for the host rare-earth ions R^{3+} (R = Sm, Ce, Nd) in $NH_4R(SO_4)_2 \cdot 4H_2O$ crystal lattices have been estimated at room-temperature from X-band EPR linewidths of Gd^{3+} impurity ion, using an appropriate expression based on the second moment for crystals consisting of two different kinds of paramagnetic spins. In addition, the τ values for Pr^{3+} ions in $NH_4Pr(SO_4)_2 \cdot 4H_2O$ lattice have been estimated in the 266–410 K temperature range from EPR linewidths of the impurity ion Gd^{3+}. The values of τ for Pr^{3+} indicate that τ^{-1} varies as T^7 (T = temperature) in the 266–296 K range, and as T^2 in the range 296–410 K. It is concluded that the T^7 behaviour is predominantly due to the sum process, while the T^2 behaviour is predominantly due to the Raman process.

1. INTRODUCTION

$NH_4R(SO_4)_2 \cdot 4H_2O$ (R = rare-earth) compounds, forming a series of isostructural crystals [1], are interesting because they exhibit multiple phase transitions below room-temperature (RT) as revealed by EPR, infrared [2–5], and differential scanning calorimetry (DSC) [6] studies. As for EPR, temperature variation of EPR linewidth (ΔB) of the impurity ion, e.g. Gd^{3+}, in these host crystals, being sensitive to temperature variation of the host crystal lattices [7], has been exploited to study phase transitions.

The impurity ion linewidths can also be used to estimate spin-lattice relaxation times (τ) of the host paramagnetic ions [8]. For the $NH_4R(SO_4)_2 \cdot 6H_2O$ hosts, characterized by R = Sm, Ce and Nd, estimates of spin-lattice relaxation times have been reported by Malhotra *et al.* [2] and by Buckmaster *et al.* [3], using Gd^{3+} EPR linewidths. However, in their calculations, they employed a frequently-used erroneous expression, applicable to the presence of only one kind of magnetic spin in the system, valid only for a simple cubic lattice [9]. Misra and Orhun [8] derived the correct expression for τ, for the presence of two different kinds of magnetic spins in the system, typical of the EPR situation wherein the host ions are paramagnetic. The purpose of the present paper is to estimate τ of the host ions R^{3+} in the $NH_4R(SO_4)_2 \cdot 4H_2O$ crystals, for R = Sm, Ce, Nd at room temperature, and for R = Pr in the temperature range 266–296 K, by the use of the correct expression [8], employing experimentally observed Gd^{3+} impurity-ion EPR linewidths. The power-law temperature dependence of the values of τ for Pr^{3+} will be used to discern the spin-lattice relaxation processes governing the host Pr^{3+} ions in the $NH_4Pr(SO_4)_2 \cdot 4H_2O$ lattice. To this end, the X-band data of Misra and Sun [4] for Gd^{3+} EPR linewidths in the $NH_4Pr(SO_4)_2 \cdot 4H_2O$ crystal will be used.

2. CRYSTAL STRUCTURE

$NH_4R(SO_4)_2 \cdot 4H_2O$ crystals are monoclinic, characterized by the space group C_{2h}^5, containing four formula units per unit cell [1]. The unit-cell parameters for crystals, where R = Nd, Ce, Sm and Pr, are listed in Table 1. In the absence of reported experimental data for the positions of the four R^{3+} ions in the unit cell, required to estimate the spin-lattice relaxation time (τ) of the host ions, the R^{3+} positions have been presently deduced, using the information provided in the literature [1, 3] to be (0.5, 0.1321, 0.0), (0.5, 0.3677, 0.5), (0.5, 0.6323, 0.5) and (0.5, 0.8678, 0.0), as shown in Fig. 1; they are labeled as 1, 2, 3 and 4, respectively. The R^{3+} ions 1 and 2 form a pair, being related by symmetry to the other pair, formed by the ions 3 and 4, through an inversion plane.

* On leave of absence from the Center of Materials Analysis, Nanjing University, Nanjing, Jiangsu, The People's Republic of China.

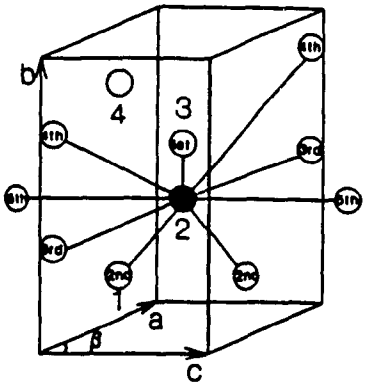

Fig. 1. Positions of the four R^{3+} ions in the unit cell of the $NH_4R(SO_4)_2 \cdot 4H_2O$ hosts. They are marked as 1, 2, 3 and 4, respectively. The positions of the nine R^{3+} ions (one 1st, two 2nd, two 3rd, two 4th and two 5th nearest neighbors) surrounding the impurity Gd^{3+} ion, substituting for the R^{3+} ion 2, are also exhibited. Similar considerations apply when the Gd^{3+} ion replaces any one of the R^{3+} ions 1, 3 or 4.

3. ESTIMATE OF τ

3.1. Theoretical expression

τ of the host paramagnetic ions in doped crystals can be estimated from impurity ion EPR linewidth (ΔB), using the expression [8]

$$\tau = (3\Delta B g^2 \mu_B)/(110 h g' \langle \Delta\nu^2 \rangle), \quad (1)$$

where μ_B, h, g, and g are respectively Bohr's magneton, Planck's constant, the impurity-ion Lande's factor, and the host-ion Lande's factor. In equation (1) $\langle \Delta\nu^2 \rangle$ is the second moment for the impurity ion. Misra and Orhun [8] showed that $\langle \Delta\nu^2 \rangle$ for crystals containing two different species of magnetic ions, for the case when the distances between the impurity ions are sufficiently large, and when the number of host-ion neighbors considered is limited to N, can be expressed as [8]

$$\langle \Delta\nu^2 \rangle = \tfrac{1}{3} S'(S'+1) h^{-2} \Big[N J_p^2 + (gg')^2 \mu_B^4 \mu_0^2 \times \sum_k^N (1 - 3\gamma_{jk}^2)^2 r_{jk}^{-6} + 2 J_p g g' \mu_B^2 \mu_0 \sum_k^N (1 - 3\gamma_{jk}^2) r_{jk}^{-3} \Big]. \quad (2)$$

In equation (2) S', J_p, μ_0, r_{jk}, and γ_{jk} are the effective spin of the host-ion, the average impurity-host ion-pair exchange constant, the permeability constant, the distance between j and k' ions and the direction cosines of r_{jk} with the external Zeeman field, respectively. (The primed quantities refer to the host ions while the unprimed ones to the impurity ions.)

3.2. Numerical estimates

In order to compute τ, using equations (1) and (2), one first needs to know the values of the various quantities appearing therein. A computer programme was used to generate the various $NH_4R(SO_4)_2 \cdot 4H_2O$ (R = Nd, Ce, Sm, and Pr) lattices required to calculate the distances r_{jk} and the corresponding direction cosines (γ_{jk}) of the external field. For the calculation of the second moment, $\langle \Delta\nu^2 \rangle$, using equation (2), it was found sufficient to consider only up to the fifth-nearest neighbors ($N = 9$), the contributions of the farther-lying neighbors were found to be negligible. Table 2 lists the calculated distances for these neighbors of an impurity Gd^{3+} ion, while their positions are shown in Fig. 1. As for the values of S', g' and J_p, the following considerations were made. The effective spin of each of the Kramer's ions Ce^{3+}, Nd^{3+}, and Sm^{3+}, as well as that of the non-Kramer's ion Pr^{3+}, is $S' = 1/2$ [7, 10]. ($S' = 1/2$ for Pr^{3+} is true for the case of lower symmetry, being equivalent to the presence of local distortions superimposed on higher symmetry due to Jahn-Teller effect). Further, for Pr^{3+}, $g_\parallel' = 2\langle \xi_0 | S_z' | \xi_0 \rangle$, where $|\xi_n\rangle$ is one of the time-conjugate states for the ground state of Pr^{3+}, and $g_\perp' = 0$ [7]. No experimental g' values have been reported for the host

Table 1. Unit-cell parameters of $NH_4R(SO_4)_2 \cdot 4H_2O$ single crystals (R = Nd, Ce, Sm and Pr) [1]

R	a(Å)	b(Å)	c(Å)	β
Nd	6.625	18.928	8.789	97.06°
Ce	6.676	19.005	8.821	97.28°
Sm	6.582	18.886	8.736	96.88°
Pr	6.644	18.963	8.798	97.18°

Table 2. Distances (in Å) between Gd^{3+} and the neighbor R^{3+} ions. There are one 1st-, two 2nd-, two 3rd-, two 4th- and two 5th-nearest neighbors (nn)

R	1st *nn*	2nd *nn*	3rd *nn*	4th *nn*	5th *nn*
Pr	5.02	6.27	6.44	8.17	8.80
Sm	5.00	6.24	6.58	8.26	8.74
Nd	5.01	6.26	6.62	8.31	8.79
Ce	5.03	6.28	6.68	8.36	8.82

ions in the presently considered crystals. However, the coordinations around a R^{3+} ion in $NH_4R(SO_4)_2 \cdot 4H_2O$ lattice are the same as that of a R^{3+} ion in the $Y(C_2H_5SO_4)_3 \cdot 9H_2O$ lattice, so that the g' values for R^{3+} ions in the two lattices are about the same [12]. A theoretical calculation yields $g'_\parallel = 3.81$, $g'_\perp = 0.20$ for Ce^{3+} in $Y(C_2H_5SO_4)_3 \cdot 9H_2O$ [11]. Similarly, one has for the Pr^{3+}, Nd^{3+} and Sm^{3+} ions $(g'_\parallel, g'_\perp) =$ (1.6, 0.0), (3.65, 1.98), and (0.73, 0.40), respectively [12, 13]. In the numerical estimates made presently for τ, the direction of the external field has been assumed to be along the principal Z magnetic axis, i.e. the principal axis of the b_2^0 tensor, of the Gd^{3+} ion [2–4]; the Z axis for the Gd^{3+} ion in $NH_4Pr(SO_4)_2 \cdot 4H_2O$ has been determined by Misra and Sun [4] to be along the 4-fold axis of a distorted-monocapped-square antiprism, making approximately the angles (51°, 45°, 72°) relative to the (a, b, c) axes. However, the principal magnetic axes (Z') for the host R^{3+} ions are not necessarily parallel to the respective principal Z axes of the impurity Gd^{3+} ion. In this case, the averages of $g'_\parallel$ and $g'_\perp$ values, listed in Table 3, for the host ions were chosen for g' in equations (1) and (2) for estimating τ. This does not lead to any significant error in the calculated values of τ, because of some uncertainty in other factors. The required g values of the Gd^{3+} ion have been reported previously [2–5], and are listed in Table 3. As for the values of J_p, they have not been determined experimentally for the Gd^{3+}–Nd^{3+}, Gd^{3+}–Pr^{3+}, Gd^{3+}–Sm^{3+}, and Gd^{3+}–Ce^{3+} pairs. The present calculations of τ have been made for $J_p = 0.1$, 1.0, 5.0, 10.0 GHz values, which cover the possible range of values.

The room-temperature τ values for Sm^{3+}, Ce^{3+}, and Nd^{3+} were estimated from equations (1) and (2), using the reported experimental Gd^{3+} EPR linewidths in the $NH_4R(SO_4)_2 \cdot 4H_2O$, R = Sm, Ce, and Nd hosts [2, 3, 5]. As for the estimate of τ for the Pr^{3+} ion, the Gd^{3+} EPR linewidths, as reported by Misra and Sun [4], in the 266–410 K temperature range, in the $NH_4Pr(SO_4)_2 \cdot 4H_2O$ host, were used. No estimates were made for τ for Pr^{3+} in $NH_4Pr(SO_4)_2 \cdot 4H_2O$ host crystal at temperature above 410 K, or below 266 K, because of the unavailability of ΔB values. This is because below 266 K the crystal underwent a phase transition, while above 410 K the crystal deteriorated due to dehydration [4].

The τ values estimated at room temperature for Sm^{3+}, Ce^{3+}, Pr^{3+} and Nd^{3+}, are listed in Table 3, along with the previously reported values of τ by Malhotra *et al.* [2] and Buckmaster *et al.* [3], estimated using the incorrect expression, for comparison purposes.

As for Pr^{3+}, Fig. 2 exhibits the log–log plot of τ^{-1} vs. temperature in the 266–410 K range for $J_p =$ 5 GHz; the calculated τ values being listed in Table 4 along with the required experimental linewidths at different temperatures.

3.3. *Discussion of τ values*

As seen from Table 3, the τ values for Sm^{3+}, Ce^{3+}, Pr^{3+} and Nd^{3+}, computed using the correct expression, equation (1), for various values of J_p, are quite different, by up to an order of 3, from those calculated using the incorrect expression. The large differences arise because of the inclusion of dipolar interactions, along with exchange interactions, between two different kinds of ions (host and impurity) in $\langle \Delta v^2 \rangle$,

Table 3. Calculated room-temperature spin-lattice relaxation times (τ) for Sm^{3+}, Ce^{3+}, Nd^{3+} and Pr^{3+} ions in $NH_4R(SO_4)_2 \cdot 4H_2O$ lattices. The values of S', g, g', J_p, and the impurity-ion (Gd^{3+}) linewidth (ΔB), used in the present calculations, are also listed. τ values are expressed in seconds, while the figures inside the round brackets following τ are J_p values in GHz

R	Sm	Nd	Pr	Ce
S'	1/2	1/2	1/2	1/2
g	1.9922	1.9830	1.9949	1.9930
g'	0.57	2.82	0.80	2.01
ΔB (Gs)	44	64	53	51
τ (0.1)*	3.09×10^{-11}	3.76×10^{-13}	1.35×10^{-11}	8.54×10^{-13}
τ (1.0)*	5.04×10^{-12}	3.45×10^{-13}	3.95×10^{-12}	6.70×10^{-13}
τ (5.0)*	2.12×10^{-13}	5.91×10^{-14}	1.84×10^{-13}	6.95×10^{-14}
τ (10.0)*	5.26×10^{-14}	1.56×10^{-14}	4.55×10^{-14}	1.76×10^{-14}
$\tau^\wedge$	2.10×10^{-10}	2.10×10^{-12}	–	1.00×10^{-11}

*Calculated presently

^Reported in [2] and [3].

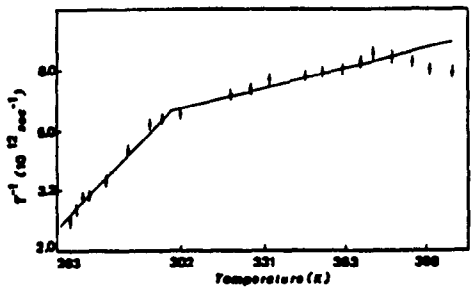

Fig. 2. A log–log plot of the inverse of spin-lattice relation time (τ^{-1}) versus the temperature (T), in the 266–410 K range, for the host paramagnetic ion Pr^{3+} in the $NH_4Pr(SO_4)_2 \cdot 4H_2O$ crystal for $J_p = 5.0$ GHz. (The values of the slopes do not change for different values of J_p, as seen from equations (1) and (2).)

given by equation (2). It is also seen from Table 3, for Pr^{3+} and Sm^{3+} ions, that their τ values fluctuate by three orders of magnitude, while this fluctuation is only by one order of magnitude for Nd^{3+} and Ce^{3+} ions, for J_p values ranging from 0.1 to 10 GHz. However, as seen from equations (1) and (2), the T power-law dependence of τ^{-1}, which enables one to discern the spin-lattice relaxation process in effect, is independent of a particular J_p value. For Pr^{3+} host ions in $NH_4Pr(SO_4)_2 \cdot 4H_2O$, a T^7 dependence of τ is found in the temperature range 266–296 K, while a T^2 dependence in the temperature interval 296–410 K.

4. SPIN-LATTICE RELAXATION MECHANISM FOR Pr^{3+} IN $NH_4Pr(SO_4)_2 \cdot 4H_2O$

A least-squares fitting of τ to temperature indicates that the τ values of Pr^{3+} in $NH_4Pr(SO_4)_2 \cdot 4H_2O$, as calculated presently for $J_p = 5.0$ GHz, can be fitted well to $\tau = BT^{-7}$ with $B = 3.79 \times 10^4$ s. K^7 in the temperature range 266–296 K, and to $\tau = CT^{-2}$ with $C = 1.61 \times 10^{11}$ s. K^2 in the temperature range 296–410 K. It is now possible, from these T^7 and T^2 temperature dependences of τ^{-1}, to deduce as to which mechanisms are responsible for SLR in the two temperature regions. Surveys of the various SLR mechanisms have been provided by Abragam and Bleaney [7], and by Shrivastava [14].

As for the T^7 dependence of τ^{-1} for a non-Kramers ion, such as Pr^{3+}, it is caused by the following processes: (i) at *low* temperature, by Raman processes, specifically Raman spin-one phonon interaction in second order, Raman spin-two-phonon interaction, and Raman process effected by short wave-length phonons. (ii) At *low* temperatures, by a process involving three phonons, described by Le Naour [15], in which first the small wave-vector approximation is used to obtain a transition from an upper level E_b to another upper level E_c by the emission of two phonons, and integration is made over all the phonons from 0 to Δ_c ($= E_c - E_a$, where E_a is the ground state). This is followed by the calculation of a Raman process using phonons from Δ_c to Debye cutoff, thus making full use of the Debye spectrum. (iii) At *intermediate* temperatures, by the "sum" process [16, 17], in which a spin transition is achieved by means of emission or absorption of two phonons; the range of temperature being centered at about 0.14 Δ_c [17], depending very sensitively on the structure of levels in the host crystal [16, 17]. From the temperature ranges over which the processes (i), (ii) and (iii) are applicable, it appears that the presently-observed T^7 behaviour of τ^{-1} in the range 266–296 K may be explained to be due predominantly to the sum process, since this tempera-

Table 4. The calculated spin-lattice relaxation times (τ) of the Pr^{3+} ion and the observed Gd^{3+} EPR linewidths (ΔB) in the $NH_4Pr(SO_4)_2 \cdot 6H_2O$ host at various temperatures (T) for $J_p = 5$ GHz. The error for ΔB is ± 3 Gs

T (K)	ΔB (Gs)	τ (s)	T (K)	ΔB (Gs)	τ (s)
266	116	4.03×10^{-13}	333	39	1.35×10^{-13}
269	106	3.68×10^{-13}	347	38	1.32×10^{-13}
271	96	3.33×10^{-13}	354	37	1.28×10^{-13}
273	95	3.30×10^{-13}	362	36	1.25×10^{-13}
278	85	2.95×10^{-13}	369	34	1.18×10^{-13}
285	67	2.33×10^{-13}	374	32	1.11×10^{-13}
292	55	1.91×10^{-13}	383	33	1.15×10^{-13}
296	53	1.84×10^{-13}	392	34	1.18×10^{-13}
303	51	1.77×10^{-13}	400	36	1.25×10^{-13}
319	44	1.53×10^{-13}	410	37	1.28×10^{-13}
326	42	1.46×10^{-13}			

ture range is more appropriately "intermediate", rather than "low".

As for the T^2 behavior of τ^{-1} in the range 296–410 K, it can be explained to be due to any one of the various Raman processes, described above, as well as due to the sum process, all of which predict T^2 dependence of τ^{-1} at high temperatures. However, the sum process has *negligible* contribution compared to that of the usual Raman process, particularly because in the sum process only the lowest-energy phonons are required, whose number diminishes considerably at *high* temperatures; in addition, the value of the integral required in the expression for τ^{-1} for the sum process becomes quite small at elevated temperatures [16, 17]. To explain further, at elevated temperatures, the number of phonons for which $\omega_1 - \omega_2 = \omega$, required for the usual Raman process, is extemely large compared to that for which $\omega_1 + \omega_2 = \omega$ required for the sum process. (Here $\hbar\omega$ is the difference in the two levels of the spin system and ω_1, ω_2 are the frequencies of the phonons involved in the Raman, or sum, processes.) This is because the energy density of phonons depends on temperature as $x^2/(e^x - 1)$, where $x = \hbar\omega/k_B T$, which tends to zero as T approaches zero, or infinity, from an intermediate value [7]. Thus, the number of phonons required for the sum process, which come from the lowest part of the phonon spectrum because $\omega = \omega_1 + \omega_2$, is negligible at high temperatures, while the number of phonons required for the Raman process is large, because they can belong to any part of the phonon spectrum, including those belonging to the highest phonon density, as long as $\omega = \omega_1 - \omega_2$. Thus, the Raman process is the predominant mechanism for SLR of host Pr^{3+} ions in $NH_4Pr(SO_4)_2 \cdot 4H_2O$ in the 296–410 K temperature range.

Finally, as seen from Fig. 2, the τ^{-1} values for Pr^{3+} in $NH_4Pr(SO_4)_2 \cdot 4H_2O$ exhibit a sudden transition from T^7 to T^2 behavior at 296 K as the temperature is increased. If only one of the above-mentioned processes, which is capable of exhibiting both T^7 and T^2 dependence of τ^{-1} as one goes from low to high temperature, were operative over the entire temperature range 266–410 K, a gradual, and not sudden, transition from the T^7 to T^2 behavior for τ^{-1} would be observed. The sudden transition of the T dependence of τ^{-1} is, most likely, due to the *simultaneous* presence of a number of competing SLR mechanisms which are in force at the transiton temperature 296 K, depending on the Pr^{3+} energy levels in a complex manner. Such a sudden transition, from T^{n_1} to T^{n_2} behaviour of τ^{-1}, is in conformity with the various experimental data exhibited in [7] and [14].

5. CONCLUDING REMARKS

The main results of the present numerical computations of τ are as follows:

(i) The correct expression, equations (1) and (2), yields much shorter τ values for the host R^{3+} ions in the $NH_4R(SO_4)_2 \cdot 4H_2O$ crystals, where R = Ce, Nd and Sm, than those estimated using the incorrect expression.

(ii) The power-law dependence on temperature of τ^{-1} values of the Pr^{3+} ion, which is independent of J_z, suggests the dominance of the sum relaxation process in $NH_4Pr(SO_4)_2 \cdot 4H_2O$ crystal in the temperature range 266–296 K (T^7 dependence of τ^{-1}), and that of the Raman process in the 296–410 K range (T^2 dependence of τ^{-1}). For $NH_4R(SO_4)_2 \cdot 4H_2O$ (R = Sm, Ce and Nd) Malhotra *et al.* [2] and Buckmaster *et al.* [3] predicted an Orbach process. However, this conclusion was only guessed by comparison with other systems and not arrived at by a study of temperature variation of τ, as only room-temperature values of τ were estimated.

Acknowledgement — The authors are grateful to the Natural Sciences and Engineering Research Council of Canada for partial financial support (grant No. OGP0004485).

REFERENCES

1. E. Eriksson, L.O. Larsson, L. Niinisto & U. Skoglund, *Inorg. Chem.* 13, 290 (1974).
2. V.M. Malhotra, H.A. Buckmaster & H.D. Bist, *Can. J. Phys.* 58, 1667 (1980).
3. H.A. Buckmaster, V.M. Malhotra & H.D. Bist, *Can. J. Phys.* 59, 596 (1981).
4. S.K. Mista & J. Sun, *Phys. Status Solidi (b)*, to be published.
5. V.M. Malhotra, H.D. Bist & G.C. Upreti, *Chem. Phys. Lett.* 28, 390 (1974).
6. S.G. Jasty & V.M. Malhotra, *EPR Symposium, Rocky Mountain Conference*, 1988.
7. A. Abragam & B. Bleaney, *Electron Paramagnetic Resonance of Transition Ions*, Clarendon, Oxford (1970).
8. S.K. Misra & U. Orhun, *Phys. Rev.* B39, 2856 (1989).
9. P.W. Anderson & P.R. Weiss, *Rev. Mod. Phys.* 25, 269 (1953).
10. S.A. Al'tshuler & B.M. Kozyrev, *Electron Paramagnetic Resonance*, Academic Press, New York (1964).
11. G.H. Larson & C.D. Jeffries, *Phys. Rev.* 141, 461 (1966).
12. S.A. Al'tshuler & B.M. Kozyrev, *Electron Paramagnetic Resonance in Compounds of Transition Elements*, Keter, Jerusalem (1974).

13. W.T. Gray IV & H.J. Stapleton, *Phys. Rev.* **B9**, 2863 (1974).
14. K.N. Shrivastava, *Phys. Status Solidi (b)* **117**, 437 (1983).
15. R. Le Naour, *Phys. Rev.* **B1**, 2007 (1970).
16. K.N. Shrivastava, *Phys. Status Solidi* **42**, K177 (1970).
17. K.N. Shrivastava, *Phys. Status Solidi (b)* **92**, K19 (1979).